THE UNIVERSITY
of EDINBURGH

Application of global methods for sensitivity analysis and uncertainty assessment of atmospheric chemistry transport models

Ksenia Aleksankina

THE UNIVERSITY *of* EDINBURGH

A thesis submitted in fulfilment of the requirements

for the degree of Doctor of Philosophy

The University of Edinburgh

2019

Lay summary

Air pollution adversely affects human health and the environment both in developed and developing countries and contributes to acidification and eutrophication that damages ecosystems. High levels of ground-level ozone affect natural and semi-natural vegetation and lead to a reduction in yields of agricultural crops. Additionally, pollutants such as particulate matter (PM), ozone (O_3), and nitrogen dioxide (NO_2) negatively affect human health and lead to an increased risk of premature death.

Poor air quality is both a local and a global issue as air pollution can travel over long distances and over national boundaries. Therefore, various approaches to help understand and improve air quality are continuously being developed at all levels of government, from global conventions to policy initiatives at local levels.

Atmospheric chemistry transport models (ACTMs) are model descriptions of the atmosphere that incorporate aspects such as emissions of the pollutants, their transport by weather systems, their chemical processing in the atmosphere and their eventual removal from the air by wet or dry deposition. ACTMs play an essential role in improving our understanding of the interrelationships of atmospheric processes and provide scientific support for policy-related decision-making by providing opportunities for assessment of past and potential future policy interventions to mitigate air pollution. Therefore, it is important to have a quantitative estimate of uncertainty in the predictions made using ACTMs.

In this study, the uncertainty in model outputs introduced by the uncertainty inherent to input data of anthropogenic emissions of air pollutants is investigated and quantified. Additionally, the sensitivity of different model outputs to changes in the model input emissions is assessed. To determine which specific input datasets drive the change in model outputs, and to what extent, a global sensitivity analysis approach is applied. This study investigates two ACTMs of different complexity: the Fine

Resolution Atmospheric Multi-pollutant Exchange (FRAME) model and the UK regional application of the European Monitoring and Evaluation Programme (EMEP4UK) model.

The results of sensitivity analyses for the FRAME model indicate that changes in surface concentrations of sulfur dioxide (SO_2), nitrogen oxides (NO_x), and ammonia (NH_3), and the deposition of sulfur and nitrogen species, are predominantly driven by the changes in the emissions of relevant precursor or primary pollutants. However, secondary air pollutants formed after emissions, such as particulate sulfate (SO_4^{2-}), nitrate (NO_3^-), and ammonium (NH_4^+) were found to be sensitive to multiple inputs, and their sensitivity was found to be complex and geographically variable. The overall ranges of uncertainty estimated for the model outputs were also found to vary spatially.

For the EMEP4UK model, two different sets of input uncertainty ranges were investigated. The ranges of predicted model output uncertainty for the FRAME and EMEP4UK models given the same uncertainty in the input emissions were found to be substantially different in both magnitude and spatial pattern. Additionally, uncertainty in the same output species was found to be driven by different inputs in the two models. This leads to the conclusion that ranges of uncertainty for different model outputs are model specific and results obtained for one model cannot be directly transferred to another.

The EMEP4UK model can be used to estimate the surface concentrations of O_3, NO_2, and $PM_{2.5}$, the pollutants associated with the adverse effects on human health. In this study, the highest level of uncertainty for these pollutants was found to occur in the grid cells comprising urban areas. This finding is important as the surface concentrations of the aforementioned pollutants predicted by the EMEP4UK model are often used for estimating the health effects induced by exposure to the air pollutants.

Additionally, an emulator-based approach to global sensitivity analysis and uncertainty assessment has been demonstrated in this study. This approach made possible global sensitivity analysis and uncertainty propagation for EMEP4UK model, that would otherwise be prohibitively computationally expensive because of a large number of model runs required.

Abstract

Atmospheric concentrations of air pollutants remain high, and air quality is still an issue that requires attention in many countries including the UK. Atmospheric chemistry transport models (ACTMs) are widely used to provide scientific support for policy development in relation to the mitigation of the detrimental effects of air pollution on human health and ecosystems. Hence it is important to assess the level of uncertainty associated with model predictions.

In this work, the application of global sensitivity analysis and uncertainty assessment methods is investigated for two ACTMs of different complexity: the Fine Resolution Atmospheric Multi-pollutant Exchange (FRAME) model and the UK regional application of the European Monitoring and Evaluation Programme (EMEP4UK) model. For both models, the uncertainties in the outputs resulting from uncertainties in the model input emissions are quantified and apportioned. Additionally, the overall model response to variations in the input emissions within a ± 40 % range from the baseline is investigated as this range of variation is typically used for future scenario simulations.

FRAME is a Lagrangian ACTM with 5 km × 5 km horizontal resolution over the UK domain that is used to estimate annual average concentrations and deposition of sulphur and nitrogen species. In the model, air columns with 33 vertical layers of varying thickness (from 1 m at the surface to 100 m at the top of the mixing layer) move from the boundary of the domain along straight-line trajectories with different starting angles at a 1° resolution. The model utilises annually averaged meteorology to define the column trajectories and rainfall. The chemical scheme includes gaseous- and aqueous-phase reactions. FRAME supplies Source-Receptor Relationship (SRR) matrices for the UK Integrated Assessment Model, which directly underpins UK air pollution control policies.

EMEP4UK is a 3-D Eulerian model with a horizontal resolution of 5 km × 5 km over the British Isles and 20 vertical levels, extending from the ground to 100 hPa, which is also extensively used to inform UK air quality assessment. The chemical scheme implemented in the model is EmChem09 with the MARS equilibrium module for gas-aerosol partitioning of secondary inorganic aerosol. In addition to the pollutants modelled by FRAME, EMEP4UK is capable of modelling ozone (O_3) and speciated particulate matter ($PM_{2.5}$ and PM_{10}) concentrations, all at hourly temporal resolutions.

In this study, the uncertainty ranges for the input emissions from UK anthropogenic land-based sources were assigned according to the data provided by the UK National Atmospheric Emissions Inventory. For the FRAME model, the uncertainties in the outputs were propagated from the uncertainties in the emissions of SO_2, NO_x, and NH_3. For the EMEP4UK model, an increased number of input variables was used; the emissions of NO_x, SO_2, NH_3, VOC, and primary $PM_{2.5}$ were split into 13 model inputs based on the contributions from different emission source sectors. The optimised Latin hypercube sampling design was used for both models to construct model runs that covered a chosen range of input emission perturbations.

The FRAME model was investigated using several regression techniques. The response of the model to emission perturbations within a ± 40% range from the baseline value was found to be substantially linear. Surface concentrations of SO_2, NO_x, and NH_3 together with the deposition of S and N were found to be predominantly sensitive to the emissions of the respective pollutant, while sensitivities of secondary species such as HNO_3 and particulate SO_4^{2-}, NO_3^-, and NH_4^+ to pollutant emissions were more complex and geographically variable. Additionally, the uncertainty in the surface concentrations of NH_3 and NO_x and the depositions of NH_x and NO_y was shown to be due to uncertainty in a single input variable, NH_3, and NO_x respectively. In contrast, the uncertainty in concentration and deposition of sulfur containing species were affected by the uncertainties in both NH_3 and SO_2 emissions. Similarly, the relative uncertainties in the modelled surface concentrations of each of the secondary pollutant variables were affected by the uncertainty range of at least two input variables.

An emulator-based approach was used to propagate and apportion uncertainty in EMEP4UK outputs and investigate the model response to input perturbations. A separate Gaussian process emulator was used to estimate model predictions at unsampled points in the space of the uncertain model inputs for every modelled grid cell. For the surface concentrations of O_3, NO_2, and $PM_{2.5}$ (pollutants associated with the adverse effects on human health) the highest level of uncertainty was found to occur in the grid cells comprising urban areas, up to ± 7%, ± 9%, and ± 9% respectively. However, overall uncertainty calculated for the land-based grid cells for the variables above was found to be low, which indicates that the outputs may be more sensitive to variation in other model input parameters, such as chemical or physical constants. Alternatively, UK land-based concentrations of O_3, NO_2, and $PM_{2.5}$ may be dominated by the precursor emissions and long-range transport of pollutants from outside the UK. Investigating seasonal changes in uncertainty and sensitivity for the monthly-averaged model outputs allowed determination of the importance of the inputs that drive uncertainty changes throughout the year. For example, uncertainty in O_3 was driven more by uncertainty in VOC emissions during the summer, and for $PM_{2.5}$ the importance of NH_3 in driving overall uncertainty increased during spring and summer.

The aim of the global methods for sensitivity analysis and uncertainty assessment presented here is to quantify the confidence in model predictions associated with particular aspects of model operation. Furthermore, the model runs and emulators created for the analyses can be used to predict the ACTM response for any other combination of perturbed input emissions within the ranges set for the original Latin hypercube sampling design without the need to re-run the ACTM. This makes exploring different emission perturbation scenarios possible at a significantly reduced computational cost. The methods discussed in this study can be applied to any operational aspect of any ACTM.

Declaration

I declare that this thesis was composed by myself, that the work contained herein is my own except where explicitly stated otherwise in the text, and that this work has not been submitted for any other degree or professional qualification except as specified. Parts of this work have been published in

Aleksankina, K., Heal, M. R., Dore, A. J., Van Oijen, M., and Reis, S.: Global sensitivity and uncertainty analysis of an atmospheric chemistry transport model: the FRAME model (version 9.15.0) as a case study, Geosci. Model Dev., 11, 1653-1664, https://doi.org/10.5194/gmd-11-1653-2018, 2018.

and

Aleksankina, K., Reis, S., Vieno, M., and Heal, M. R.: Advanced methods for uncertainty assessment and global sensitivity analysis of a Eulerian atmospheric chemistry transport model, Atmos. Chem. Phys. Discuss., https://doi.org/10.5194/acp-2018-690, in review, 2018.

Ksenia Aleksankina

February 2019

Acknowledgements

Firstly, I would like to thank my supervisors Mathew Heal and Stefan Reis for their constructive suggestions during the planning and development of this research work, as well as their continual support and enthusiastic encouragement.

I am grateful to the people at the Centre for Ecology & Hydrology, Tony Dore for the valuable support with setting up the FRAME model and providing helpful advice, Marcel Van Oijen for always finding time to discuss statistical questions, and Massimo Vieno for his guidance with the EMEP4UK model.

I would like to thank all members of Mathew Heal's group and the MACAQUE (Modelling and measuring atmospheric chemistry and air quality at Edinburgh) group for their support. Our meetings have always been a source of challenging questions and valuable feedback. I am particularly grateful for the assistance given by Riinu, who helped with getting the models to run. I am also thankful to everyone in the Kings Buildings office for creating a friendly atmosphere.

I am very grateful to my mother and grandmother for all their support. Finally, I am thankful to Nikolai who believed in me and kept me motivated.

Contents

List of Figures

List of Tables

List of Abbreviations

ACTM	Atmospheric Chemistry Transport Models
ADIFOR	Adjoint Sensitivity Analysis and Automatic Differentiation in FORTRAN
AQEG	Air Quality Expert Group
BFM	Brute Force Method
CEIP	Centre for Emission Inventories and Projections
CI	Confidence Interval
CLRTAP	Convention on Long-range Transboundary Air Pollution
DDM	Decoupled Direct Method
DICE	Deep Inside Computer Experiments
EC	European Commission
EEA	European Environment Agency
EMEP MSC-W	European Monitoring and Evaluation Programme Meteorological Synthesizing Centre-West
EMEP4UK	UK regional application of the European Monitoring and Evaluation Programme
EPA	Environmental Protection Agency
FAST	Fourier Amplitude Sensitivity Test
FRAME	Fine Resolution Atmospheric Multi-Pollutant Exchange
GAM	Generalised Additive Model
GEM-SA	Gaussian Emulation Machine for Sensitivity Analysis
GFS	Global Forecast System
GP	Gaussian process
GUI	Graphical User Interface
HDMR	High-Dimensional Model Representation
HPC	High-Performance Computing
IIR	Informative Inventory Report

IPCC	Intergovernmental Panel on Climate Change
LHS	Latin hypercube sampling
LOESS	Locally Weighted Regression
MUCM	Managing Uncertainty in Complex Models
NCAR	National Center for Atmospheric Research
NCEE	National Center for Environmental Economics
NCEP-GFS-FNL	National Centers for Environmental Prediction Final Global Forecast System
OAT	One-at-a-time
PDF	Probability Density Function
PM	Particulate Matter
RC	Regression Coefficient
SNAP	Selected Nomenclature for Air Pollutants
SOA	Secondary Organic Aerosols
SRC	Standardised Regression Coefficient
SRS	Simple Random Sampling
VOC	Volatile Organic Compound
WHO	World Health Organisation
WRF	Weather Research and Forecast model

Chapter 1

Introduction

1.1 Air pollution

Air pollution is defined by the World Health Organisation (WHO) as "contamination of the indoor or outdoor environment by any chemical, physical or biological agent that modifies the natural characteristics of the atmosphere" (WHO, 2015) and it is a concern not only for developing countries but also for European countries. In Europe, emissions of many air pollutants have decreased substantially over the past decades, resulting in improved air quality in the region. However, many air pollutant concentrations remain above the recommended levels, and air quality problems persist in the UK and elsewhere globally.

According to WHO, air pollution is a significant environmental risk to health, and it is linked to stroke, heart disease, chronic and acute respiratory diseases and premature mortality (WHO, 2013). Pollutants of major public health concern include particulate matter ($PM_{2.5}$ and PM_{10}), tropospheric ozone (O_3), and nitrogen dioxide (NO_2). The effects of these pollutants on human health have been reported in a number of studies (Anderson et al., 2012; Anenberg et al., 2010; Chen et al., 2007; Heal et al., 2012; Hoek et al., 2013; Im et al., 2018; Kampa and Castanas, 2008; Tuet et al., 2017). Air pollution also damages ecosystems; emissions of nitrogen oxides (NO_x), SO_2 and ammonia (NH_3) contribute to acidification and eutrophication, which adversely affects vegetation and aquatic environments (Bobbink et al., 1998; Bouwman et al., 2002; Krupa, 2003; Schindler, 1988). Ground-level ozone is shown to damage vegetation and decrease crop yields (Benton et al., 2000). Additionally, O_3 and particulate matter contribute to climate change through radiative forcing (IPCC, 2013; Stevenson et al.,

2013). Therefore, in order to prevent detrimental effects, air pollution needs to be monitored and controlled.

1.2 Application of models to underpin policy decisions

Policies and legislation regarding air pollution and human health and ecosystem protection are developed continuously at all levels of government, from global conventions and European legislations to policy initiatives at local levels. One of the first international agreements was the 1979 Geneva Convention on Long-range Transboundary Air Pollution (CLRTAP). The convention has created a framework for controlling and reducing air pollution and its damaging effects. In the European Union, the limits for ambient concentrations of air pollutants are set by the Ambient Air Quality Directive (EC Directive, 2008). The national air quality objectives for the UK are summarised by Defra (Defra, 2018).

As emissions ceilings get tighter, it becomes more important to quantify the effect of policy measures, which are complex and cannot easily be estimated. In order to assess if the existing objectives are likely to be met, a wide range of atmospheric chemistry transport models (ACTMs) are utilised. These models are used to project how pollutants emitted from different sources are distributed in, and deposited from, the atmosphere. ACTMs can also be used for source attribution and calculation of source-receptor relationship matrices.

With the increase in availability of computational resources, mathematical models have become prominent tools in the decision-making process. Any model is a simplified representation of the real world, and it is impossible to build a perfect model that would completely replicate the system of interest. The choice of model type and complexity heavily depends on the application; modelling complex chemical transformations and transport of multiple species over time requires more computationally demanding models than modelling the transport of a single chemical species. However, increasing model complexity does not always result in a better

quality of output predictions. Increasing the refinement of the model also increases the number of parameters with uncertain values which in turn may result in greater overall output uncertainty.

Additionally, the presence of a large number of interconnected processes in a model decreases its transparency to users and reviewers and presents a difficulty for model evaluation. The computational time required to run the model also needs to be considered; increased model runtime reduces the number of alternative scenario simulations that can be performed and hence makes some models inadequate for certain applications. Examples of such applications are the impact assessment studies that require a large number of scenarios to be simulated or the calculation of detailed source-receptor relationships (Oxley et al., 2003, 2013).

The approaches commonly used to model air pollutant behaviour in the atmosphere are described below.

1.2.1 Types of process-based atmospheric models

The simplest atmospheric model is the zero-dimensional box model (Fig. 1.1) in which the air mass over a region is treated as a single static box. The pollutant species are introduced into the box by emission or net advection in and out and undergo chemical transformations and deposition. The air mass inside the box is assumed to be well mixed, and pollutant concentrations are assumed to be uniform (Finlayson-Pitts and Pitts, 2000; Holmes and Morawska, 2006).

More sophisticated ACTMs are used to simulate how pollutants are dispersed from emission sources as well the chemical transformations they undergo on the way to receptor sites. In a Lagrangian model (Fig. 1.2) pollutants are emitted into an air column which can be split into several vertical layers and moves over a geographical domain along a defined trajectory. The chemical transformations take place in the air column layers with appropriate vertical transport processes between layers. The deposition takes place in the lowest layer (Lin et al., 2012).

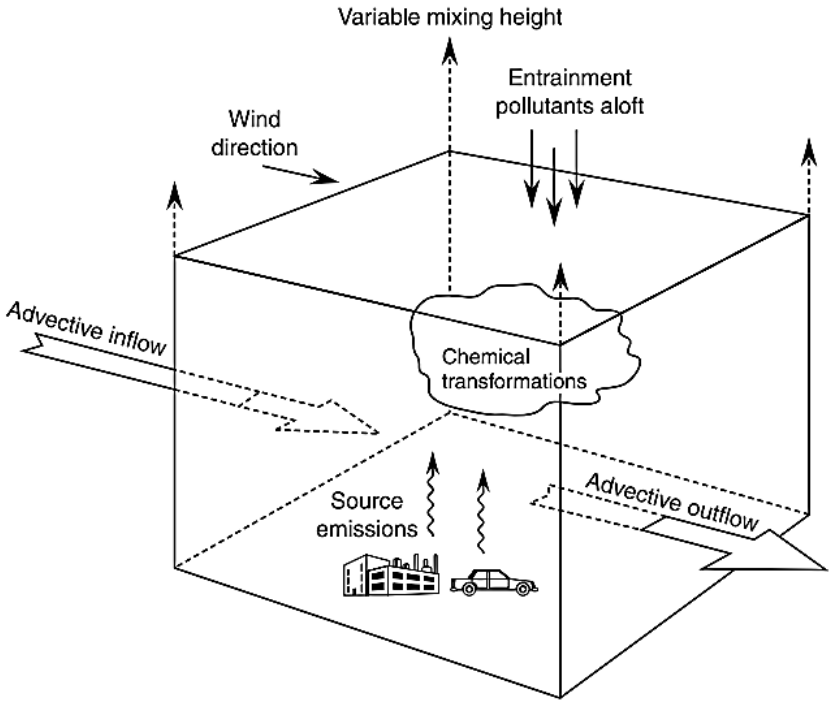

Figure 1.1 Schematic diagram of a box model *(Finlayson-Pitts and Pitts, 2000).*

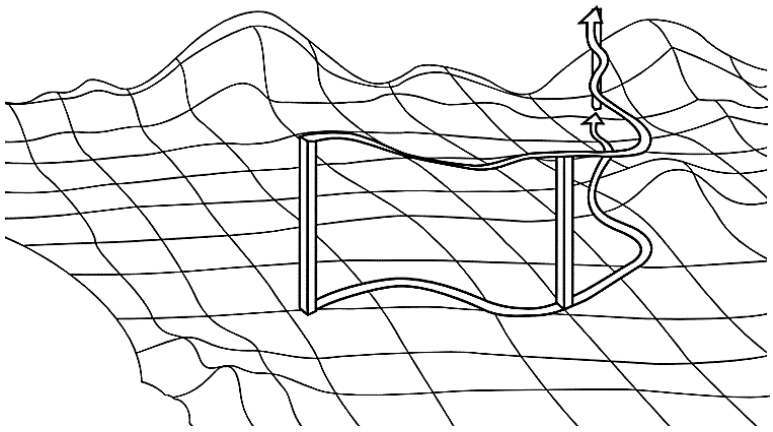

Figure 1.2 Schematic representation of the air column movement in a Lagrangian modelling approach *(Finlayson-Pitts and Pitts, 2000).*

The most comprehensive and complex model type is the Eulerian model (Fig 1.3). In this model, the entire 3-D domain to be modelled is divided into a series of boxes within a static coordinate frame. At each time step, the model simulates all chemical transformation and deposition processes within each box, and the relevant mass

transport between adjacent boxes, leading to 3-D spatial and temporal concentration maps and time series (Finlayson-Pitts and Pitts, 2000; Simpson et al., 2012).

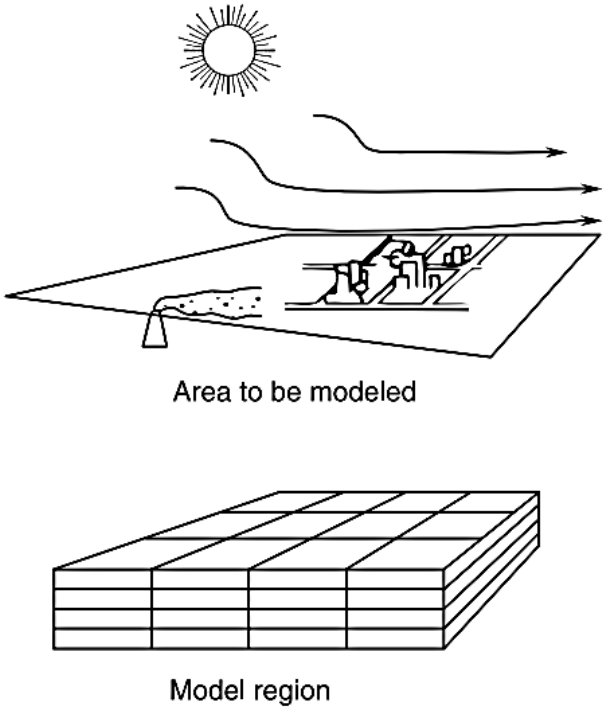

Figure 1.3 Schematic representation of a Eulerian modelling approach *(Finlayson-Pitts and Pitts, 2000).*

1.2.2 Model evaluation

Model evaluation is a crucial part of the development process and is essential for models used in both scientific research and regulatory decision making. The main aim of evaluation is to determine if the model sufficiently represents the system of interest. This allows the adequacy of conclusions made from the model predictions to be assessed.

Typically, when evaluating ACTM performance emphasis is placed on the model validation process, i.e. comparison of model predictions against a set of observations. A number of performance indicators such as root mean square error, correlation coefficient, and normalised mean bias are widely accepted as the assessment criteria

of how well model outputs correspond with observations. Boylan and Russell (2006), Dennis et al. (2010), and Thunis et al. (2012) discuss the suitability of different model performance criteria for the evaluation of air quality models. The Taylor diagram (Fig. 1.4) introduced by Taylor (2001) and the target diagram (Fig. 1.5) introduced by Jolliff et al. (2009) are commonly used to visualise and compare performance characteristics of different models. The Taylor diagram displays the standard deviation, Pearson correlation coefficient, and root mean square error values. The target diagram typically displays a bias measure on the *y*-axis, and a root mean square on the *x*-axis. These values could be presented as normalised by the standard deviation of the observations (Jolliff et al., 2009) or normalised by the uncertainty values assigned to the observation data (Thunis et al., 2012).

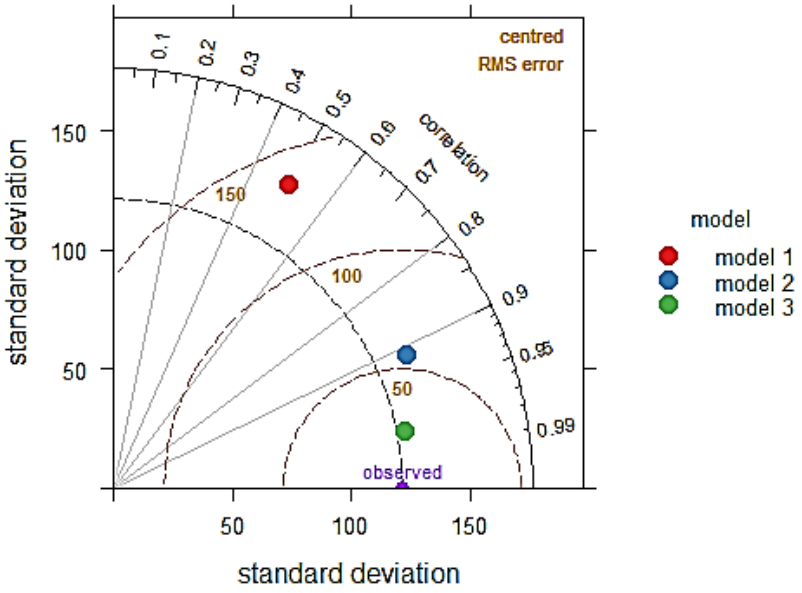

Figure 1.4 A Taylor diagram illustrates a statistical comparison of model outputs with observation data. The diagram illustrates Pearson correlation coefficient values, standard deviation, and root mean square error values for three different models. This illustrative example of a Taylor diagram is produced using code from the example presented in the openair package manual *(Carslaw and Ropkins, 2018)*.

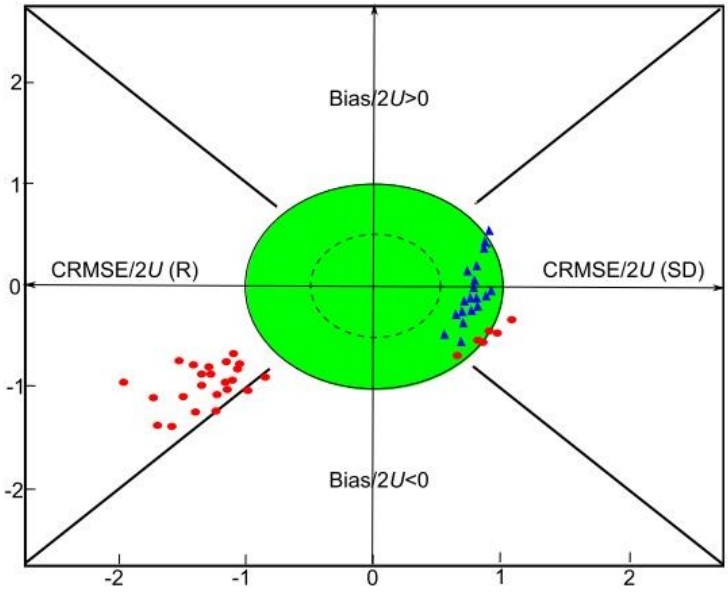

Figure 1.5 A target diagram from Thunis et al. (2012) visualises model performance for two different locations (red and blue). The green area represents model performance that fulfils desirable performance criteria set in the study; the x-axis displays centred root mean square error and y-axis displays bias, both normalised by the uncertainty in the observations.

Although model validation indicators are informative and are easy to interpret, there is an issue associated with their use. Firstly, it is usually assumed that observed or measured values are the true values, i.e. uncertainty in the observations is acknowledged but not included in the calculation of the performance indicators. Secondly, the model performance indicators provide information about the difference between modelled and observed values only and cannot help to identify the reason for the discrepancy. Additionally, the current increase in computational resources makes increasingly complex models more accessible. As the model complexity increases, it becomes more difficult to predict which inputs are driving the outputs of interest, and the amount of uncertain information that needs to be specified in the model increases. Hence, in addition to model validation, uncertainty assessment and sensitivity analysis should be included as an integral part of the model evaluation.

In the context of model evaluation, uncertainty assessment provides information on how uncertainties in different model parameters and inputs are propagated to get the uncertainty range for the outputs of interest. An uncertainty assessment allows a credible range of predicted values for the model outputs, rather than a single best estimate, to be presented. This information is especially valuable when models are used to inform decision making. Sensitivity analysis aims to provide an understanding of how a model depends upon the information fed into it. It can be used to quantify the response of the model to changes in the input data and to determine to what extent different inputs contribute to the overall model uncertainty. Uncertainty assessment and sensitivity analysis approaches are discussed in detail in the following chapters.

The US Environmental Protection Agency guidelines on environmental model development, evaluation, and application (EPA, 2009) and the technical guide on the use of models with regard to the ambient air quality directive in Europe (EEA, 2011) both recommend implementation of uncertainty assessment and sensitivity analysis as a part of model development and evaluation. Despite these recommendations, there are only a few published studies that report uncertainty assessment methodology development or application for ACTMs. Additionally, most of the published sensitivity analyses use a one-at-a-time approach to investigate the model response to different inputs without acknowledging the possible drawbacks and limitations of this approach (this issue is discussed in detail in Chapter 2). The reason for this could be the comparatively high computational cost associated with uncertainty propagation and global sensitivity analysis as they require a large number of model simulations to be performed which may not have been feasible previously. However, continued increase in the availability of computational resources and the development of techniques such as emulation make these techniques more accessible.

1.3 Scope and aims

In this thesis, the application of global uncertainty and sensitivity analysis techniques to atmospheric chemistry transport models (ACTMs) is introduced. These analyses are aimed to get a quantitative understanding of the uncertainty magnitude expected for predictions made using ACTMs. Additionally, global approaches provide an understanding of how ACTMs respond to input emission perturbations and help to identify the model inputs that drive resulting uncertainty the most. In addition to quantifying the confidence in model predictions these analyses allow us to gain insight into model behaviour.

Chapter 2 discusses sensitivity and uncertainty analysis methods and gives an overview of the use of sensitivity analysis in the field of ACTM development and application. Chapter 3 provides a detailed description of two ACTMs investigated in this study (FRAME and EMEP4UK), and also includes an overview and comparison of sampling and analysis techniques as well as comparison of packages and tools for emulation. Chapter 4 discusses the results of global sensitivity and uncertainty analysis applied to the FRAME model. Chapter 5 covers the uncertainty assessment study of health-relevant pollutants modelled with EMEP4UK. In Chapter 6 a comprehensive assessment of the results obtained for both ACTMs is presented. Finally, Chapter 7 elaborates on the conclusions and suggestions for further research needs identified by this work.

Chapter 2

Literature overview

This chapter provides an overview of methods used for uncertainty assessment and sensitivity analysis of mathematical models in different research fields. The aim of this review is to summarise the methods available and assess the suitability of these methods for quantifying uncertainty in ACTMs and assessing how variation model inputs affects the outputs. The second part of this chapter presents a systematic overview of sensitivity analysis methods used for model performance assessment in the field of atmospheric modelling. The aim of this section is to assess the current trends in sensitivity analysis methods used in the field.

The increase in computing power coupled with abundance of available data has made the use of mathematical models more widespread in all research areas. However due to the continuous development of models and the inclusion of more processes at greater resolution the complexity of the mathematical models also continues to increase. This increase in model complexity results in an increase in the number of potential sources of uncertainty and the relationship between model inputs and outputs not being analytically tractable. As a result, most complex models, including ACTMs, are being treated as black-box systems.

The uncertainty propagation for complex models relies on the use of Monte Carlo techniques, which require large numbers of model simulations to be performed. In addition to uncertainty propagation it is also of interest to know how a model responds to perturbations of different inputs and what inputs most affect variation in the model output. For this purpose, sensitivity analysis is conducted. It is good practice to perform uncertainty assessment together with sensitivity analysis so as to gain the most

information about the model response to perturbations in the inputs and confidence levels of model outputs (Saltelli et al., 2008).

There are good examples of the application of global uncertainty and sensitivity analysis techniques within the earth sciences. For example, these methods have been successfully applied in fields such as hydrological (Shin et al., 2013; Yatheendradas et al., 2008), ecological (Lagerwall et al., 2014; Makler-Pick et al., 2011; Song et al., 2012), and atmospheric aerosol (Carslaw et al., 2013; Chen et al., 2013; Lee et al., 2011) modelling. However, in atmospheric chemistry and transport modelling, uncertainty assessment has been largely overlooked, and sensitivity analysis is performed by varying model inputs one-at-a-time, which can lead to erroneous conclusions regarding the model response.

2.1 Uncertainty assessment and quantification

Uncertainty is typically defined as a lack of knowledge about the true value of a variable. Walker et al. (2003) defines uncertainty as "any departure from the unachievable ideal of complete determinism", which emphasises that there is always inherent uncertainty in any measured value or any process represented by a model.

Without quantitative estimate of uncertainty, it is difficult to assess the robustness of the conclusions made based on any model output. The European Commission (EC, 2009) and the United States Environmental Protection Agency (EPA, 2009) emphasise the importance of uncertainty quantification in environmental modelling in general, and the European Environment Agency (EEA, 2011) in air quality modelling specifically. One of the major attempts to develop a framework and tools to address uncertainty in all areas of modelling was undertaken by the MUCM (Managing Uncertainty in Complex Models) project (http://mucm.ac.uk). Although this project covered a variety of environmental models, ACTMs were not included.

In order to correctly choose and implement techniques for the uncertainty assessment it is crucial to have information about the types of uncertainty present in the model. The two main types of uncertainty are epistemic uncertainty, due to imperfect

knowledge (reducible), and stochastic uncertainty, due to inherent variability (non-reducible). The types of uncertainty can be further classified as shown in the diagram in Figure 2.1. This classification was introduced by Brown (2004) and further modified by Refsgaard et al. (2007). According to this classification quantitative analysis methods can be applied to both statistical uncertainty and qualitative uncertainty, given that unknown probabilities for all outcomes can be estimated with a level of confidence. Scenario analysis is applicable in situations when it is not possible to formulate the probability of any particular outcome, but the outcome is known. In some cases, if there is awareness that knowledge is missing (recognised ignorance), expert elicitation techniques can be used to estimate outcomes and associated uncertainties.

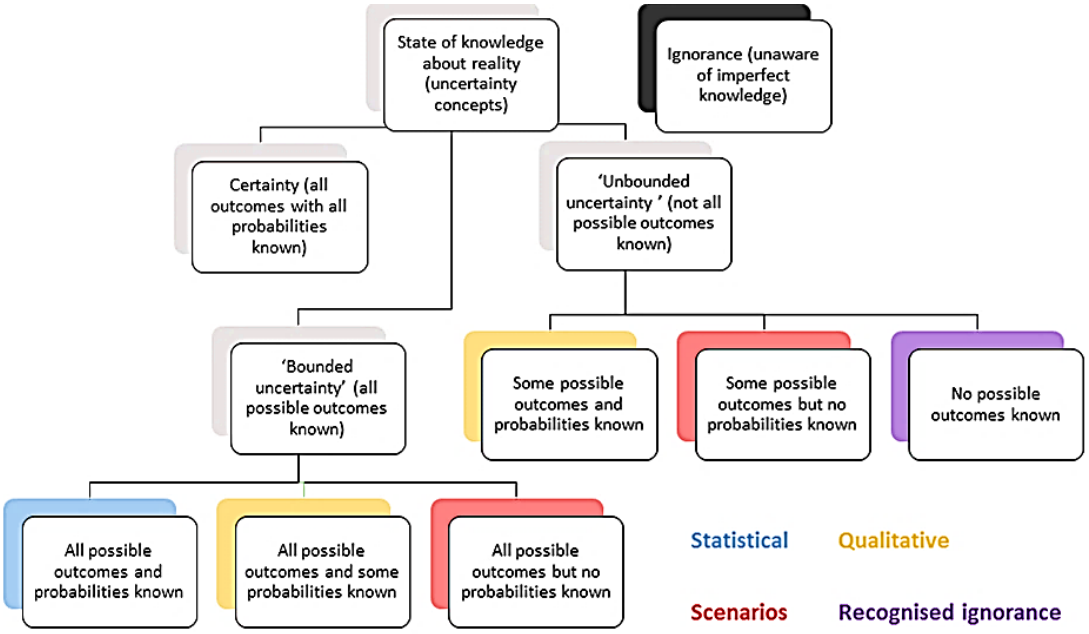

Figure 2.1 Taxonomy of imperfect knowledge. The diagram is based on the figures presented in papers by Brown (2004) and Refsgaard et al. (2007).

Uncertainty can also be classified according to the source into the following four categories: context, input, model structure, and application (Krupnick et al., 2006; Walker et al., 2003).

Context: All models are imperfect simplifications of a real system. It is essential to choose the right model for the given application. At the stage of choosing the model, the main source of uncertainty is the selection of one model form over another and the boundaries that are set for the modelled system.

Input: At this stage, the main sources of uncertainties are the uncertainty in input emissions, for example possibility of over- or underestimating the magnitude of emissions from a particular source, not being able to accurately estimate spatial and temporal variability of emissions or having a disagreement between alternate sources of information. Other major sources in input include the uncertainty in the boundary conditions and in external driving forces (mainly meteorology).

Model: Model structure uncertainty includes simplifications of the model structure (e.g. parameterisations of complex processes), structural choices, incompleteness, value judgments, and extrapolation errors. Additionally, there is model technical uncertainty (e.g. software or hardware issues and bugs in the model code). The parameter uncertainty in the model comes from errors in measuring data or difficulty in finding the right value of a parameter due to disagreement between alternate sources of information. Another major source of uncertainty is variation in the data used for model validation and calibration. Most of the uncertainty at this stage is considered to be epistemic.

Application: Models are widely used to investigate variations in environmental effects resulting from future emission scenarios. At this level scenario choice is important. Three major uncertainties in scenario preparation are i) variability in human behaviour, ii) social, economic and cultural dynamics, and iii) technological developments.

2.1.1 Approaches to uncertainty assessment

Many methodologies and tools for uncertainty assessment have been developed, implemented, and reported in the scientific literature. The choice of the suitable methodology depends on the purpose of the analysis and the type of the model. The most commonly applied methods are briefly discussed below.

Error propagation

The error propagation method is based on error propagation equations and is widely used for combining uncertainties coming from multiple sources. This method is commonly applied when estimating uncertainties in compiled emission inventories (IPCC, 2000). This method is applicable when the effect of model input uncertainties on the model outputs is of interest. Equations 2.1 and 2.2, where U_i is the uncertainty in the variable x_i, are used to estimate total percentage uncertainty, $U_{total,}$ where uncertain variables are combined by addition (Eq. 2.1) or by multiplication (Eq 2.2).

$$U_{total} = \frac{\sqrt{U_1 {x_1}^2 + U_2 {x_2}^2 + \cdots + U_n {x_n}^2}}{x_1 + x_2 + \cdots + x_n} \tag{2.1}$$

$$U_{total} = \sqrt{U_1^2 + U_2^2 + \cdots + U_n^2} \tag{2.2}$$

In order to be able to estimate combined uncertainty in the model output using this method certain assumptions have to hold. The input variables whose uncertainties are being combined, should not be correlated, the uncertainties associated with the variables should be normally distributed, and model response to changes in input variables needs to be linear or very close to linear. These assumptions rarely hold for complex models.

For the non-linear model response to the change in an input variable or a combination of variables Taylor series expansion can be used to represent input-output relationship and to obtain an error propagation equation (Bücker et al., 2006).

Monte Carlo analysis

The Monte Carlo method is a reiterative process which is used to estimate the model output uncertainty due to combined effects of parameter and input data uncertainties. This method provides ability to sample from high dimensional distributions.

The first step of the Monte Carlo method involves selecting parameters to be sampled and defining their probability density functions (PDFs). An assumption here is that the parameter value has a continuous distribution with defined PDF. The most common shapes of probability density function for a variable are normal, log-normal, uniform, and triangular are illustrated in Figure 2.2.

In the next step a random set of parameter values for all parameters under test is sampled, where the probability that a parameter value has a given value is determined by the PDF assigned to that parameter, and a model run is performed to generate an output. The process is repeated many times to create a probability density function for model outputs. Similarly to error propagation, the Monte Carlo analysis helps to estimate uncertainty stemming from model inputs.

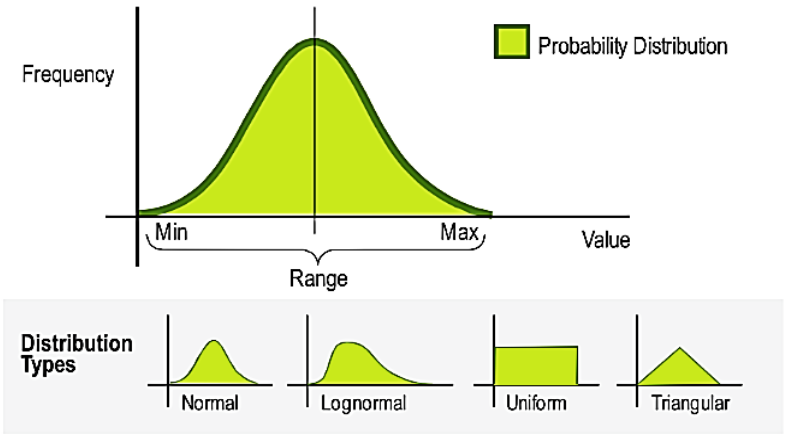

Figure 2.2 Illustration of probability distribution and different PDF shapes *(Passant et al., 2013)*

The Monte Carlo method is especially useful when correlations in input data or between parameters are present and when the model output shows non-linearity. This makes the method advantageous compared to other available techniques. This method is the most comprehensive and widely used, but it also is one of the most demanding as it requires all probability distributions for all inputs and parameter as well as all correlations, co-variances to be specified. In addition, evaluating a model multiple

times, typically several thousand times, is computationally intensive and most of the time the computational cost is prohibitively high.

There are variations of the Monte Carlo method such as Bayesian Monte Carlo, which can take into account model performance and adjust uncertainty estimates accordingly. This is done by applying a continuous likelihood function which gives weighting to the results of individual runs. A higher weighting is given to the results closely matching the observations and lower weightings are given to the outputs that match measurements poorly. This method can be used to refine estimates of model parameters (Bergin and Milford, 2000; Qian et al., 2003).

Expert elicitation

Expert elicitation is a formal method of obtaining data from experts (IPCC, 2000). This method is widely used in cases where summary statistics (central tendency, range of variation or skewness) is scarce or not available at all or empirical data is missing. This technique is also frequently used as a first step of Monte Carlo uncertainty analysis, which requires formal information about probability density functions of variables of interest (Hanna et al., 2001; Hannaa et al., 1998; van der Sluijs et al., 2005). Expert elicitation allows all available knowledge, which cannot be formalised otherwise, to be obtained. This approach can be used in both quantitative and qualitative assessment of uncertainty originating from any source.

In the context of atmospheric models, the expert elicitation method is most commonly used for uncertainty estimation when compiling emission inventories, for example when estimating emission factors and their probability distributions.

The main disadvantage of this method is that it is prone to conscious and unconscious biases in expert judgement. An example of unconscious biases is representativeness bias, i.e. having limited data or experience to base judgements on and fully consider alternative outcomes. An example of conscious biases includes motivational bias, when an expert tries to influence outcome or tries not to contradict prior beliefs on the issue (IPCC, 2000).

There are a lot of web-based tools and procedure protocols available to help ensure reproducibility of elicitation. An example of a comprehensive expert tool is the MATCH Uncertainty Elicitation Tool (Morris et al., 2014).

Scenario analysis

Scenario-based uncertainty assessment is widely applied when models are used to make predictions about the future. The scenarios are sets of model inputs that describe how the system and its driving forces are likely develop in the future. The focus of this approach is on the exploration of different alternative futures and its effects of the model outputs of interest. The scenario-based uncertainty assessment results in a range of possible outcomes; however it does not yield the probability associated with any particular outcome occurring (Petersen et al., 2013). This method is commonly used for climate or environmental models especially for integrated assessment modelling that couples economic and ecological or climate systems (EPA NCEE, 2014; Zhu et al., 2011). The method concentrates on context and application uncertainty rather than input or model uncertainty.

Multiple model analysis

The multiple model analysis aims to address uncertainty associated with simplifications, assumptions, and parametrisations in the model structure. In this type of analysis, numerous models that predict values of the same variable of interest for the same domain are run with a common set of inputs. The analysis of the output ensembles allows estimation of the robustness of modelled predictions, which increases with the number of relevant models included in the analysis. This method has been applied in climate modelling (Parker, 2013; Tebaldi and Knutti, 2007) and hydrological modelling (Breuer et al., 2009; Exbrayat et al., 2010). An example of multi-model study with ACTMs is presented in the study by Dore et al. (2015). Although this study does not directly address the uncertainty assessment of the modelled variables, it illustrates the principles of a multi-model analysis and model intercomparison.

The main disadvantage of multiple model uncertainty analysis is that it estimates uncertainty due to difference in model structure but does not allow identification of the causes of the uncertainty that arises. Additionally, the potential difficulty in setting up the analysis may arise due to the fact that different models are typically supported and developed by different researchers, hence performing this analysis can be constrained by logistical issues.

2.2 Sensitivity analysis

Uncertainty assessment conducted for a mathematical model provides very important information regarding the confidence in the model results; however uncertainty assessment conducted on its own does not allow us to make conclusions regarding the origin of the uncertainty. It is equally of interest to know how uncertainty can be apportioned to different sources and to be able to identify the major cause of variation in the model outputs. For this purpose, sensitivity analysis is conducted.

It can be argued that performing uncertainty analysis without the sensitivity analysis provides limited information; typically, the uncertainty quantification requires multiple model simulations to be performed and if the experimental design for these simulations is created with sensitivity analysis in mind it is possible to learn a lot more about the model performance, i.e. how model output responds to input variable perturbations.

The sensitivity analysis for mathematical and simulation models is defined as the study of how uncertainty in the model output can be apportioned to different sources of uncertainty in the model input (Saltelli, 2002). It can be used to map input-output relationships to determine which variables contribute the most to the output behaviour, to determine the non-influential inputs to enable model reduction, and as a quality assurance tool that can reveal unexpected dependences which are indicative of conceptual or coding errors (Ghanem et al., 2017; Rabitz, 1989; Saltelli et al., 2008).

Modelling guidelines from the U.S. Environmental Protection Agency (EPA, 2009) and impact assessment guidelines from the European Commission (EC, 2009)

recommend the use of sensitivity analysis as a tool to ensure quality and robustness of model-based predictions.

2.2.1 Overview of commonly used sensitivity analysis methods

Local methods

In the local sensitivity analysis, the impact of perturbations occurring around nominal values of model inputs is assessed. This method relies on calculating partial derivatives of the output functions with respect to the input variable at the specific points in the input space (Saltelli et al., 2000; Turanyi, 1990).

The most commonly used local method is one-at-a-time (OAT) where the value of each variable of interest is varied while all the other inputs are fixed to their nominal values and the resulting model response is assessed. The OAT sensitivity index is typically represented as the ratio of the change in the model output, *Y*, in response to the change in the input, x_i, and the change in the input itself, Δx_i (Eq. 2.3).

$$\frac{Y(x_i + \Delta x_i) - Y(x_i)}{\Delta x_i} \tag{2.3}$$

When sensitivity analysis is performed in the field of atmospheric chemistry transport modelling it is most likely to be local OAT sensitivity analysis; sometimes it is also referred to as the Brute Force Method (BFM). This method is popular because of the ease its implementation, ease of interpretation of the analysis results, and the relatively small computational cost (only a few model runs are performed). However, the local OAT method has significant disadvantages: it is only appropriate if the model response is linear for the range of investigated inputs and the effects of the different inputs are all independent of each other, i.e. there are no interactions between model inputs that result in synergistic response (Saltelli and Annoni 2010). Additionally, as the number of model inputs examined using the local OAT approach increases, the fraction of input space investigated tends to zero (Jimenez and Landgrebe, 1998).

Another type of local sensitivity analysis used in atmospheric chemistry transport modelling is decoupled direct method (DDM). In this method the sensitivity is determined by directly solving sensitivity equations derived from the equations governing the model (Cohan et al., 2010; Dunker et al., 2002; Koo et al., 2007). This method operates integrally within the model which determines both its advantages and disadvantages; this sensitivity analysis approach is computationally efficient as it does not require any extra model runs. However, it has to be implemented directly into the model source code which is not always possible.

Global methods

In contrast to local methods, global sensitivity analysis considers the entire domain of possible input parameter variations and hence allows investigation of the model response to the simultaneous perturbation of all inputs of interest over their entire range. In this analysis, firstly, the input space generated by the joint probability distribution of the inputs of interest is sampled using a suitable space-filling sampling design (e.g. Latin hypercube sampling, more details in Chapter 3). Then the model is run with the chosen set of inputs and the corresponding input-output relationships are analysed. Compared to the local sensitivity analysis, the global approach is more computationally demanding, but does not require any assumptions about the model structure, accounts for interactions between variables, and does not depend on the choice of the nominal values of model inputs (Ghanem et al., 2017; Helton et al., 2006; Homma and Saltelli, 1996; Oakley and O'Hagan, 2004; Saltelli et al., 1999, 2010). In addition to apportioning uncertainty, variance-based sensitivity analysis helps to gain insights into model structure; for input parameters with high sensitivity, a small perturbation may result in exaggerated effects on the outputs and hence it is important to understand if this could be true or if there is potential error in the model structure (Borgonovo, 2006).

As was mentioned previously, the goal of global sensitivity analysis is to determine which model inputs have the greatest effect on model outputs and quantify this effect. For this purpose, variance-based global sensitivity analysis methods are the most widely used. In the variance-based analysis the total (unconditional) variance of an output of a deterministic model is apportioned to the variation in the model inputs.

Consider the following generic model (Eq.2.4) where Y is the model output and X_1 to X_k are the inputs of interest.

$$Y = f(X_1, X_2, \dots, X_k) \tag{2.4}$$

The first-order sensitivity indices, S_i, represent the fraction of total variance of the output Y (i.e. the proportion of the overall uncertainty) explained by the variance in the X_i input while total-order indices show the sum of the effects due to X_i and all of its interactions with other inputs, $X_{\sim}$ (Eq. 2.5). In Eq. 2.5 $V_{X_i}(E_{\boldsymbol{X}_{\sim i}}(Y|X_i))$ is the conditional variance and $V(Y)$ is the unconditional variance of Y.

$$S_i = \frac{V_{X_i}(E_{\boldsymbol{X}_{\sim i}}(Y|X_i))}{V(Y)} \tag{2.5}$$

The first application of variance-based sensitivity analysis can be traced back to the study by Cukier et al. (1973), where the authors discussed effects of uncertainty in chemical reaction rate coefficients on the solutions of large sets of coupled nonlinear rate equations, and proposed the use of conditional variances for the sensitivity analysis. The methods described by Cukier et al. (1978) are now referred to as the Fourier Amplitude Sensitivity Test (FAST). Following the work by Cukier, Sobol (1993) proposed a generalised probabilistic framework for computing sensitivity measures for arbitrary groups of variables, which gave rise to Sobol sensitivity indices (first-order sensitivity indices). The Sobol method was further developed by Homma and Saltelli (1996) who introduced the total effect index, S_{Ti}, which includes the first-order effect of the variable and all its interactions with other variables (Eq. 2.6).

$$S_{Ti} = \frac{E_{X_{\sim i}}\left(V_{X_i}(Y|X_{\sim i})\right)}{V(Y)} \tag{2.6}$$

Since then, multiple studies have presented the methods for computation of first and higher order sensitivity indices based on Monte Carlo experimental designs (Jansen, 1999; Saltelli, 2002; Saltelli et al., 2010; Sobol, 2001).

A full set of first-order and total effect indices for a model with k inputs can be computed as follows (Saltelli et al., 2008). Firstly, two sampling matrices A and B of size (N, k) where N is the sampling size and k is the number of input variables are generated. Then a third matrix C_i is formed by taking all but *i*th column of B and *i*th column of A. Then three N×1 vectors of model outputs Y_A, Y_B, and Y_C are computed. The scalar product of these vectors is to estimate S_i and S_{Ti} for a given input variable X_i as demonstrated in Eq. 2.7-2.9.

$$S_i = \frac{Y_A \cdot Y_{C_i} - f_0^2}{Y_A \cdot Y_A - f_0^2} \tag{2.7}$$

$$S_{T_i} = 1 - \frac{Y_B \cdot Y_{C_i} - f_0^2}{Y_A \cdot Y_A - f_0^2} \tag{2.8}$$

where

$$f_0^2 = \left(\frac{1}{N} \sum_{j=1}^{N} Y_A^{(j)} \right)^2 \tag{2.9}$$

Another family of global sensitivity analysis methods can be classified as regression-based methods. These methods involve generation and exploration of the mapping from the model inputs to the outputs. The sensitivity of the model outputs to its inputs is assessed with the help of regression analysis that provides an algebraic representation of the relationships between the model output and one or more of the inputs (Helton et al., 2006). The simplest approach is the multiple linear regression, which yields standardised regression coefficients (SRCs) or their rank equivalents in case of non-linearity in the input-output relationship. The SRCs can be interpreted as

the magnitude of the response of an output to the unit change in a particular input when all other inputs are allowed to vary (Iooss and Lemaître, 2015; Saltelli and Annoni, 2010). One of the main benefits of the regression-based methods is that the sign of the effect of the input factor on the output is determined. This, in addition to the input importance ranking, provides the information regarding the nature of the input output correlation. However, if the model response to input perturbations is highly non-linear and non-additive or non-monotonic, the regression coefficients become uninformative. Other regression approaches have also been used in sensitivity analysis such as generalised linear models and additive models (Makler-Pick et al., 2011; Storlie and Helton, 2008).

2.3 Application of emulators and meta-models in global sensitivity analysis and uncertainty assessment

Although global analysis methods have many advantages, the computational cost associated with obtaining the thousands of data points required to calculate sensitivity indices is prohibitively high for complex models such as ACTMs. In recent years the use of meta-models and emulators to tackle this issue has been increasing (Gladish et al., 2017; Iooss and Lemaître, 2015; Ratto et al., 2012; Yang, 2011).

Meta-models and emulators are classed as surrogate models, which are statistical representations of the original simulation models that, for any point in the input space, produce outputs sufficiently similar to the original model. The surrogate models are built from an experimental design with a limited number of simulation model runs and can be evaluated many times at a much lower computational cost relative to the original model (Castelletti et al., 2012; O'Hagan, 2006). As defined by O'Hagan (2006), an emulator is a surrogate model, fitted values of which are exactly equal to the outputs of the training data (e.g. Gaussian process regression) for a deterministic simulation model. In contrast regression methods such as generalised additive models are referred to as meta-models (Ryan et al., 2017).

Different surrogate model-based approaches have been used for uncertainty and sensitivity analysis; these techniques include locally weighted regression (LOESS), generalised additive model (GAM) (Storlie et al., 2009; Storlie and Helton, 2008), Gaussian process emulator (Oakley and O'Hagan, 2004), high-dimensional model representation (HDMR) (Rabitz and Alış, 1999; Ziehn and Tomlin, 2009), and polynomial chaos expansion (Sudret, 2008). The choice of a surrogate model depends on the previous knowledge or assumptions about the nature of the input-output relationships in the simulator model. For example, it is useful to know if model response to input perturbations is non-monotonic or has discontinuities.

The steps involved in the emulator-based sensitivity analysis and uncertainty assessment are illustrated in Figure 2.3. Firstly, it is necessary to create a space-filling sampling design with *n* points taken from the whole input space. Then the simulator model is evaluated at *n* chosen points. This step can be skipped if the emulator is being constructed based on the given data points (e.g. model runs performed previously with the model of interest) and there is no possibility to generate the new experimental design. The next step involves creating an emulator and validating it. Depending on the type of chosen emulator (or meta-model) the necessary parameters or hyperparameters are estimated and the emulator is validated using the test data. The test dataset can be generated separately as described by Bastos and O'Hagan (2009) or taken as a subset of the whole dataset like in the cross-validation approach (Gladish et al., 2017; Urban and Fricker, 2010). After the emulator is successfully validated it is used to estimate outputs of the original model for any point in the previously defined input space, which makes global sensitivity analysis possible.

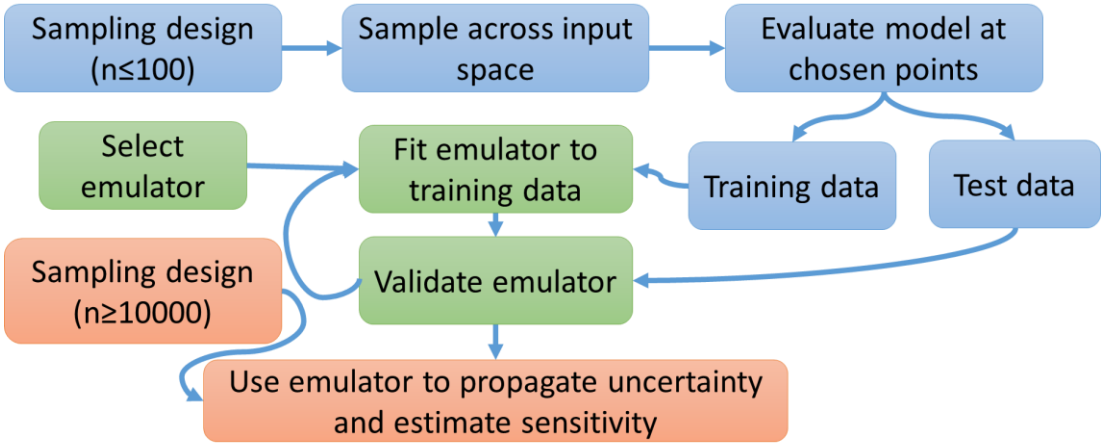

Figure 2.3 Typical workflow for emulator based global sensitivity analysis and uncertainty propagation. Steps in blue involve simulations made with the original mathematical model, steps in green are involved in creating an emulator, and steps in orange are involved in sensitivity and uncertainty analyses.

2.4 Systematic overview of the application of sensitivity analysis in atmospheric chemistry transport modelling

The publication by Ferretti et al. (2015) illustrates that recently the number of published studies that include sensitivity analysis has been increasing. The study reports that although there is an increase in the application of global sensitivity analysis techniques in all research fields that utilise modelling, the local OAT sensitivity analysis is still commonly used even in cases where assumptions about the linearity and additivity of the model under investigation are unjustified. This section presents a systematic overview of atmospheric chemistry transport modelling studies that include sensitivity analysis as a part of model assessment.

2.4.1 Overview methodology

For the systematic overview of the published literature a search was conducted using two databases: Scopus (https://www.scopus.com/, accessed 18 December 2017) and Web of Science (https://clarivate.com/products/web-of-science/, accessed 18 December 2017). The search terms were set to include terms associated with atmospheric chemistry transport modelling and the term "sensitivity analysis". The exact search strings for the databases were as follows.

Web of Science: TS = ("sensitivity analysis") AND TS = (model* AND atmospher* AND pollut* AND emission*) AND TS = (chemistry OR transport) Refined by: DOCUMENT TYPES: (ARTICLE)

Scopus: (ABS ("sensitivity analysis") AND ALL (chemistry OR transport) AND ALL (concentration* OR deposition* OR output*) AND ALL (assessment* OR respon* OR behaviour*) AND TITLE-ABS-KEY (model* AND atmospher* AND pollut* AND emission*))

In the above search strings, TS, ABS, ALL, and TITLE-ABS-KEY indicate topic, abstract, all fields, and a search field that combines title, abstract, and key words of a document respectively. The "*" indicates any zero or more characters.

The combined resulting search yielded 114 publications and after excluding the irrelevant publications at the title and abstract level a total of 63 relevant publications were identified and reviewed. The excluded papers were review papers, studies that looked at pollutant measurements, papers investigating models other than ACTMs, and publications with restricted access or in language other than English. Only articles published from 1990 to 2017 were included in this review (for the full details see Appendix A).

The sensitivity analysis approach used in the publications was classified as local OAT in cases where it was clear that one or more parameters were changed relative to their baseline value one-at-a-time. Decoupled direct method, scenario-based methods, and factorial designs with a small number of investigated input combinations were

classified under “other local”. Variance-based or regression-based sensitivity analyses were classified as global approaches. It was also noted if uncertainty assessment was presented in the reviewed publication.

2.4.2 Overview results

Figure 2.4 illustrates the number of publications that report using different sensitivity analysis methods; in some publications more than one sensitivity analysis method was used. From the figure it can be seen that local sensitivity analysis is the most often used approach with one-at-a-time sensitivity analysis reported in 29 out of 63 publications. Scenario analysis was the second most reported approach. In contrast to OAT, in scenario analysis multiple inputs may be varied simultaneously to estimate model response to a certain scenario relative to the baseline model run. For example a paper by Zhou et al. (2017) reports sensitivity of $PM_{2.5}$ and O_3 concentrations to removing all pollutant emissions from power, iron, steel, and cement plants in China. Scenarios can also include using different emission inventories as a model input (Lauer et al., 2007) or different algorithms implemented in an ACTM (Canepa and Ratto, 2003).

The methodology reported for ADIFOR (adjoint sensitivity analysis and automatic differentiation in FORTRAN) methods did not provide enough information to clearly classify methods as local or global; whether the response of an ACTM outputs to the perturbation in the inputs is explored locally or globally depends on the design of the adjoint model. ADIFOR is a derivative-based approach similar to DDM and its classification could be also application specific. Hence for the purposes of this review the two aforementioned methods are classified as “other”.

The implementation of global sensitivity analysis methods was reported in 11% of reviewed publications. In the paper by Rodriguez et al. (2007) standardised regression coefficients were used as a sensitivity measure, in six other studies, variance based methods were applied. In order to conduct a variance based sensitivity analysis in all studies a surrogate model was created for the ACTM under investigation; three studies reported using Gaussian process emulator (Beddows et al., 2017; Carslaw et al., 2013;

Lee et al., 2011), two reported high dimensional model representation (Chen et al., 2012; Chen and Brune, 2012), and Shrivastava et al. (2016) implemented generalised linear modelling.

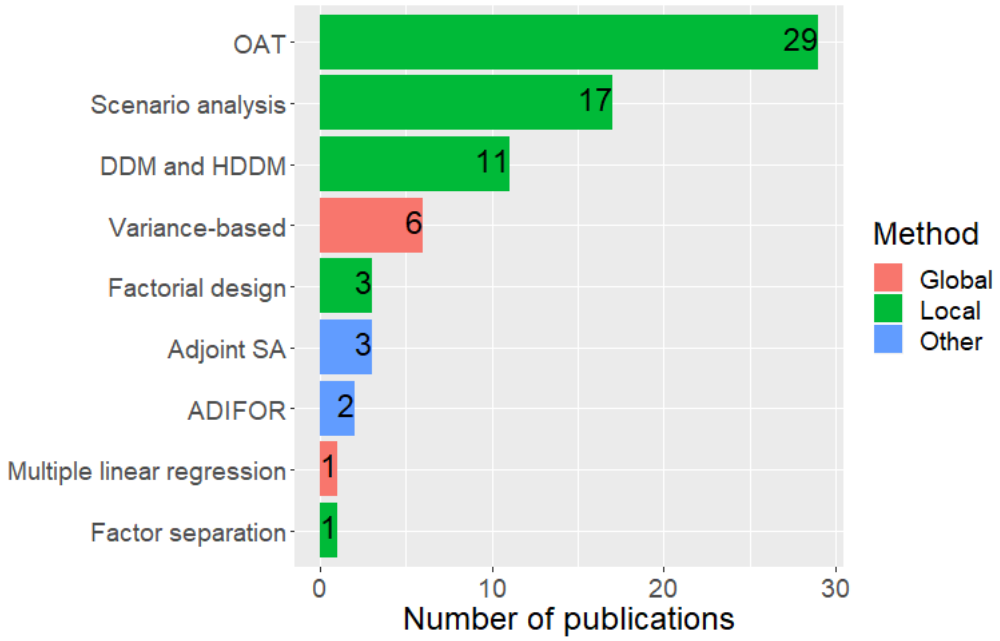

Figure 2.4 Sensitivity analysis methodologies reported in the reviewed publications. In some publications multiple methodologies were used.

An uncertainty assessment was reported in 10 out of 63 publications. None of the studies that included OAT or scenario-based sensitivity analysis included an uncertainty assessment. This finding indicates that, in the field of atmospheric chemistry and transport modelling, sensitivity analysis is mainly conducted to investigate a particular model behaviour and not the potential robustness of the model outputs. Furthermore, most studies that included local sensitivity analysis did not discuss the shortcomings associated with the approach.

Additionally, the publications that included sensitivity analysis most often investigated the response of O_3 to various input perturbations (40% of publications) or included O_3 as one of multiple pollutants of interest (20% of publications). Only 2 out of 63 studies investigated deposition output variables.

The systematic overview presented in this section indicates that the use of global methods for uncertainty and sensitivity analysis is not common in the field of atmospheric chemistry transport modelling despite the benefits these methods can offer for model assessment and development.

Chapter 3

Methods

The overall focus of the studies presented in this thesis is to investigate application and results of the global sensitivity and uncertainty analyses performed for two different atmospheric chemistry transport models. The description of the models utilised is provided in this chapter.

Although the exact description of the choice of model input emissions and their ranges as well as details of the calculations performed are study-specific and are reported in further chapters (Chapter 4, 5, and 6), this chapter provides an overview of the sampling designs implemented and the computational tools.

3.1 Model description

3.1.1 FRAME model

Model overview

The FRAME model is a Lagrangian model that calculates annual average surface concentrations of sulfur dioxide (SO_2), nitrogen oxides ($NO_x = NO_2 + NO$), ammonia (NH_3), and nitric acid (HNO_3), particulate ammonium (NH_4^+), sulfate (SO_4^{2-}), and nitrate (NO_3^-) together with dry and wet deposition of oxidised sulfur (SO_y), oxidised nitrogen (NO_y) and reduced nitrogen (NH_x) at 5 km × 5 km horizontal resolution over the UK (Dore et al., 2012; Fournier et al., 2002, 2005; Matejko et al., 2009; Singles et al., 1998). The main atmospheric processes, such as emission, diffusion, chemistry,

and deposition take place in a constant-volume air column which is advected along straight-line trajectories following specified wind fields. The wind fields are defined by an annual wind rose and annually-averaged wind speed generated from the output of the Weather Research and Forecast model (www.wrf-model.org) (Skamarock et al., 2008) version 3.7.1. The air column contains 33 vertical layers of varying thickness from 1 m at the surface to 100 m at the top of the mixing layer. The vertical mixing between layers is calculated using *K*-theory eddy diffusivity (Fournier et al., 2004). In this study, the model was run at a 5 km × 5 km horizontal resolution over the UK with boundary and initial conditions based on the National Centers for Environmental Prediction Final Global Forecast System (NCEP-GFS-FNL) data (https://rda.ucar.edu/datasets/ds083.2/).

A detailed evaluation of model outputs with annually averaged measurements of pollutant concentrations in air and precipitation is discussed elsewhere (Dore et al., 2015). In this study, all model runs were performed using emissions and meteorology data for the year 2012 and FRAME model version 9.15.0.

Input emissions

Gridded emissions of SO_2, NO_x, and NH_3 were obtained from the UK National Atmospheric Emission Inventory (NAEI, http://naei.beis.gov.uk/) at 1 km × 1 km spatial resolution (maps are shown in Fig. B.1 in Appendix B). Input emissions of SO_2 and NO_x are split into three categories: UK area, point source, and shipping emissions. FRAME treats SO_2 emissions as 95% SO_2 and 5% H_2SO_4, and NO_x emissions as 95% NO and 5% NO_2. For NH_3 emissions there are only UK area and point source categories. The NH_3 emissions from livestock are distributed spatially according to Hellsten et al. (2008). All emissions are injected into the air column at different heights according to the classification of emission sources.

Chemistry scheme

The chemistry scheme is described in Fournier et al. (2004) and includes gaseous and aqueous-phase oxidation reactions and conversion of the gases NH_3, SO_2, and NO_x to particulate matter (NH_4^+, NO_3^-, SO_4^{2-}). The gaseous-phase reactions of oxidised

nitrogen include the photolytic dissociation of NO_2 to form NO, the oxidation of NO by O_3 to form NO_2, and the oxidation of NO_2 to form NO_3^-. Nitric acid (HNO_3) is formed by the reaction of NO_2 and the hydroxyl radical (OH). The main reaction of NH_3 with oxidised nitrogen is the formation of NH_4NO_3 by the equilibrium reaction between HNO_3 and NH_3. Nitrate aerosols are also formed by the uptake of HNO_3 onto sea salt or large particles. The most important gaseous-phase reaction of oxidised sulfur is the reaction of SO_2 with the hydroxyl radical (OH) which leads to the formation of H_2SO_4. H_2SO_4 reacts with NH_3 to form $(NH_4)_2SO_4$ and this reaction is assumed to be instantaneous and irreversible. The aqueous-phase reactions include the oxidation of S(IV) by O_3, and the metal catalysed reaction with O_2. The oxidation of S(IV) is strongly dependent on pH and increases with increasing pH values.

Deposition scheme

Modelled dry deposition is land-cover dependent (the land classes are: forest, grassland, moorland, arable, urban, and water) and is treated by assigning a deposition velocity to each chemical species. These velocities are derived from a dry deposition model (Smith et al., 2000). Wet deposition is calculated using scavenging coefficients, and it is driven by rainfall rate; there is no difference between in-cloud and below-cloud processes. The rainfall is modelled using a constant drizzle approach based on the measured spatial distribution of annual average rainfall data with the assumption of an enhanced washout rate over elevated areas (Fournier et al., 2004; Kryza et al., 2013; Matejko et al., 2009).

3.1.2 EMEP4UK model

Model overview

The EMEP4UK model is a regional application of the EMEP MSC-W (European Monitoring and Evaluation Programme Meteorological Synthesizing Centre-West) open source ACTM (www.github.com/metno/emep-ctm, version rv4.8). The model is capable of calculating concentration and deposition of various primary and secondary pollutants and has been used for scientific studies and policy-related purposes. The

detailed description of EMEP MSC-W is available in Simpson et al. (2012), and the EMEP4UK model is described by Vieno et al. (2010, 2014, 2016a).

EMEP4UK is a 3-D one-way nested Eulerian model with a horizontal resolution of 5 km × 5 km over the British Isles nested within an extended European domain with 50 km × 50 km resolution. The model has 20 vertical levels, extending from the ground to 100 hPa with the lowest vertical layer of ~90 m. The model time-step is 20 s for chemistry, 5 min for the advection in the inner domain, and 20 min for the advection in the outer domain. The meteorological fields were computed using the Weather Research and Forecast model version 3.1.1 (www.wrf-model.org) (Skamarock et al., 2008). The WRF model initial and boundary conditions are derived from the US National Center for Environmental Prediction (NCEP)/National Center for Atmospheric Research (NCAR) Global Forecast System (GFS) at 1˚ resolution, including Newtonian nudging every 6 h (NCEP, 2000).

A detailed evaluation of model performance is discussed elsewhere (Dore et al., 2015; Lin et al., 2017; Vieno et al., 2010, 2016b). In this study, all model runs were executed using meteorology and emissions data for the year 2012.

Input emissions

The anthropogenic emissions of SO_2, NO_x, NH_3, primary $PM_{2.5}$, primary PM_{coarse}, CO, and non-methane VOC for the UK were derived from the National Atmospheric Emissions Inventory (http://naei.beis.gov.uk/). For the outer domain, the emissions are provided by the Centre for Emission Inventories and Projections (CEIP, http://www.ceip.at/). All emissions are split across a set of emission source sectors defined by the Selected Nomenclature for Air Pollutants (SNAP) described in Table 5.2. Hour-of-day, day-of-week and monthly emission factors are used to distribute the annual total emissions temporally to hourly resolution as described in Simpson et al. (2012). The international shipping emissions were derived from ENTEC UK Ltd. (now Amec Foster Wheeler). Biogenic emissions of dimethyl sulfide in addition to monthly in-flight aircraft, soil, and lightning NO_x emissions are included as described in Simpson et al. (2012). Biogenic emissions of monoterpenes and isoprene are

calculated by the model for every grid cell and time step. The emissions of sea salt and wind-blown dust are also included.

Chemistry scheme

The chemistry and the aerosol formation is described in detail in Simpson et al. (2012). The chemistry scheme, EmChem09, has 72 species and 137 reactions. The scheme contains both long-lived species that are included in advection and chemical equations and short-lived (non-advected) species concentrations of which are controlled by local chemistry. SO_2 is oxidised to sulfate in both the aqueous and the gaseous phase. The oxidation reaction rates are scaled by the solubility and the cloud fraction in the grid volume. In the gaseous phase, SO_2 is oxidised by OH and in the aqueous phase by O_3, H_2O_2, and O_2 are catalysed by metal ions. The formation of sulfate is also pH dependent. For the nitrate formation, the reaction between N_2O_5 and deliquescent aerosols plays an important role. The gas-aerosol partitioning of secondary inorganic aerosols is described by the MARS equilibrium module presented by Binkowski and Shankar (1995). The species treated in the MARS module include HNO_3, NH_3, and H_2O in gaseous or vapour phase; SO_4^{2-}, HSO_4^-, NH_4^+, NH_3, and H_2O in the aqueous phase; H_2SO_4 and HNO_3 with corresponding neutralised salts $(NH_4)_2SO_4$ and NH_4NO_3 in aerosol phase. The production and ageing of secondary organic aerosols (SOA) are modelled using the volatility basis set framework described in Bergström et al. (2012).

Deposition scheme

The dry and wet deposition schemes are described in detail in Simpson et al. (2012). The dry deposition flux of gases is modelled using deposition velocity, which is calculated with a resistance approach. The calculation involves estimating aerodynamic resistance, quasi-laminar layer resistance, and canopy resistance, which is the most complex out of the three variables and depends on the surface characteristics and the chemical characteristics of the depositing gas. For aerosols, instead of resistance approach, the mass-conservative equation is implemented. This means that the dry deposition velocity at a particular height is calculated using a settling velocity and a sum of the aerodynamic resistance and the inverse of compound-specific surface deposition velocity. The overall deposition rate of larger

particles is affected by the settling velocity which is size-dependent. To account for this, a log-normal particle size distribution is assumed, and settling velocity calculations are integrated over the aerosol sizes. The calculation of aerodynamic resistance is land-use category dependent.

The parametrisation of the wet deposition is described by Berge and Jakobsen (1998). It includes in-cloud and sub-cloud scavenging of particles and gases. For soluble components of gases and particles, the in-cloud scavenging is calculated using compound-specific in-cloud scavenging ratios. In below-cloud scavenging the distinction is made between gases and particles; for gases, the sub-cloud scavenging ratio is used, and for particles, the calculation makes use of size-dependent collection efficiency of aerosols by raindrops and raindrop fall speed.

3.2 Uncertainty assessment and global sensitivity analysis

3.2.1 Sampling design

The first step in the uncertainty assessment and global sensitivity analysis is creating a sampling design with the aim to explore the entire space of inputs of interest. Sampling designs for computer experiments with deterministic models differ from designs for physical experiments in that they do not require replication. The reason for this is the absence of noise in the model response to perturbations of the input parameters (Jones and Johnson, 2009). Hence, the desirable properties of a good sampling design for a computational experiment are adequate coverage of the entire multidimensional sampling space, sufficient density and distribution of the sample that allows characterisation of non-linearity in the model response, and a sample size that does not make computational execution of the model prohibitive.

The most commonly used sampling strategies for computational experiments are: simple random sampling (SRS), full and fractional factorial designs, Latin hypercube sampling (LHS), and sampling using quasi-random or low discrepancy sequences.

The SRS is conceptually the simplest method, which utilises pseudo-random number generation. It is known to have low efficiency compared to other sampling approaches as the points are not evenly distributed across the sampling interval. Simple random samples tend to have gaps and clusters, which results in poor representation of the input space (Fig. 3.1). The clusters in the sample can lead to overemphasised function values, and gaps can result in underrepresentation in the region of space where they occur (Saltelli et al., 2008).

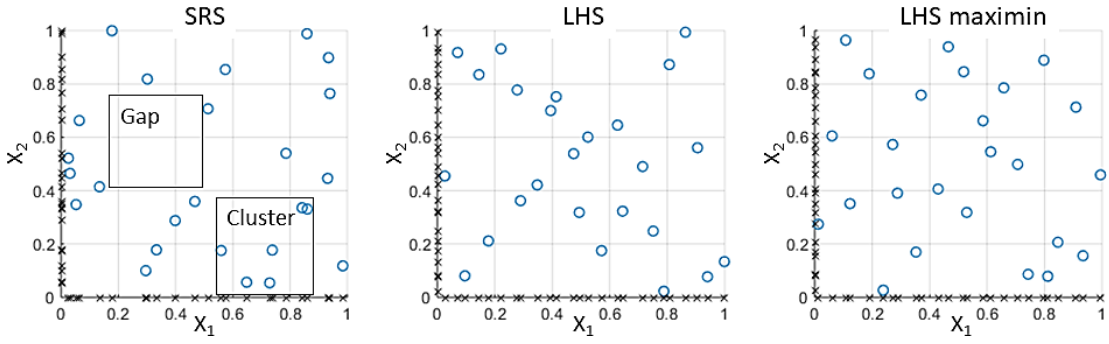

Figure 3.1 Example of 25 points sampled in two dimensions using simple random sampling (SRS), Latin hypercube sampling (LHS), and Latin hypercube sample optimised according to maximin criterion (LHS maximin) which aims to maximise the minimum distance between points. The sample was generated using MATLAB built-in functions.

In fractional factorial design (Box and Hunter, 1961), two levels of every input variable are sampled, and combinations of all levels are created. This sampling approach is typically used for screening purposes, where the aim is to detect the influential model inputs for further analysis. However, this approach does not allow effective exploration of the whole input space because the information is typically obtained only from two levels of each variable, hence there is a gap in the sampling space.

LHS is a stratified, space-filling sampling technique. In LHS each variable is stratified over a number of layers, and each layer contains the same number of points. Since it was first introduced by McKay et al. (1979) many efforts have been made to develop LHS with better space filling properties. Different optimality criteria such as maximin

(Johnson et al., 1990; Morris and Mitchell, 1995) or integrated mean squared error minimisation (Park, 1994) have been successfully applied for that purpose. Until recently, the major drawback of LHS was the requirement to generate the whole sample at once without the possibility of adding extra design points. However recently a sequential sampling, where sample size can grow progressively was introduced (Sheikholeslami and Razavi, 2017).

Quasi-random sampling involves taking a subset of points from low-discrepancy sequences such as Sobol (Sobol, 1976) or Halton (Halton, 1960) sequences. The discrepancy of the sampling sequence is defined as a maximum absolute difference between the area (or volume) fraction of the sampling space and the fraction of points in that space (Saltelli et al., 2008). The main advantages of a low-discrepancy sequence are its space-filling properties and the possibility of adding extra design points to an already existing sampling design. The Sobol sequence (Sobol, 1967, 1976; Sobol and Levitan, 1999) is arguably the most popular choice for variance based sensitivity analysis; however it might not work well or at all for a small number of sampling points (Saltelli et al., 2008). Examples of sampling designs created using a Sobol sequence are shown in Figure 3.2.

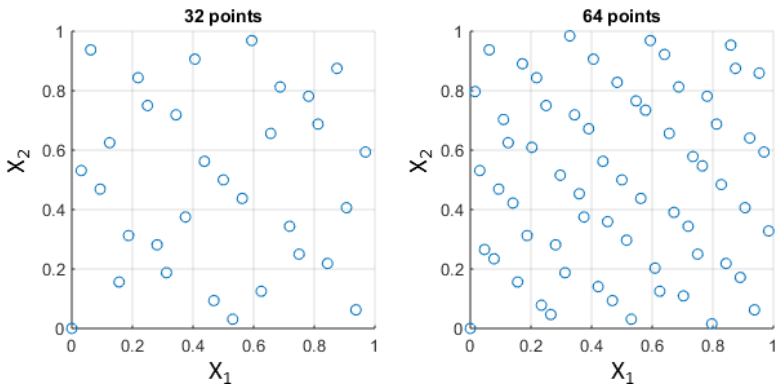

Figure 3.2 Two-dimensional sampling designs with 32 and 64 points based on the Sobol sequence. The sample was generated using MATLAB built-in functions.

In this study, several optimised LHS designs were implemented. The details of each sampling design, i.e. the number of variables, sampling ranges, number of points, and optimisation criteria, for the specific experiment are provided in Chapters 4 and 5.

In this study the response of FRAME and EMEP4UK models to changes in various input emissions was investigated. The assumption was made that the emissions of various pollutant species from different sources are independent and hence magnitudes and directions of changes in these emissions are uncorrelated. Therefore, all model inputs under investigation (i.e. model input emissions) were assumed to be statistically independent, i.e. the value or the change in the value of any single input did not have an effect on values of any other inputs.

Quasi-random sampling based on Sobol sequences was implemented in the calculation of the first-order and total sensitivity indices for EMEP4UK model outputs presented in Chapters 5 and 6.

3.2.2 Uncertainty propagation

The details of uncertainty propagation, for example, uncertainty ranges assigned to the model inputs emission variables, varied for different case studies. Therefore, the details of the methodology used are reported in the following chapters (Chapters 4, 5, and 6).

3.2.3 Model response investigation and uncertainty apportionment

The first step in investigating the model response to perturbations in the input variables is the exploratory data analysis using scatterplots (Kleijnen and Helton, 1999; Saltelli et al., 2008). The linearity in the output response and the importance of different input variables can initially be assessed from the scatterplots. Figure 3.3 illustrates the response of surface concentrations of O_3 modelled with EMEP4UK. The scatterplots

with the fitted local regression visualise how the model response to the input emission perturbations changes with different temporal resolution.

In this study, it was not possible to fully investigate input-output relationships for FRAME and EMEP4UK models using scatterplots as that would require inspecting over 10,000 sets of scatterplots for each model (one per grid cell). Therefore, it was chosen to present regression coefficients and Sobol first-order and total sensitivity indices as the measures to quantify model response to input emission perturbations and to assess how uncertainty in different model inputs contributes to the overall uncertainty in the outputs.

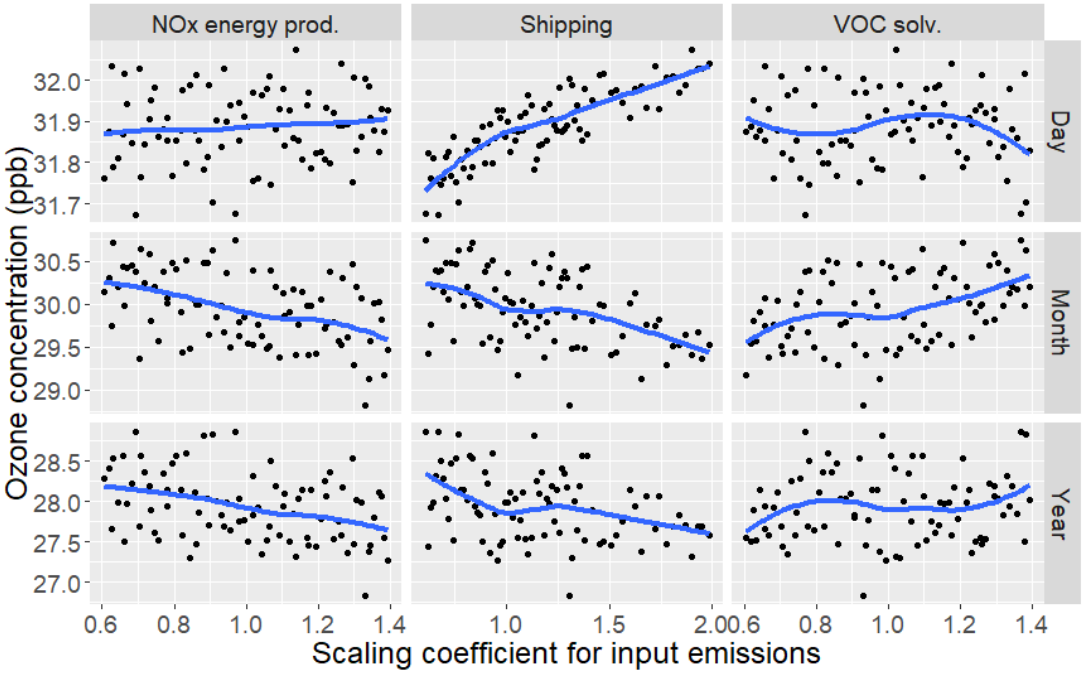

Figure 3.3 Scatterplots of O_3 concentration (modelled with EMEP4UK) versus scaling coefficients applied to the input emissions of NO_x from the energy production sector, VOC from solvent use, and all shipping emissions. The scatter plots are shown for daily (1st of July 2012), monthly (July 2012), and annually (2012) averaged model outputs for a single grid cell. Local regression (LOESS) lines (blue) help to visualise the input-output relationship.

Regression coefficients (RCs) for both FRAME and EMEP4UK models were estimated by performing multiple linear regression. The model inputs and outputs were

substituted by the corresponding values of fractional change. The definition of fractional change is given by Equation 3.1, where m_n is a variable (input or output) in the model run with emissions altered and m_0 is the baseline value. The interpretation of RCs is shown in Table 3.1.

$$Fractional\ change = \frac{m_n - m_0}{m_0} \tag{3.1}$$

Table 3.1 Example of interpretation of regression coefficient values

Value of RC	Interpretation
RC = 0	Change in the input does not lead to any change in the output value.
RC = 1	A certain relative change in the input leads to the same relative change in the output, e.g. 30% reduction in the input emissions of an air pollutant leads to the 30% reduction in the surface concentration of the model output of interest.
RC < 0	Change in the model output is reversely proportional to the change in the input

The first-order (S_i) and total (S_{Ti}) Sobol sensitivity indices were used to apportion the overall uncertainty in model outputs to the uncertainty in the input variables. The indices are defined as follows (Homma and Saltelli, 1996; Sobol, 1993).

For the model with a scalar output $Y=f(\boldsymbol{X})$, where $\boldsymbol{X}$ is the vector of inputs $\{X_1, \ldots, X_n\}$, the first-order sensitivity index represents the ratio of the variance of the mean of Y when one input variable (X_i) is fixed, $V_{Xi}(E_{X\sim i}(Y|X_i))$, to the unconditional variance of Y, $V(Y)$ (Eq. 3.2).

$$S_i = \frac{V_{X_i}(E_{\boldsymbol{X}_{\sim i}}(Y|X_i))}{V(Y)} \tag{3.2}$$

The total sensitivity index measures the total effect of a variable, which represents the sum of the first and higher order effects for that variable (Eq. 3.3), where $\boldsymbol{X}_{\sim i}$ denotes the matrix of all variables but X_i.

$$S_{Ti} = 1 - \frac{V_{\boldsymbol{X}_{\sim i}}\left(E_{X_i}(Y|\boldsymbol{X}_{\sim i})\right)}{V(Y)} \tag{3.3}$$

The computation of both sensitivity indices directly from model evaluations was not possible as it required *n(k+2)* model runs to be performed, where *n* is the sampling size chosen typically between 500 and 1000 and *k* is the number of inputs of interest (Saltelli, 2002). Therefore, emulator-based approaches described below were investigated, and the most suitable approach was applied.

3.3 Emulator

An approach utilising a Gaussian process (GP) emulator was chosen in this study in order to predict model outputs at a large number of sampled points in the model input space to fulfil sampling requirements for the variance-based sensitivity analysis. The GP emulator was constructed for the EMEP4UK model; the relationships between FRAME model input and output variables were found to be sufficiently linear, and hence further analysis did not suggest a need for the application of emulators (details are discussed in Chapter 4).

Each EMEP4UK simulation for a full year takes approximately 10 hours to complete on 8 nodes (16 cores each) of a high-performance computing (HPC) cluster, which gives a computing time of 1,280 core hours per simulation. In contrast, using an emulator to predict model outputs for 10^4 to 10^6 points sampled from the input space

takes less than a minute on a single core of a desktop computer. Below, three different approaches to GP emulator-based sensitivity analysis are described and compared.

Gaussian process emulator provides an approximation, $\hat{f}(.)$ for a simulator that can be represented as function *f(.)* which maps inputs of interest **x** into an output $y = f(\mathbf{x})$. In addition to providing mean value, $\hat{f}(\mathbf{x})$, GP emulators also provide the probability distribution around that mean which reflects the associated uncertainty. For the training points the emulator returns $\hat{f}(x_i) = y_i$ with no uncertainty, as the true value of the simulator output is known at that point (Figure 3.4).

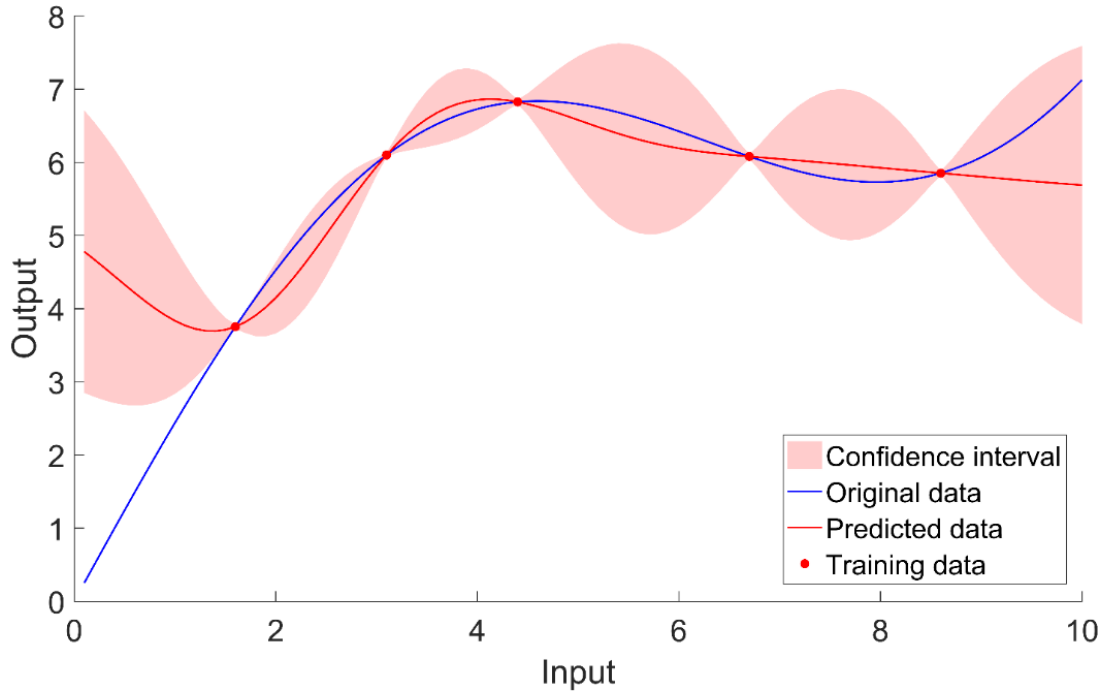

Figure 3.4 Example output of a Gaussian process emulator fitted to the training data from a model with one-dimensional input.

Gaussian process (Eq. 3.4-3.6) is specified by its mean function *m(**x**)* and covariance function *cov(**x**, **x**′)* (Rasmussen and Williams, 2006),

$$f(\boldsymbol{x}) \sim \mathcal{GP}(m(\boldsymbol{x}), cov(\boldsymbol{x}, \boldsymbol{x}')) \tag{3.4}$$

where $m(\boldsymbol{x})$ and $cov(\boldsymbol{x}, \boldsymbol{x}')$ are defined as follows.

$$m(\boldsymbol{x}) = \mathbb{E}[f(\boldsymbol{x})] \tag{3.5}$$

$$cov(\boldsymbol{x}, \boldsymbol{x}') = \mathbb{E}[(f(\boldsymbol{x}) - m(\boldsymbol{x}))(f(\boldsymbol{x}') - m(\boldsymbol{x}'))] \tag{3.6}$$

The covariance between $f(\boldsymbol{x})$ and $f(\boldsymbol{x}')$ is represented by Equation 3.7, where $c(\boldsymbol{x}, \boldsymbol{x}')$ is the correlation function, and σ^2 is a hyperparameter that represents the variance of the Gaussian process.

$$cov\{f(\boldsymbol{x}), f(\boldsymbol{x}')|\sigma^2\} = \sigma^2 c(\boldsymbol{x}, \boldsymbol{x}') \tag{3.7}$$

GEM-SA

The Gaussian Emulation Machine for Sensitivity Analysis (GEM-SA, http://www.tonyohagan.co.uk/academic/GEM/, last access: 10 July 2017) is an open-source software and has been successfully used in studies by Carslaw et al. (2013), Lee et al. (2011), and Marrel et al. (2009).

The techniques implemented in the software to create a GP emulator are described by Kennedy and O'Hagan (2001) and O'Hagan (2006) and the software is described by Kennedy (2004). In GEM-SA, mean function can be represented as a constant or a simple linear regression function and the form of the correlation function is described by Kennedy (2004).

The sensitivity indices are calculated as a percentage of the total variance explained; first-order and total terms, as well as second-order interaction terms are calculated. The information about the exact estimator used is not provided in the software description.

UQLab

UQLab, is a MATLAB-based set of modules for emulation, uncertainty quantification, and sensitivity analysis (Lataniotis et al., 2017; Marelli and Sudret, 2014). UQLab modules allow creating stand-alone GP emulators or integrate emulation as a part of uncertainty quantification and sensitivity analysis. The main advantage of UQLab emulation module is its computational speed and the possibility of fine-tuning the emulator parameters, such as mean and correlation functions, and hyperparameter optimisation options.

DiceKriging

DiceKriging is an R package developed by the DICE (Deep Inside Computer Experiments) consortium (Roustant et al., 2012). Similarly to UQLab, emulators created with the DiceKriging package can be fully customised. A number of studies have been published that utilise this package (Beddows et al., 2017; Lee et al., 2013; Ryan et al., 2018). The calculation of variance-based sensitivity indices in R requires a separate package 'sensitivity' which is described by Bertrand et al. (2018).

3.3.1 Comparison of GP emulation tools

The three aforementioned tools for creating GP emulators and conducting subsequent uncertainty quantification and sensitivity analysis were compared.

The GEM-SA software did not provide options for defining mean and covariance functions for the emulator; in UQLab and DiceKriging mean functions were chosen to have a linear form. For the covariance function, *c(x,x')*, Matérn 5/2 was chosen (Eq. 3.8). In Eq. 3.8 h represents the absolute distance between x and x', and θ is a length-scale parameter that determines the smoothness of the mean function from Eq. 3.5.

$$c(x, x') = \left(1 + \frac{\sqrt{5}|h|}{\theta} + \frac{5\,h^2}{3\theta^2}\right) \exp\left(-\frac{\sqrt{5}|h|}{\theta}\right) \tag{3.8}$$

The calculation of sensitivity indices GEM-SA did not provide customisable options. In UQLab and R package 'sensitivity' Monte Carlo estimation of the Sobol sensitivity indices was done using the estimator presented by Janon et al. (2014).

For the uncertainty assessment and sensitivity analysis of the EMEP4UK model, the input emissions were split into 13 categories and an LHS design with 84 points was created. The detailed description of the design and input variable definitions are presented in Chapter 5. For the comparison presented here, the definition of the input variables is not important.

As an example, the mean, standard deviation, and sensitivity indices for the surface concentration of $PM_{2.5}$ estimated using an emulator (for a single grid cell of the EMEP4UK output domain) are presented here (Tables 3.2 and 3.3). In this calculation all input variables were assigned a ± 40% (2σ) variation range from their baseline value.

No substantial difference was found between results of the calculations performed with the GEM-SA software and packages for MATLAB and R (Tables 3.2 and 3.3). Therefore, preference was given to the UQLab module as it provided better scalability. For the uncertainty assessment and sensitivity analysis described in Chapters 5 and 6 a separate emulator was created for every land-based grid cell (over 10,000) of the model domain, hence scalability of the calculation was a determining factor when choosing the suitable tool for the analysis.

Table 3.2 Mean and standard deviation estimated for the surface concentration of $PM_{2.5}$ for a single grid square. The values are shown for annually-averaged and monthly-averaged (single month) model outputs.

	Year		Month	
	Mean (μg m^{-3})	σ (μg m^{-3})	Mean (μg m^{-3})	σ (μg m^{-3})
Gem-SA	8.58	0.23	8.78	0.42
UQLab	8.56	0.23	8.78	0.41
DiceKriging	8.57	0.27	8.78	0.41

Table 3.3 First-order (S_i) and total (S_{Ti}) sensitivity indices calculated using different software packages for EMEP4UK model. The values are presented in percent units. X1-X13 represent the categories of the input emissions. For the comparison purposes the exact definition of each of the 13 categories is not important.

	GEM-SA		UQLab		DiceKriging	
	S_i (%)	S_{Ti} (%)	S_i (%)	S_{Ti} (%)	S_i (%)	S_{Ti} (%)
X1	15.2	15.3	15.0	15.1	14.9	15.1
X2	2.6	2.6	2.4	2.6	2.3	2.6
X3	0.8	0.9	0.8	1.0	0.5	0.8
X4	0.2	0.2	0.3	0.5	0.0	0.3
X5	1.7	1.8	1.9	2.1	1.9	2.2
X6	1.7	1.8	1.4	1.6	1.5	1.6
X7	0.3	0.3	0.2	0.4	0.1	0.3
X8	5.4	5.5	5.7	5.8	5.2	5.6
X9	34.6	34.8	35.9	36.3	34.2	34.8
X10	13.2	13.2	13.8	14.1	13.0	13.3
X11	7.6	7.6	7.2	7.5	7.1	7.2
X12	5.2	5.4	5.2	5.3	5.0	5.0
X13	11.1	11.4	10.3	10.7	10.9	11.2

Chapter 4

Global sensitivity and uncertainty analysis of an atmospheric chemistry transport model: the FRAME model as a case study

This chapter is based on a research paper published in 'Geoscientific Model Development' (Aleksankina, K., Heal, M. R., Dore, A. J., Van Oijen, M., and Reis, S.: Global sensitivity and uncertainty analysis of an atmospheric chemistry transport model: the FRAME model (version 9.15.0) as a case study, Geosci. Model Dev., 11, 1653-1664, https://doi.org/10.5194/gmd-11-1653-2018, 2018). I developed the experimental design, set up and performed model runs, analysed data, and prepared the manuscript. The co-authors, Prof Mathew Heal and Dr Stefan Reis, provided valuable advice on the interpretation of results and aided with manuscript preparation and editing. Dr Anthony Dore provided support with model setup and Dr Marcel Van Oijen provided statistical advice, both also provided feedback for the manuscript.

4.1 Introduction

Typically, model assessment studies focus on uncertainties in the model parameter values (Derwent, 1987; Konda et al., 2010; De Simone et al., 2014) and model-specific structure (Simpson et al., 2003; Thompson and Selin, 2012). However, for ACTMs the uncertainty in the model input emissions data could be dominating; for example, previous dispersion model uncertainty studies identified input emissions as a primary source of uncertainty in model outputs (Bergin et al., 1999; Hanna et al., 2007; Sax and Isakov, 2003). It is also the case that a major role of ACTMs is to estimate the impact of potential future changes in emissions on atmospheric composition (Boldo et al., 2011; Crippa et al., 2016; Heal et al., 2013; Vieno et al., 2016a; Xing et al., 2011; Zhang et al., 2010).

Thus the focus of this study is to demonstrate a systematic approach for quantifying model output sensitivity and uncertainty as a function of the variation in model input emissions. Fine Resolution Atmospheric Multi-pollutant Exchange (FRAME) model was used here as a case study. FRAME is a Lagrangian model that outputs, at a 5 km × 5 km horizontal resolution over the UK, annual average surface concentrations of sulphur dioxide (SO_2), nitrogen oxides (NO_x), ammonia (NH_3), nitric acid (HNO_3), and particulate ammonium (NH_4^+), sulphate (SO_4^{2-}), and nitrate (NO_3^-), together with dry and wet deposition of oxidised sulphur (SO_y), oxidised nitrogen (NO_y), and reduced nitrogen (NH_x) (Dore et al., 2012; Matejko et al., 2009; Singles et al., 1998). The model is extensively used to provide policy support including generation of source-receptor matrices for the UK Integrated Assessment Model (UKIAM) and estimation of critical load exceedances (Matejko et al., 2009; Oxley et al., 2013). Source receptor matrices link concentration and deposition with individual emission sources and are used to automate procedures to estimate the impact of future emission reduction scenarios. Integrated assessment modelling incorporates technical emissions abatement costs with cost-benefit analysis and source-receptor data to indicate cost-effective solutions to protect natural ecosystems from acidic and nitrogen deposition above defined critical thresholds and to protect human health from particulate concentrations (Oxley et al., 2003, 2013).

FRAME uses emissions input data from the UK National Atmospheric Emissions Inventory (NAEI, http://naei.beis.gov.uk/), which are compiled following the international 'Guidelines for Reporting Emissions and Projections Data under the Convention on Long-range Transboundary Air Pollution (United Nations Economic Commission for Europe, 2015). We used the uncertainties published by the NAEI in the Informative Inventory Report (Misra et al., 2015) as the foundation of the uncertainty propagation for the FRAME concentration and deposition outputs with respect to UK emissions of SO_2, NO_x, and NH_3. The uncertainty ranges for different pollutants reported by the NAEI are estimated using a Monte Carlo technique which corresponds to the IPCC Tier 2 approach (IPCC, 2006). In this approach uncertainty ranges for each source for both emission factor and activity statistics are associated with a probability distribution and further used as inputs in a stochastic simulation which calculates output distributions of total UK emissions for each pollutant. The

uncertainties are expressed as plus or minus half the confidence interval width relative to the estimated emissions value.

Previously, local one-at-a-time (OAT) sensitivity analysis has been used to investigate ACTM sensitivity because it is less computationally demanding than global sensitivity analysis that requires a large number of simultaneous perturbations of all inputs of interest. However, there are significant disadvantages associated with OAT analysis: the interactions between the input parameters and non-linearities in the model response cannot be identified; additionally as the number of input parameters increases the fraction of parameter space investigated tends to zero (Jimenez and Landgrebe, 1998; Saltelli and Annoni, 2010). Therefore local OAT sensitivity analysis is only applicable when the effects of the different inputs are all independent from each other and model response is linear for the range of investigated inputs. Many previous publications that include ACTM sensitivity analysis use the OAT approach but fail to acknowledge its limitations (Appel et al., 2007; Borge et al., 2008; Capaldo and Pandis, 1997; Labrador et al., 2005; Makar et al., 2009).

Hence this study focuses on demonstrating the use of global methods capable of revealing non-linearity in the model response and the presence of interactions between inputs in addition to revealing the spatial pattern of the model response to changes in the input emissions. Global sensitivity and uncertainty analyses have been applied in many earth science fields such as hydrological modelling (Shin et al., 2013; Yatheendradas et al., 2008), ecological modelling (Lagerwall et al., 2014; Makler-Pick et al., 2011; Song et al., 2012), and atmospheric aerosol modelling (Carslaw et al., 2013; Chen et al., 2013; Lee et al., 2011). Increasing computational resource means this approach is now starting to be applied to ACTMs (Christian et al., 2017).

In a global sensitivity analysis a sample space is created for all inputs under investigation from which a set of combinations of model inputs for different model runs are chosen. The sampling design for model inputs for uncertainty and sensitivity analysis must balance the needs of covering the full multidimensional input parameter space at sufficient density to allow characterisation of any non-linearities and interactions in the model response with a small enough number of samples for the total number of model runs to remain computationally tractable. Therefore, in this work,

Latin hypercube sampling (LHS) (McKay et al., 1979), which is a stratified space-filling sampling technique, was used. Advances have been made to optimise the space filling properties of LHS including maximin sampling (Johnson et al., 1990; Morris and Mitchell, 1995) and integrated mean squared-error minimisation (Park, 1994).

In summary, this work demonstrates application of global uncertainty and sensitivity analysis to an ACTM using the FRAME model as an example.

4.2 Methods

4.2.1 Sensitivity and uncertainty analysis

For both sensitivity and uncertainty analyses a Latin hypercube sampling design was chosen as it is superior to quasi-random sampling for small numbers of samples (Saltelli et al., 2008). A uniform LHS design was created using the R package 'lhs'(Carnell, 2016), with the sample optimised by maximising the mean distance between the design points. The LHS design was created for the scaling coefficients applied to the model input emissions of UK SO_2, NO_x and NH_3 and not for the actual values of the input emissions. This means that emissions from all sources of a particular pollutant were varied by the same fraction across all grid squares in a particular model run.

For the sensitivity analysis a uniform LHS sample of size n = 100 within a range of ± 40 % relative to the baseline for each of the three input variables was created. This range was chosen to test the overall model response to changes in emissions (for example to identify non-linearities) as it encompasses the range of variations in input emissions used for future scenario simulations with the FRAME model.

Regression coefficients (RC) were used as the measure of the sensitivity of the model response, derived as follows. For each model grid cell, and for each model output variable, a multiple linear regression (Eq. 4.1) was performed using the data from the n = 100 model runs. To obtain the RCs (b_i in Eq. 4.1) the model inputs X_i, and outputs Y, were substituted by corresponding values of fractional change relative to the

baseline value. This simplifies interpretation of the resulting RCs. A RC represents the relative effect of changing input X_i on the output Y, e.g. RC = 0.5 signifies a 15 % reduction in the output variable value if an input is reduced by 30 %. The coefficients of determination (R^2) were evaluated for each fitted model (for every grid cell) to identify if a significant level of non-linearity in the input-output relationship was present.

$$Y = b_0 + \sum_{i=1}^{3} b_i X_i \tag{4.1}$$

For the uncertainty propagation, the input sampling space was constrained to the specific uncertainty ranges assigned to the emissions of SO_2, NO_x and NH_3 in the UK Informative Inventory Report (Misra et al., 2015) with a new LHS sample n = 100. These uncertainty ranges are derived following published guidelines on quantifying uncertainties in emissions estimates (IPCC, 2006; Pulles and Kuenen, 2016). According to the guidelines, uncertainties are expressed as lower and upper limits of the 95 % confidence interval as a percentage of the central estimate. The assigned emissions uncertainties have ± 4 %, ± 10 % and ± 20 % ranges, for SO_2, NO_x and NH_3 respectively. The probability distributions were not specified, therefore it was chosen to use uniform distributions for the variable ranges from which the LHS sample was created. It is also acknowledged that a number of other aspects of emissions uncertainty are not included. For example, the FRAME model cannot capture uncertainty in assigned seasonal and diurnal cycles in emissions. Uncertainties in the spatial distributions or in height of elevated emissions are also not included.

The uncertainty values for each grid square were calculated as a half of the 95% confidence interval relative to the mean value of the output as recommended in the EMEP/EEA and IPCC Guidebooks (IPCC, 2006; Pulles and Kuenen, 2016). Relative uncertainty values are presented here.

To assess the contribution of uncertainties in the emissions of SO_2, NO_x and NH_3 to the overall output uncertainty standardised regression coefficients (SRCs) were calculated as shown in Eq. 4.2. A multiple linear regression was performed using the

data from the 100 model simulations for the case of constrained input sampling space. The SRCs (β_i in Eq. 4.2) were calculated by multiplying the RC by the ratio between the standard deviations of the input σ_i, and output σ_Y (σ_Y is the same for all the β_i values for a given output variable).

$$\beta_i = b_i \frac{\sigma_i}{\sigma_Y} \tag{4.2}$$

The squared value of SRC (Eq. 4.3) for linear additive models is equal to the ratio of variance of mean of Y when one input variable is fixed, $V_{X_i}(E_{X_{\sim i}}(Y|X_i))$, to the unconditional variance of Y, $V(Y)$ (Saltelli et al., 2008). Thus SRC squared represents the fractional contribution of the uncertainties in the model inputs to the overall uncertainty in the output. For the case of non-linear models, variance decomposition methods are described in more detail elsewhere (Homma and Saltelli, 1996; Saltelli, 2002; Saltelli et al., 2010; Sobol, 1993). In the case where a large number of model simulations is not possible an emulator based approach can be used for the uncertainty and sensitivity analysis (Blatman and Sudret, 2010; Lee et al., 2011; Shahsavani and Grimvall, 2011; Storlie and Helton, 2008).

$$\beta_i^2 = \frac{V_{X_i}(E_{X_{\sim i}}(Y|X_i))}{V(Y)} \tag{4.3}$$

4.3 Results and discussion

4.3.1 Global sensitivity analysis

Figure 4.1 summarises the distributions of the regression coefficient (RC) global sensitivity measure across all model grid cells. RCs show the sensitivity of each model output variable to the three input emissions variables (SO_2, NO_x and NH_3), and can be interpreted as a magnitude of the response of an output to the unit change in a particular input when all other inputs are allowed to vary. The magnitude of the RCs provides

useful information not only about the effect of the change in a particular input on a model output, but also allows input sensitivity ranking to be determined because all inputs were assigned the same range of variation (± 40 %). In the case where the ranges for inputs differ, standardised regression coefficients (SRCs) are used to obtain the input importance ranking instead.

Figure 4.1 shows that model outputs have (i) varying sensitivities, (ii) varying relative rankings in their sensitivities to SO_2, NO_x and NH_3 emissions, and (iii) that these output sensitivities to the emissions also vary spatially across the model grids, as shown by the spreads in individual box plots. The annual average concentrations of particulate NH_4^+, NO_3^-, and SO_4^{2-} and annual dry and wet deposition of SO_y for the baseline model run are presented in Appendix B Figure B.2. The actual spatial distributions of the RCs from Figure 4.1 are illustrated in Figure 4.2 for the example output variables of particulate NH_4^+, NO_3^-, and SO_4^{2-}. Figure 4.3 shows the equivalent for the example output variables of dry and wet deposition of SO_y. These five output variables were chosen to illustrate the spatial distribution of uncertainty and sensitivity metrics. Figures B.3 and B.4 in Appendix B show the spatial distribution of RCs for other FRAME outputs displayed in Figure 4.1.

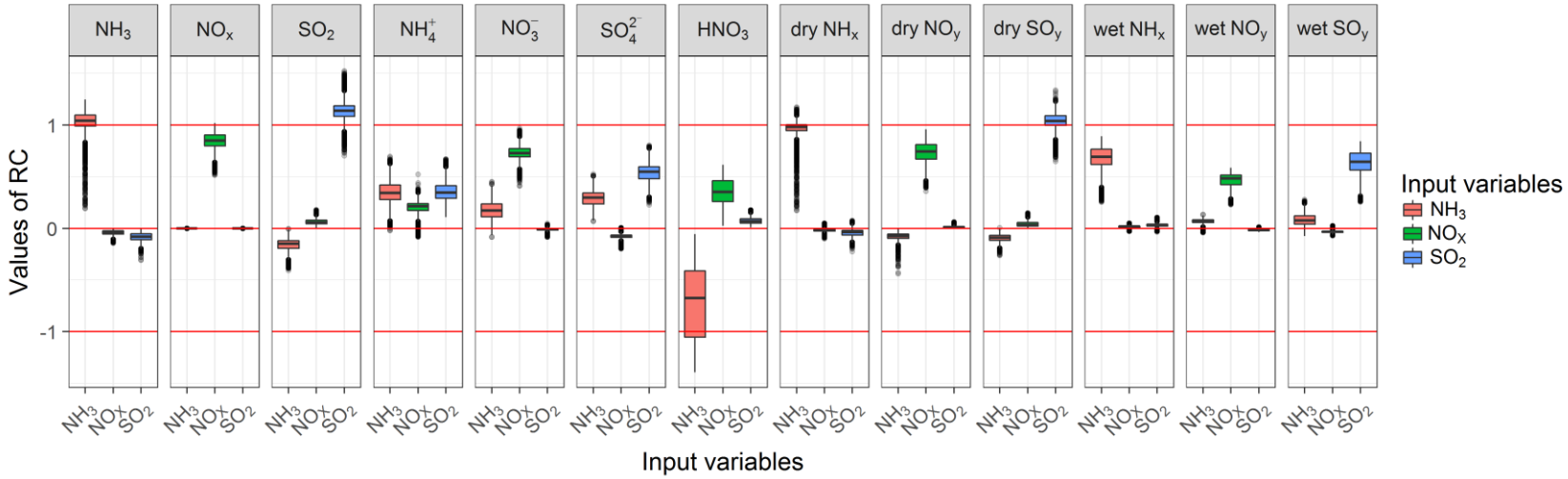

Figure 4.1 Box plots of the values of regression coefficients (RC) across all UK land-based model grid squares. Boxes demarcate the median and lower/upper quartiles of the distributions; whiskers extend to 1.5 times the interquartile range.

RC is a first-order sensitivity measure and it quantifies the average response of model output to varying a model input X_i when all inputs are allowed to vary. In this study no second, or higher, order interaction terms were quantified as their contribution was assumed to be negligible. This was concluded from the values of the coefficients of determination (R^2) obtained from multiple linear regressions performed; for most output variables, values of R^2 were on average > 0.98 with the exception of a slightly lower value for HNO_3 (R^2 > 0.96). Hence less than 2 % (4 % for HNO_3) of variance in the output could not be explained by the linear combination of inputs. This finding allows us to conclude that the FRAME model response is in fact fairly linear within the ± 40 % emission perturbation range investigated. The fact that the FRAME model input-output response fits linear model well indicates that the current use of the FRAME model to produce source-receptor matrices for the use in the UK Integrated Assessment Model is not subject to undue error from varying emissions one-at-a-time. Without conducting the global sensitivity analysis it is not possible to predict a priori for a given model output variable either the relative sensitivities to the different input factors, such as emissions, or the spatial variation in these sensitivities that are illustrated in Figures 4.1, 4.2 and 4.3.

With respect to findings from this FRAME model sensitivity analysis for particulate inorganic components in the UK context, Figure 4.1 shows that the modelled surface concentrations of particulate NH_4^+ are sensitive to changes in emissions of all three pollutants, being similarly sensitive (on average) to emissions of NH_3 and SO_2, and slightly less sensitive to emissions of NO_x. The sensitivities of NH_4^+ to SO_2, NO_x and NH_3 emission changes were found to vary substantially around the UK (top row of Figure 4.2). Sensitivity of NH_4^+ to SO_2 emissions is generally lowest in south-east England, and rises on moving north and west across the UK. Reductions in emissions are always associated with reductions in NH_4^+. The broad geographical pattern of relative sensitivity across the UK of NH_4^+ to NH_3 emissions is approximately the reverse of that to SO_2 emissions although with substantial spatial heterogeneity as well. Figure 4.2 shows that there are instances in north-west Scotland of negative RCs for the sensitivity of NH_4^+ to NO_x emissions, i.e. areas where NH_4^+ increases when NO_x emissions are decreased.

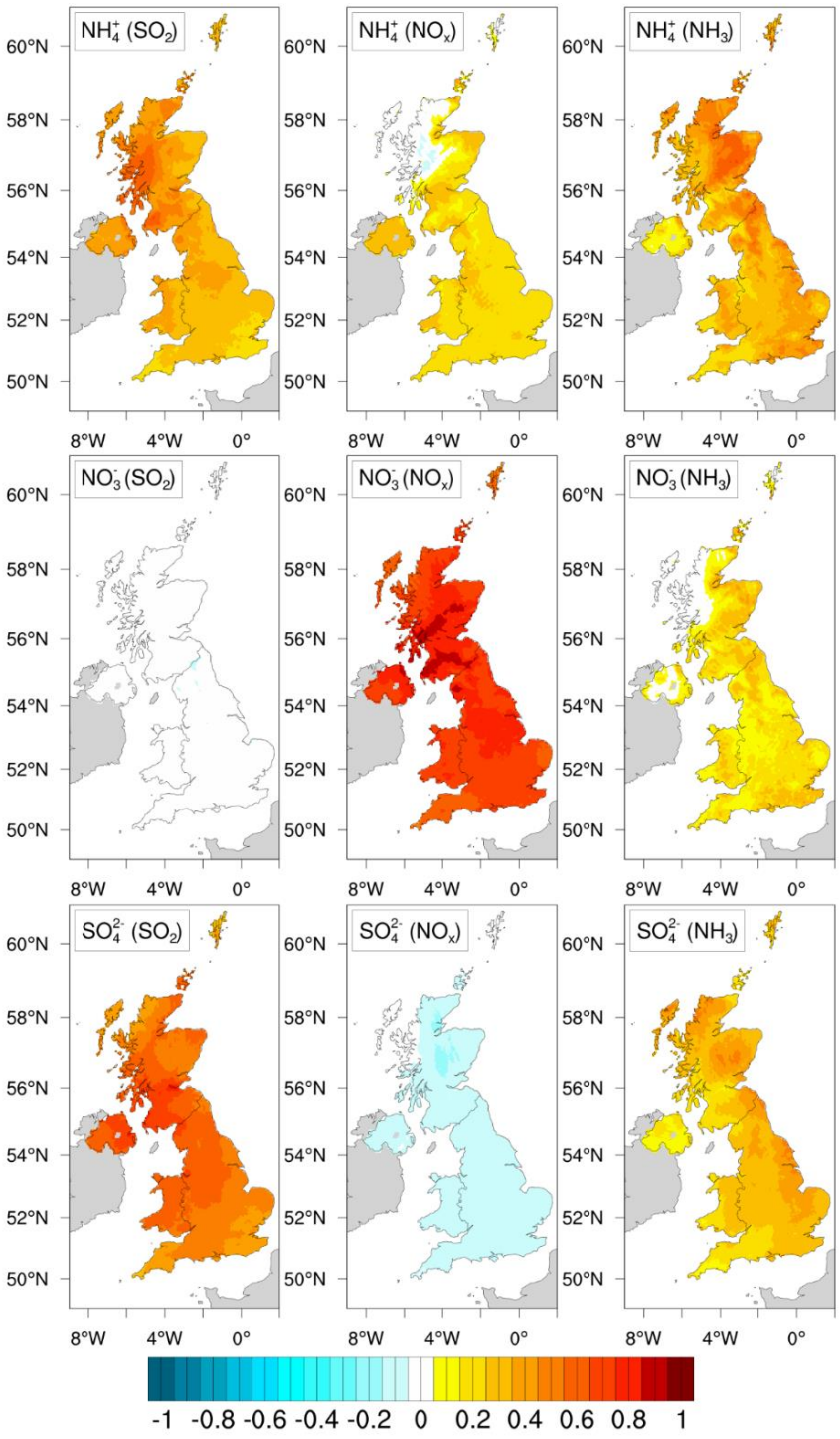

Figure 4.2 Spatial distributions (at the 5 km × 5 km model grid resolution) of RCs for particulate NH_4^+, SO_4^{2-}, and NO_3^- as a function of variation in input emissions of SO_2, NO_x or NH_3. The model input emissions for which the RC quantifies the output variable sensitivity is given in brackets in each panel.

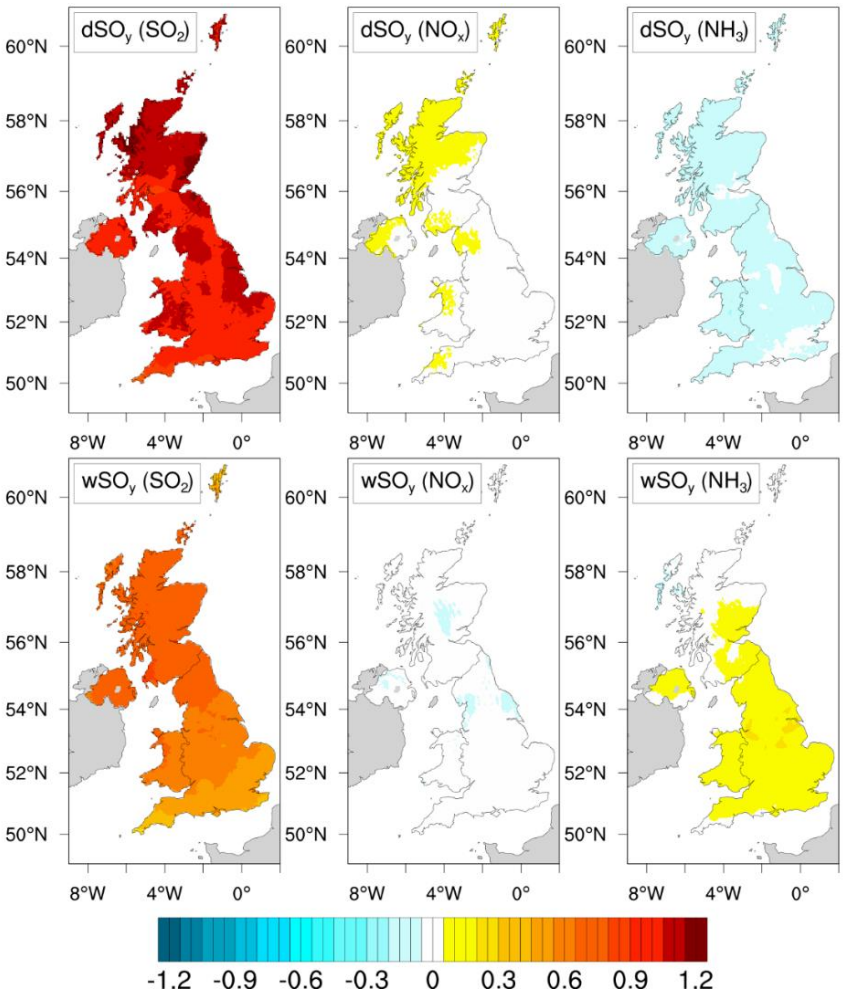

Figure 4.3 Spatial distributions (at the 5 km × 5 km model grid resolution) of RCs of dry (d) and wet (w) deposition of SO_y as a function of variation in input emissions of SO_2, NO_x or NH_3. The model input emissions for which the RC quantifies the output variable sensitivity is given in the brackets in each panel.

Figure 4.1 similarly shows that surface concentrations of particulate SO_4^{2-} are sensitive to changes in emissions of all three of SO_2, NO_x and NH_3 (most sensitive to SO_2 emissions) but with a universally negative sensitivity (albeit relatively weak) to NO_x emissions, i.e. particulate SO_4^{2-} concentrations increase everywhere by approximately 3 % if NO_x emissions are reduced by 40 % (lower row of Figure 4.2). This is due to competition between HNO_3 and H_2SO_4 to react with NH_3 and form particles, i.e. reducing NO_x emissions means NH_3 is more readily available to react with H_2SO_4. The positive values of RCs of SO_4^{2-} to SO_2 emissions are geographically fairly uniform

(somewhat lower sensitivity in the eastern UK), but the relative sensitivity to NH_3 emissions is more heterogeneous and greater in the east.

The sensitivity of particulate NO_3^- concentrations to the emissions is more straightforward than for particulate NH_4^+ and SO_4^2, being dominated by its positive sensitivity to NO_x emissions, weakly sensitive to NH_3 emissions and essentially not sensitive at all to SO_2 emissions (Figure 4.1 and middle row of Figure 4.2). The sensitivity to NO_x emissions is almost unity, such that for example a 30 % reduction in NO_x emissions results in almost the same 30 % reduction in surface NO_3^-. The spatial distribution of RCs that represent sensitivity of NO_3^- concentrations to NO_x (and NH_3) emissions is also geographically more homogenous across the UK than the sensitivities of NH_4^+ and SO_4^{2-} concentrations (middle row of Figure 4.2).

The concentrations of the three inorganic particulate matter components are determined by the reactions that lead to formation of $(NH_4)_2SO_4$ and NH_4NO_3. Formation of the former is irreversible whilst the latter exists in reversible equilibrium with gas-phase NH_3 and HNO_3. Changes in emissions of NH_3 have an impact on formation of both $(NH_4)_2SO_4$ and NH_4NO_3 very quickly, and therefore close to the source of the NH_3 emissions, because it reacts directly as NH_3. In contrast the influence of changes in SO_2 and NO_x emissions is not so localised. Before they influence the formation of $(NH_4)_2SO_4$ and NH_4NO_3 these gases must be oxidised in the atmosphere to H_2SO_4 and HNO_3, during which time the air is undergoing transport. The spatial pattern of the sensitivities of $(NH_4)_2SO_4$ and NH_4NO_3 formation to changes in the UK precursor emissions is therefore the outcome of many interacting factors: i) the magnitude of background import of precursors from outside the UK which could explain lower sensitivity of inorganic particulate matter components to SO_2 emissions in south-east England, ii) the magnitude and spatial pattern of the UK precursors, iii) the time taken for chemical oxidation in relation to atmospheric transport of air masses, and iv) the varying dry and wet deposition spatial patterns that remove from the atmosphere both the precursor gases and particulate products.

In summary, the broad patterns of the sensitivity results in Figures 4.1, 4.2, and 4.3 can be explained as follows. The surface concentrations of the directly emitted pollutants NH_3, NO_x, and SO_2 are predominantly sensitive only to their respective

emissions (Figure 4.1). This is also the case for the deposition of oxidised S, and of oxidised and reduced N. Dry deposition is dominated by the gas-phase components so the variations in the dry deposition of NH_x and SO_y are dominated by the variations in the emissions of NH_3 and SO_x respectively with the RC values being close to 1. For the dry deposition of NO_y, both NO_2 and its oxidation product HNO_3 are important. This is illustrated by the weaker response of dry NO_y deposition to changes in NO_x emissions. Wet deposition is a more complex process as this is dominated by washout of the particles which are the product of chemical reactions in the atmosphere. This explains lower values of RC for wet compared to dry deposition.

The considerably more ubiquitous sources of NO_x emissions compared with SO_2 emissions means that atmospheric concentrations of gaseous oxidised N are generally higher than for oxidised S so the former usually has greater influence on NH_3 chemistry. Therefore particulate NO_3^- is predominantly controlled by NO_x emissions, and changes in SO_2 emissions have very little effect on particulate NO_3^-. However, because lower NO_x emissions lead to lower NH_4NO_3 formation more NH_3 is available which means lower NO_x emissions leads to greater $(NH_4)_2SO_4$ formation this explains the inverse correlation between surface concentrations of SO_4^{2-} and NO_x emissions. On the other hand, changes in NH_3 emissions impact on both NO_3^- and SO_4^{2-} concentrations, both in a positive direction of association, but with a magnitude sensitive to the relative amounts of the reacting species present, which in turn depends both on the magnitudes and distances of local sources and on long-range transport. Likewise, the sensitivity of NH_4^+ concentrations varies with all three sets of precursor emissions and with geographical location. The same is the case for concentrations of HNO_3. This is why, aside from some broad expectations, it is not easily possible to predict the spatial patterns of the sensitivities of ACTM model output to changes in emissions and a formal sensitivity analysis is needed.

4.3.2 Uncertainty propagation

The global uncertainty propagation approach for FRAME output variables was based on the assigned uncertainties in the estimates of the total UK emissions of SO_2 (± 4 %), NO_x (± 10 %) and NH_3 (± 20 %) (Misra et al., 2015). As explained in the Methods, the

uncertainties in the input emissions were assigned uniform distributions, and no uncertainties in either the spatial or temporal aspects of the emissions are included. No substantial difference in the resulting model output uncertainty ranges was observed when the probability distributions of the input emissions were changed to normal. The distributions of the relative uncertainties across all model grid cells for each output are shown in Figure 4.4 Example maps of the spatial distributions of the relative uncertainties from Figure 4.4 for surface concentrations of particulate NH_4^+, NO_3^-, and SO_4^{2-} and for dry and wet deposition of SO_y are shown in Figure 4.5. Equivalent maps for the relative uncertainties of the other FRAME output variables are shown in Appendix B Figure B.5.

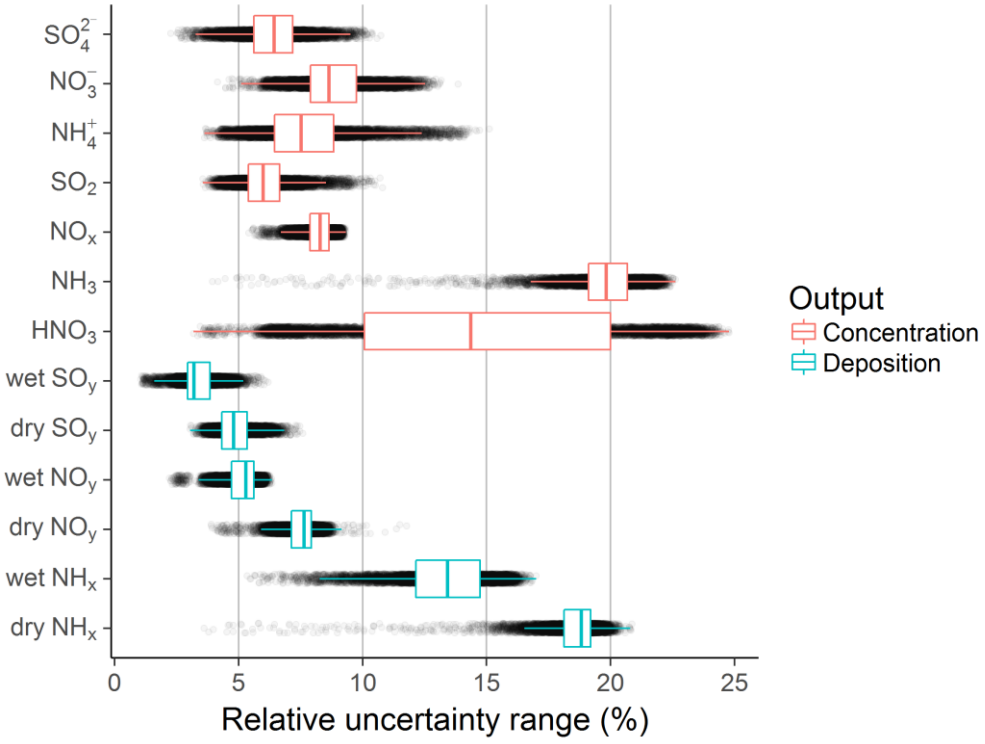

Figure 4.4 Distributions of relative uncertainty values calculated for all FRAME model outputs across all model grid squares given the following input uncertainty ranges: ± 4 %, ± 10 % and ± 20 % in emissions of SO_2, NO_x and NH_3 respectively. Boxes demarcate the median and lower and upper quartiles of the distributions; whiskers extend to 1.5 times the interquartile range.

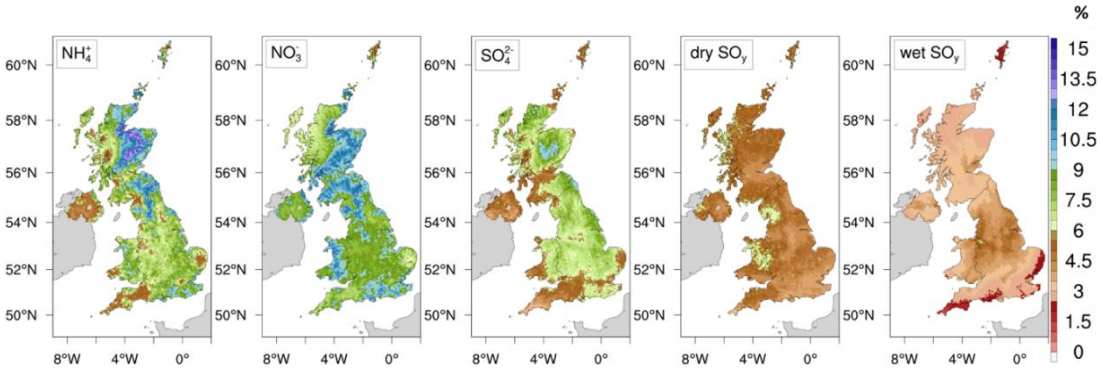

Figure 4.5 Spatial distributions (at the 5 km × 5 km model grid resolution) of the relative uncertainties in surface concentrations of particulate NH_4^+, SO_4^{2-}, and NO_3^- and dry and wet deposition of SO_y for uncertainties of ± 4 %, ± 10 %, ± 20 % in emissions of SO_2, NO_x and NH_3 respectively. The uncertainty values are represented as a range of +/- the baseline value and represent the 95 % confidence interval.

Figure 4.4 shows that the surface concentration of NH_3 is the most uncertain output (model grid median uncertainty 19.8 %). This is because the variation in NH_3 surface concentrations is almost entirely driven by variation in NH_3 input emissions (Figure 4.1) and this is the most uncertain input in the presented analysis. The uncertainty in modelled dry deposition of NH_x likewise closely matches the assigned uncertainty in NH_3 emissions (median = 18.8 %). The uncertainty in wet deposition of NH_x is somewhat less than uncertainty in dry deposition (median = 13.4 %) because wet deposition of NH_x includes some dissolved $(NH_4)_2SO_4$ component which is also sensitive to other precursor emissions whose uncertainty is estimated to be smaller than for NH_3. Surface concentrations of SO_2 and the dry and wet depositions of SO_y have least uncertainty (medians of 6.0 %, 4.8 % and 3.2 %) for the similar reason that these model outputs are predominantly sensitive to SO_2 emissions (Figure 4.1) which has the smallest of the input uncertainties (± 4 %).

Relative uncertainties of particulate SO_4^{2-} (median = 6.4 %), NO_3^- (median = 8.6 %) and NH_4^+ (median = 7.5 %) are fairly similar (Figure 4.4) even though there are substantial differences in the assigned uncertainties for emissions of SO_2, NO_x and NH_3. The explanation is that PM components are sensitive to all three inputs (for NO_3^- two out of three inputs) (Figure 4.1). There is also wide spatial variation in the

uncertainties of these PM components (Figures 4.4 and 4.5). The relative uncertainty values in surface concentration of HNO_3 show the largest variability out of all output variables. This can be explained by the fact that the concentration of this species is impacted directly by both gas and particle-phase processes. The spatial pattern of the relative uncertainty values does not correlate either with the spatial pattern of emissions or rainfall, which demonstrates again that the uncertainties of many model outputs cannot be readily predicted because of the complexity of the atmospheric processes underpinning them and consequently that formal uncertainty analysis needs to be applied.

Uncertainty apportionment

Estimated uncertainty of the model output given the uncertainties in model input emissions is presented in Figures 4.4 and 4.5, but it is also of interest to know how each of the inputs contributes to the overall uncertainty individually. This was estimated by calculating squared standardised regression coefficients (SRCs) (Eq. 4.3). As an example, Figure 4.6 illustrates the spatial distributions of the fractional contributions of the SO_2, NO_x and NH_3 emission uncertainties to the overall uncertainties in surface concentrations of particulate NH_4^+, NO_3^- and SO_4^{2-}, for the assigned uncertainties in the input emissions, whilst Figure 4.7 illustrates similar for the dry and wet deposition of SO_y. The equivalent maps for the other model output variables are presented in Appendix B Figures B.6 and B.7.

Figure 4.6 shows that across nearly all the UK, uncertainty in concentrations of particulate NH_4^+ is mainly driven by the uncertainty in NH_3 emissions. Uncertainty in NO_x emissions contributes some uncertainty to NH_4^+ concentrations, whilst the uncertainty in SO_2 emissions makes almost no contribution. Northern Ireland is an exception; here uncertainties in NO_x emissions contribute the most to the uncertainties in NH_4^+ concentrations and perturbations in NH_3 emissions have less impact. Concentrations of NH_3 in Northern Ireland are some of the highest anywhere in the UK, whilst NO_x emissions are not high; this means that NH_3 will be in excess so the formation of NH_4NO_3 will be largely controlled by HNO_3 through NO_x emissions. The major contribution to uncertainty in particulate NO_3^- derives from uncertainty in NO_x emissions (Figure 4.6). However in the east of Scotland, uncertainty in NH_3 emissions

contributes up to 78% of the total uncertainty. There is no contribution from SO_2 emissions uncertainty. An important feature of the lower panel of Figure 4.6 is that by far the major contributor to uncertainty in particulate SO_4^{2-} concentrations is the uncertainty assigned to the NH_3 emissions not the uncertainty in the direct precursor SO_2 emissions. This is because the formation of $(NH_4)_2SO_4$ is irreversibly dependent on gaseous NH_3 and emissions of NH_3 are much more uncertain than SO_2 emissions.

Figure 4.7 shows the spatial distribution of the squared SRC values for dry and wet SO_y deposition; for these output variables uncertainty in NO_x does not make any contribution to uncertainty in either case. In contrast to the situation for particulate SO_4^{2-} concentrations shown in Figure 4.6, Figure 4.7 shows that uncertainty in dry and wet deposition of SO_y is mainly driven by the uncertainty in the SO_2 emissions. Additionally uncertainty in NH_3 emissions contributes to the total uncertainty in dry and wet SO_y deposition. The contribution to uncertainty in wet deposition is higher due to wet deposition being dominated by the washout of the particles which include products of the reactions of NH_3 with oxidation products of SO_x.

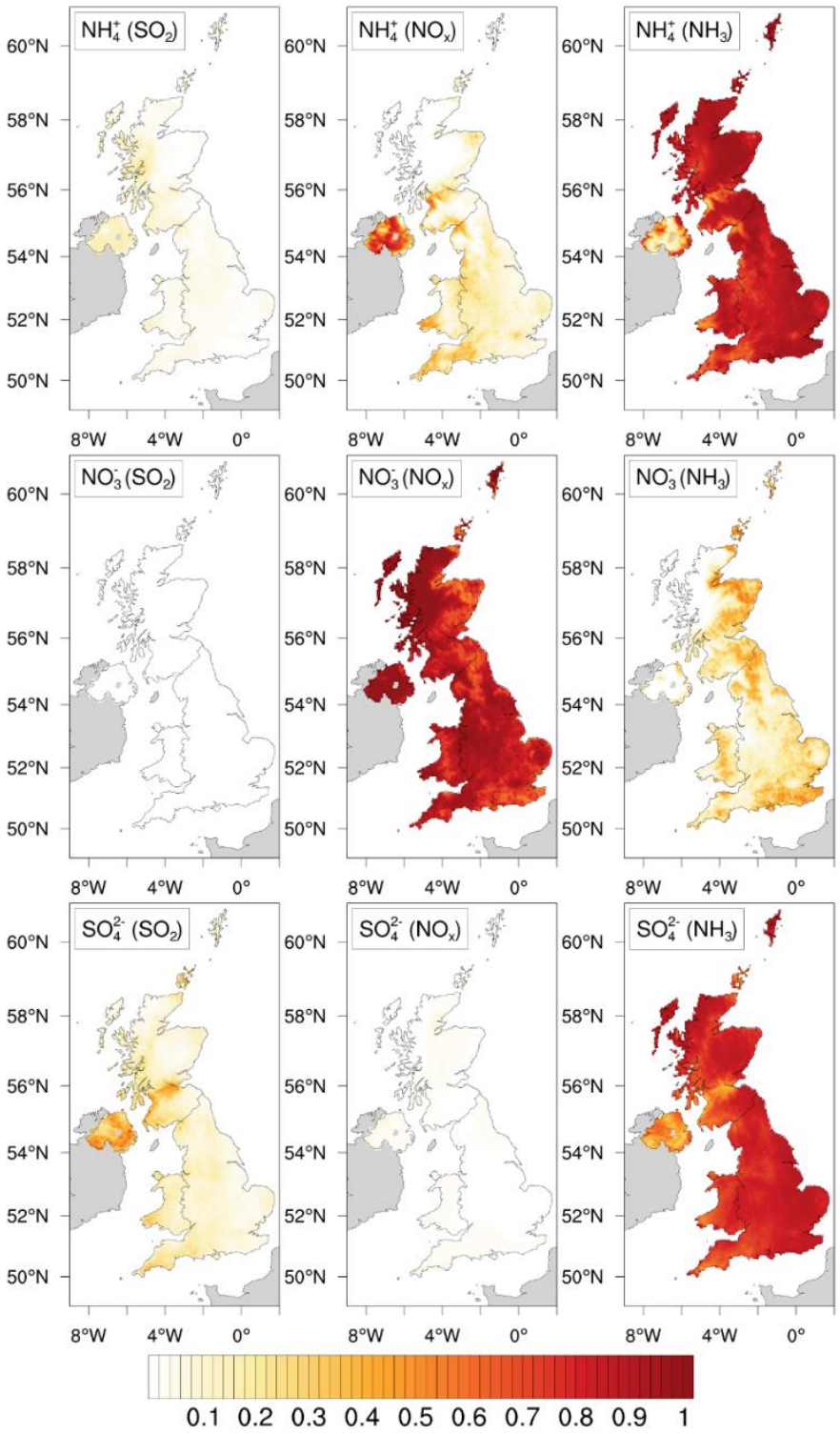

Figure 4.6 Spatial distributions (at the 5 km × 5 km model grid resolution) of the squared SRC values which represent the fractional contribution of the uncertainty in the input emissions given in brackets to the overall uncertainty in the surface concentrations of particulate NH_4^+, SO_4^{2-}, and NO_3^-. The uncertainties in the input emissions are ± 4 %, ± 10 % and ± 20 % for SO_2, NO_x and NH_3 respectively.

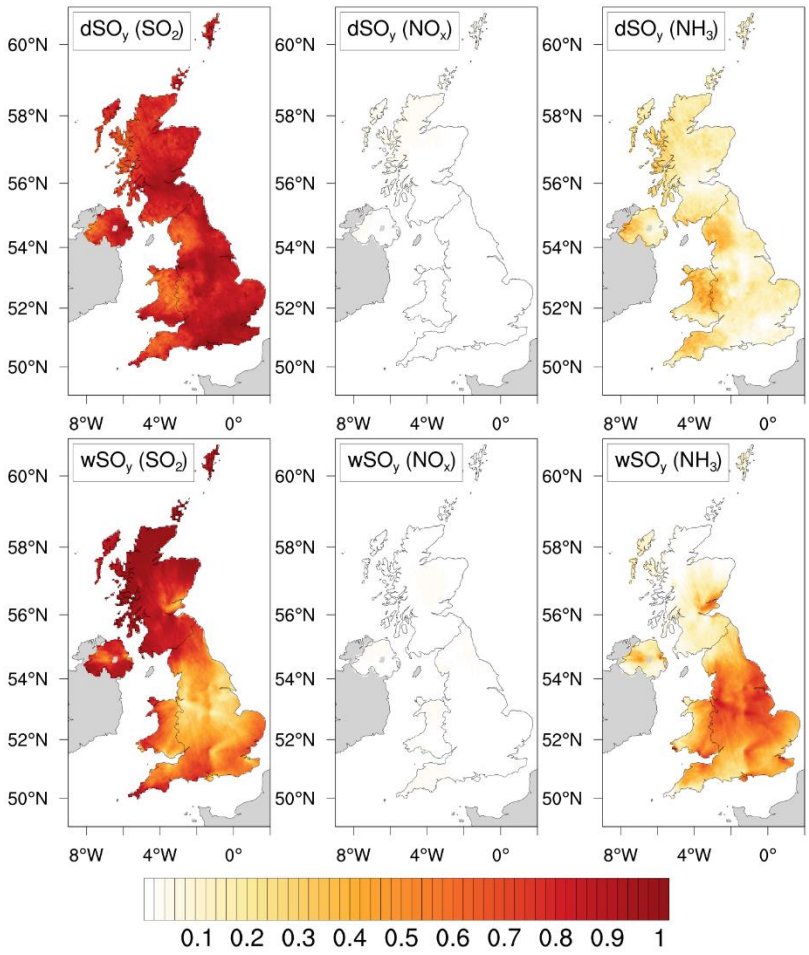

Figure 4.7 Spatial distributions (at the 5 km × 5 km model grid resolution) of the squared SRC values which represent the fractional contribution of the uncertainty in the input emissions given in brackets to the overall uncertainty in the dry and wet deposition of SO_y. The uncertainties in the input emissions are ± 4 %, ± 10 % and ± 20 % for SO_2, NO_x and NH_3 respectively.

4.4 Conclusions

Global sensitivity analysis was applied to determine the response of concentration and deposition output variables of the FRAME atmospheric chemistry transport model to perturbations of UK emissions of SO_2, NO_x and NH_3. The benefit of using systematic global sensitivity analysis is that all dimensions of variable input space are investigated

simultaneously, which is important when the response to a large number of variables is of interest, so inferences can be drawn without assumptions about the model structure. For complex models such as ACTMs, for which input-output mapping is not analytically tractable, it is not possible to predict output sensitivities to multiple input perturbations without conducting a global sensitivity analysis. Local one-at-a-time sensitivity analysis is often applied without acknowledging the shortcomings associated with it.

In this study no substantial deviations from linearity or presence of interactions between the model input variables were identified for the FRAME model in response to input emission perturbations within a ±40 % range, hence regression coefficients obtained from multiple linear regression were chosen as a sensitivity measure. This was not predictable from a local one-at-a-time sensitivity analysis.

Whilst sensitivity of surface concentrations of the primary precursor gases SO_2, NO_x and NH_3 (and of deposition of S and N) was dominated by the emissions of the respective pollutant, the sensitivities of secondary species such as HNO_3 and particulate SO_4^{2-}, NO_3^- and NH_4^+ to pollutant emissions were more nuanced and geographically variable. The dry deposition of S and N showed stronger response to changes in the emissions of the respective pollutant compared to wet deposition.

A global uncertainty analysis approach was used to estimate uncertainty ranges for all FRAME model output variables from the uncertainties assigned to the UK emissions of SO_2, NO_x and NH_3 (± 4 %, ± 10 % and ± 20 % respectively) by the UK National Atmospheric Emissions Inventory. The spatial distribution of the relative uncertainty was affected by both the sensitivity of the model output to variations in the inputs and the magnitude of this variation (i.e. the input uncertainty range); NH_3 was the most uncertain input and as a result the output variables sensitive to NH_3 showed the highest levels of relative uncertainty in the areas most sensitive to this input. The uncertainty in the surface concentrations of NH_3 and NO_x and the depositions of NH_x and NO_y was shown to be due to uncertainty in a single precursor input variable, NH_3 and NO_x respectively. In contrast, the concentration of SO_2 and deposition of SO_y was affected by uncertainties in both SO_2 and NH_3 emissions. Likewise, the relative uncertainties in the modelled surface concentrations of each of the secondary pollutant variables

(NH_4^+, NO_3^-, SO_4^{2-}, and HNO_3) were affected by the uncertainty range of at least two input variables.

This work has demonstrated a methodology for conducting global sensitivity and uncertainty analysis for ACTMs. Although, for the FRAME model used here, the response to emission perturbations was found to be substantially linear in the investigated input range, the complexity of chemical and physical processes included in ACTMs means that the input-output relationships, in particular their spatial patterns, cannot be predicted without conducting a global sensitivity analysis. The benefit of using global approaches is that all dimensions of input variable space are investigated simultaneously so model input-output relationships can be quantified without the need to make strong prior assumptions about the model response to perturbations in the inputs of interest.

Chapter 5

Advanced methods for uncertainty assessment and global sensitivity analysis of the EMEP4UK model

This chapter is based on a research paper currently undergoing review in 'Atmospheric Chemistry and Physics' (Aleksankina, K., Reis, S., Vieno, M., and Heal, M. R.: Advanced methods for uncertainty assessment and global sensitivity analysis of a Eulerian atmospheric chemistry transport model, Atmos. Chem. Phys. Discuss., https://doi.org/10.5194/acp-2018-690, in review, 2018). I developed the experimental design, set up and performed model runs, created scripts for data analysis and visualisation, and prepared the manuscript. The co-authors, Prof Mathew Heal and Dr Stefan Reis, provided valuable advice on the interpretation of results and aided with manuscript preparation and editing. Dr Massimo Vieno aided with setting up model runs and provided feedback for the manuscript.

5.1 Introduction

Air pollution has a wide range of detrimental impacts. Exposure to air pollutants such as nitrogen dioxide (NO_2), ozone (O_3), and particulate matter ($PM_{2.5}$) is associated with increased risk of stroke, cardiovascular disease, and chronic and acute respiratory diseases (WHO, 2006, 2013). Additionally, particulate matter and O_3 contribute to climate change through radiative forcing (IPCC, 2013; Stevenson et al., 2013) and O_3 has an adverse impact on natural and semi-natural vegetation and crop yields (Teixeira et al., 2011).

To reduce the harmful impact of air pollution, various policies and directives have been implemented. For example, in the European Union, the Ambient Air Quality

Directive (EC Directive, 2008) sets limit values on ambient concentrations of air pollutants, whilst other directives set source-specific emissions limits. Atmospheric Chemistry Transport Models (ACTMs) play an essential role in the evaluation of the potential outcomes of different management options aimed at improvement of future air quality.

Analytical uncertainty propagation is not feasible for complex models such as ACTMs because it requires an exact function for input-output mapping. Consequently, Monte Carlo based methods for uncertainty assessment have to be used. Uncertainty analysis should be performed in tandem with sensitivity analysis to maximise the knowledge gained (Saltelli, 2002).

The computational cost of running ACTMs to explore the entire parameter space of the uncertain inputs using Monte Carlo based uncertainty and sensitivity analyses is typically prohibitively high because the analyses require a large number of points in parameter space which translates to thousands of model simulations. To tackle this issue, the use of meta-models has been increasing in recent years (Gladish et al., 2017; Iooss and Lemaître, 2015; Ratto et al., 2012; Yang, 2011). A meta-model (or emulator) is a statistical approximation of the original simulation model that can be evaluated many times at a lower computational cost relative to the original model (Castelletti et al., 2012; O'Hagan, 2006). This approach allows the output of an ACTM for a large number of points in parameter space to be estimated efficiently making uncertainty and sensitivity analyses feasible.

Different meta-modelling approaches have been used for uncertainty and sensitivity analysis; these techniques include regression smoothers (Storlie et al., 2009; Storlie and Helton, 2008), Gaussian process emulator (Oakley and O'Hagan, 2004), high-dimensional model representation (Rabitz and Alış, 1999; Ziehn and Tomlin, 2009), and polynomial chaos expansion (Sudret, 2008). Meta-models have been applied for uncertainty and sensitivity analyses in earth science fields such as ecological modelling (Luo et al., 2013; Parry et al., 2013), hydrological modelling (Asher et al., 2015; Gladish et al., 2017), and atmospheric aerosol modelling (Carslaw et al., 2013; Chen et al., 2013; Christian et al., 2017; Lee et al., 2011).

In this study, a Gaussian process is used for emulation because of its desirable properties and available implementations (i.e. Matlab based software UQLab or R package DiceKriging). Gaussian process emulators are non-parametric statistical models that use the principles of conditional probability to estimate model outputs. The beneficial properties are the curve that fits through the training points (for deterministic models) and a measure of the uncertainty for the estimated points when using an emulator in place of the original model for the estimation of new points.

The efficiency of the emulator compared to the original model is determined by how smooth and continuous the model response is to input perturbations. For a smooth and continuous input-output relationship, the high correlation between the inputs and the simulated points means a lower uncertainty in predictions made using the emulator further away from the training points (i.e. resulting in a good emulator performance with a small number of training points) (Lee et al., 2011).

The design of computer experiments for deterministic models differs from the designs for physical experiments. As there is no random error involved in computer experiments, replication is not required (Jones and Johnson, 2009). Hence sampling techniques that have good space-filling properties and the ability to maintain uniform spacing when projected into a lower-dimensional space are used (Dean et al., 2015; Jones and Johnson, 2009). Latin hypercube sampling (LHS) introduced by (McKay et al., 1979) meets these desirable criteria.

The aim of this study is to demonstrate the method for uncertainty assessment and global sensitivity analysis for computationally demanding ACTMs. The ACTM to which the method is applied here is the EMEP4UK model (Vieno et al., 2010, 2014, 2016a), and the outputs of interest are the modelled surface concentrations of O_3, NO_2, and $PM_{2.5}$, but the methodology is generic for model and output variable. The analyses described here investigated sensitivities and uncertainties of model output to emissions from UK land-based sources and from surrounding shipping. Additionally, we identify which model inputs drive uncertainty in the output variables, and to what extent; as well as discuss how the uncertainty ranges that are obtained affect current predictions and scenario analysis outcomes (i.e. confidence in model outputs).

5.2 Methods

5.2.1 Input variables and their uncertainty ranges

For this study, emissions of five pollutants (NO_x, SO_x, VOC, NH_3, primary $PM_{2.5}$) were split into 13 model input variables based on the contributions from different emission source sectors to total annual emissions; the emissions from the dominant sector (the sector with the highest relative contribution to total emissions) for every pollutant were treated as a separate variable, while the emissions from the rest of the sectors were grouped and treated as another input variable. Shipping emissions were treated as a separate variable and were not split by the pollutant type. The description of the Selected Nomenclature for Air Pollution (SNAP) sectors is shown in Table 5.1, and the definitions of the input variables for the uncertainty and sensitivity analyses in this work are presented in Table 5.2, where variables marked with D represent emissions from a single dominant sector (D1 and D2 in case of multiple dominant sectors) and variables marked with O indicate the grouped 'other' emissions from the rest of the sectors. Emissions from 'natural' sources (e.g. lightening, soil, ocean) were not part of the uncertainty and sensitivity analyses.

Uncertainty ranges for the input emissions from UK anthropogenic land-based sources were assigned according to data in the UK Informative Inventory Report (IIR) (Wakeling et al., 2017). In the IIR, uncertainties are defined as upper and lower limits of the 95% confidence interval relative to the central estimate. There is no information on uncertainty ranges for different source sectors available for the emissions for 2012 because uncertainties split by the emission source sector were first presented in the IIR that included 2014 emissions (Wakeling et al., 2016). Hence, for this study, the most recently published data for the uncertainty ranges of pollutants split by source sector were used.

Equation 5.1 was used to aggregate uncertainties for multiple emission source sectors for the grouped-source input variables, where x is the quantity of interest and U is the uncertainty of that quantity, taken from the EMEP/EEA air pollutant emission inventory guidebook (Pulles and Kuenen, 2016).

$$U_{total} = \frac{\sqrt{(U_1 x_1)^2 + (U_2 x_2)^2 + \cdots + (U_n x_n)^2}}{x_1 + x_2 + \cdots + x_n} \quad (5.1)$$

The shipping emission variable in this study combines all emissions of all relevant pollutants, hence a 'best estimate' range for the uncertainty was chosen. The range was estimated based on the available published information. Some recently published sources (Corbett, 2003; Scarbrough et al., 2017) state that the uncertainty in shipping emissions is significant, but do not provide quantitative estimates. The most recent source of quantitative information on the uncertainty in shipping emissions is the report for the European Commission (Entec, 2002) which presents the estimates of uncertainties for emission factors of NO_x, SO_2, PM, VOC, for the ships' emissions 'at sea', 'manoeuvring', and 'in port'. The uncertainties are presented for the emissions for the year 2000 as 95% CI with the lowest values of uncertainty presented for 'at sea' emission factors (± 10-20%) and highest values for 'manoeuvring' emission factors (± 30-50%). For the total pollutant emissions for the year 2000 the percentage uncertainties around the estimates are ± 21% for NO_x, ± 11% for SO_2, ± 11% for CO_2, ± 28% for VOC and ±45% for PM. Additionally, in Moreno-Gutiérrez et al. (2015) the uncertainty in the emission factors for all pollutant compounds was estimated to be ± 20%. Using the above data, an overall uncertainty of ± 30% was assigned to the shipping emissions variable in this study (Table 5.2). It was applied to all shipping emissions within the inner British Isles domain of the EMEP4UK model.

Table 5.1 Source sector definitions for emissions of air pollutants according to the Selected Nomenclature for Air Pollutants (SNAP) (Eurostat, 2004).

SNAP 1	Combustion in energy and transformation industries
SNAP 2	Residential and non-industrial combustion
SNAP 3	Combustion in manufacturing industry
SNAP 4	Production processes
SNAP 5	Extraction and distribution of fossil fuels
SNAP 6	Solvent and other product use
SNAP 7	Road transport
SNAP 8	Other mobile sources and machinery
SNAP 9	Waste treatment and disposal
SNAP 10	Agriculture

Table 5.2 Input variable definitions for the EMEP4UK uncertainty propagation and apportionment. The quoted uncertainties for emission sources are for UK annual totals. D indicates emissions from a dominant source sector and O indicates grouped emissions from the rest of the source sectors. See main text for information on the sources of these values.

Variable used for sampling design	SNAP source sector	Contribution of source sector to total land-based emissions of that pollutant (%)	Uncertainty (as a 95% CI)	Ranges of scaling coefficients for the input emissions used in the LHS design
SOx_D	1	80	± 12 %	0.6 – 1.4
SOx_O	2-10	20	± 17 %	0.6 – 1.4
NOx_D1	1	41	± 7 %	0.6 – 1.4
NOx_D2	7	32	± 7 %	0.6 – 1.4
NOx_O	2-6, 8-10	27	± 19 %	0.6 – 1.4
VOC_D	6	39	± 22 %	0.6 – 1.4
VOC_O	1-5, 7-10	61	± 24 %	0.6 – 1.4
NH3_D	10	88	± 33 %	0.6 – 1.4
NH3_O	1-9, 10	12	± 35 %	0.6 – 1.4
PM2.5_D1	2	33	± 59 %	0.25 – 1.75
PM2.5_D2	7	21	± 59 %	0.25 – 1.75
PM2.5_O	1, 3-6, 8-10	46	± 58 %	0.25 – 1.75
Shipping	N/A	N/A	± 30 %	0.6 – 2.0

5.2.2 Gaussian process emulator for EMEP4UK

A Gaussian Process emulator was used to estimate model predictions at unsampled points in the space of the uncertain model inputs. The UQLab, a MATLAB-based software framework for uncertainty quantification (Lataniotis et al., 2017; Marelli and Sudret, 2014), was implemented to build the emulators for the uncertainty propagation and the following sensitivity analysis. The comprehensive description of the statistical theory of Gaussian process applied to uncertainty and sensitivity analysis with full

mathematical details can be found in O'Hagan (2006) and Oakley and O'Hagan (2002, 2004).

The uncertainty values and sensitivity indices were calculated for three EMEP4UK model outputs (O_3, NO_2, and $PM_{2.5}$ surface concentrations) with annual and monthly temporal resolution. For the annually-averaged outputs, an emulator was created for each modelled grid cell in the EMEP4UK domain (n = 59 400). The first-order and total sensitivity indices were calculated for the land-based grid cells only (n > 10 000). For the monthly mean model outputs, uncertainty and sensitivity analysis were performed for five selected grid cells. The five grid cells were selected to contain a UK national-network air pollution monitoring station to aid classification according to the environment (i.e. rural background, urban background, and urban traffic) and also to provide geographically representative coverage across the UK.

LHS maximin design, which maximises the minimum distance between the points in the parameter space to provide the optimum space-filling properties was used. The design was previously demonstrated suitable for Gaussian process emulators by Jones and Johnson (2009). The design with 84 data points was created for the scaling coefficients that were subsequently applied to the input emissions. This means that emissions corresponding to a particular input variable were perturbed homogeneously throughout the whole of the UK model domain. The ranges of scaling coefficient used for the sampling design are presented in Table 5.2.

In this study, the surface concentration of O_3, NO_2, and $PM_{2.5}$ for every grid cell is defined as a scalar output $Y = f(\boldsymbol{X})$ where $\boldsymbol{X}$ is the vector of input values $\{X_1, \ldots, X_{13}\}$.

A Gaussian process emulator utilises a Bayesian approach; the training data is used to update the selected prior function to produce posterior mean and covariance functions. The Gaussian process is specified by its mean function and covariance function. The mean function is given by Eq. 5.2:

$$\mathbb{E}[f(\boldsymbol{x})|\boldsymbol{\beta}] = \boldsymbol{h}(\boldsymbol{x})^{\boldsymbol{T}}\boldsymbol{\beta} \tag{5.2}$$

where $\boldsymbol{h(\cdot)}$ is a vector of regression functions and $\boldsymbol{\beta}$ is a vector of unknown coefficients. The choice of $\boldsymbol{h(\cdot)}$ incorporates any prior beliefs about the form of $f(\cdot)$. In this study, the mean function was chosen to have a linear form $\beta_o + \sum_{i=1}^{13} \beta_i x_i$.

The covariance function between $f(\boldsymbol{x})$ and $f(\boldsymbol{x}')$ is given by Eq. 5.3:

$$cov\{f(\boldsymbol{x}), f(\boldsymbol{x}')|\sigma^2\} = \sigma^2 c(\boldsymbol{x}, \boldsymbol{x}') \tag{5.3}$$

where σ^2 is the hyperparameter that represents the variance of the Gaussian process and $c(\boldsymbol{x}, \boldsymbol{x}')$ is the correlation function. The correlation function increases as the distance between $\boldsymbol{x}$ and $\boldsymbol{x}'$ decreases and equals one when $\boldsymbol{x} = \boldsymbol{x}'$. In this study Matérn 5/2 (Eq. 5.4) was used, where h is the absolute distance between $\boldsymbol{x}$ and $\boldsymbol{x}'$ and $\boldsymbol{\theta}$ is a vector of range parameters or length-scales, which define how far one needs to move along a particular axis in the input space for the function values to become uncorrelated.

$$c(x, x') = \left(1 + \frac{\sqrt{5}|h|}{\theta} + \frac{5\,h^2}{3\theta^2}\right) \exp\left(-\frac{\sqrt{5}|h|}{\theta}\right) \tag{5.4}$$

A number of emulators were built with the EMEP4UK simulation data using other available covariance functions; however, little difference was found in the performance of the emulators. The hyperparameters $\boldsymbol{\beta}$, σ^2, and $\boldsymbol{\theta}$ were estimated using a cross-validation approach.

The emulator error was estimated by implementing k-fold cross-validation (Gladish et al., 2017; Urban and Fricker, 2010). The original sample was randomly partitioned into $k = 10$ sized subsamples which allowed approximately 90% of data to be used as a training set and 10% as a validation set. Spatial distribution of cross-validation errors is presented in Appendix C (Figure C.1).

5.2.3 Uncertainty and sensitivity analysis

Uncertainty propagation

The uncertainties for the EMEP4UK output variables were estimated using a Monte Carlo approach (also described in the IPCC guidelines (IPCC, 2006) as a Tier 2 approach). The specific uncertainty ranges assigned to the input emission variables were used to constrain the input sampling space. All inputs were assigned normal distributions with baseline value as the mean and the standard deviation derived from the corresponding confidence interval (Table 5.1). For every grid cell, the emulator was used to predict model values of surface concentrations of O_3, NO_2, and $PM_{2.5}$ at the new set of input points (n = 5,000). The resulting probability distributions for each grid cell were evaluated, and the resulting uncertainty was estimated as a half of the 95% confidence interval relative to the central estimate (i.e. the mean for normally distributed values) of the output value, as described in the EMEP/EEA and IPCC Guidebooks (IPCC, 2006; Pulles and Kuenen, 2016). The re-sampling size of n = 5,000 was chosen because it minimised the error in the estimated values of the mean and the confidence interval from the corresponding probability distribution while being small enough to allow computational efficiency. The uncertainty for the monthly average modelled surface concentrations of O_3, NO_2, and $PM_{2.5}$ was calculated for five grid cells using the same approach as above. The locations of the grid cells within the UK are shown in Figure 5.1. The five grid cells selected were assigned the following environment types – the names and environment type reflect those of the national-network monitoring site within that grid cell: Auchencorth Moss and Harwell - rural background, Birmingham Acocks Green and London N. Kensington - urban background, and London Marylebone Road - urban traffic.

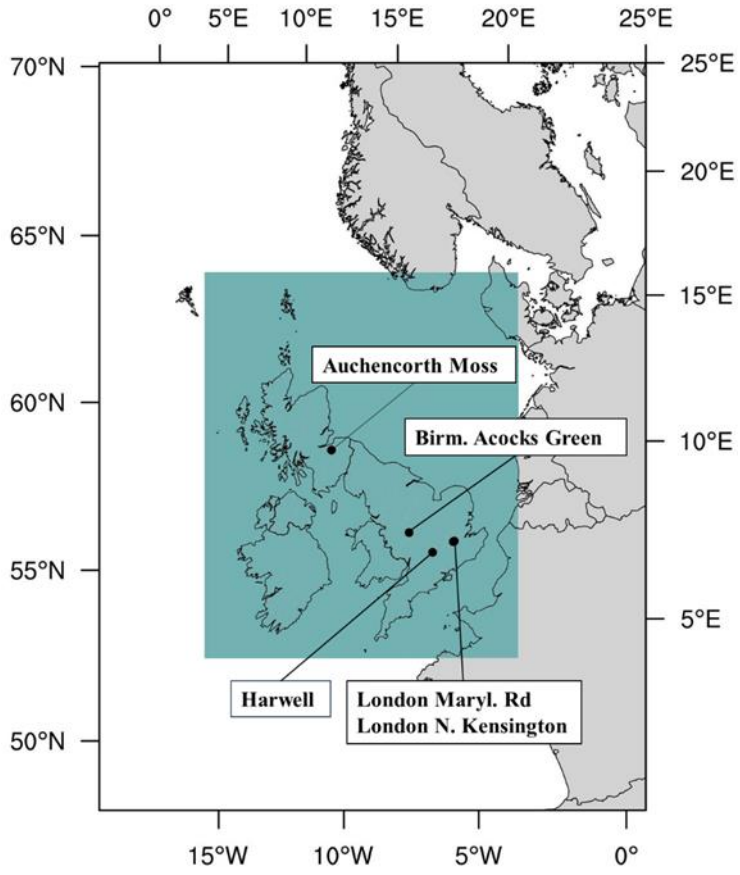

Figure 5.1 The inner shaded box illustrates the EMEP4UK model British Isles domain, which is modelled at 5 km× 5 km horizontal resolution. The location of five grid cells used for uncertainty quantification and sensitivity analysis for monthly average modelled concentrations of O_3, NO_2, and $PM_{2.5}$ are shown.

5.2.4 Global sensitivity analysis; first- order and total sensitivity indices

A variance-based global sensitivity analysis was conducted to apportion overall uncertainty in modelled variables to the uncertainty in the input emissions. Sobol first-order and total sensitivity indices were estimated (Homma and Saltelli, 1996; Janon et al., 2014; Sobol, 2001, 1993). The first-order indices represent the fraction of total variance of the output (i.e. the proportion of the overall uncertainty in Y) explained by the variance in an input X_i while total indices show the sum of the effects due to an input X_i and all of its interactions with other inputs ($X_{\sim i}$). Therefore, the values of first-

order and total indices can be compared to identify the presence of interactions between input X_i and all other model inputs.

Unlike an OAT sensitivity coefficient, a first-order sensitivity index accounts for the non-linear response of a model output to a parameter across the specified parameter variation range. Sensitivity indices in this context are also indicators of importance for the input variables.

The first-order sensitivity index is defined as the ratio of the variance of the mean of Y when one input variable is fixed, $V_{Xi}(E_{X\sim i}(Y|X_i))$, to the unconditional variance of Y, $V(Y)$ (Eq. 5.5).

$$S_i = \frac{V_{X_i}(E_{\boldsymbol{X}_{\sim i}}(Y|X_i))}{V(Y)} \tag{5.5}$$

The total sensitivity index measures the total effect of a variable, which includes its first-order effect and interactions with any other variables (Eq. 5.6).

$$S_{Ti} = 1 - \frac{V_{\boldsymbol{X}_{\sim i}}\left(E_{X_i}(Y|\boldsymbol{X}_{\sim i})\right)}{V(Y)} = \frac{E_{X_{\sim i}}\left(V_{X_i}(Y|\boldsymbol{X}_{\sim i})\right)}{V(Y)} \tag{5.6}$$

where $\boldsymbol{X}_{\sim i}$ denotes the matrix of all variables but X_i. In $E_{X\sim i}(V_{Xi}(Y \mid \boldsymbol{X}_{\sim i}))$ the inner variance of Y is taken over all possible values of X_i while keeping $\boldsymbol{X}_{\sim i}$ fixed, while the output expectation E is taken over all possible values $\boldsymbol{X}_{\sim i}$ (Ghanem et al., 2017).

For the annual average modelled surface concentrations of O_3, NO_2 and $PM_{2.5}$, the sensitivity indices were calculated for the UK land-based grid cells for the whole domain. For the monthly average modelled concentrations, sensitivity indices for five selected grid cells (discussed above) were estimated to determine whether seasonality affects the magnitude of the sensitivity indices.

5.3 Results and discussion

5.3.1 Uncertainty propagation

Figure 5.2 shows the spatial distribution of annual average surface concentrations of O_3, NO_2, and $PM_{2.5}$ modelled with EMEP4UK and their absolute and relative uncertainties given the uncertainties in UK pollutant emissions for each source sector shown in Table 5.2. The uncertainties are presented as a range of ± the baseline value and represent the 95% confidence interval. The maps represent the uncertainty in surface concentrations propagated from the uncertainties reported in the UK emissions (Wakeling et al., 2017) and estimated uncertainties in shipping emissions in the EMEP4UK model domain (Entec, 2002; Moreno-Gutiérrez et al., 2015). The uncertainties in surface concentration do not incorporate any uncertainties in the spatial and temporal aspects of the input emissions because no data on these aspects of uncertainty are provided by the compilers of the emissions inventories.

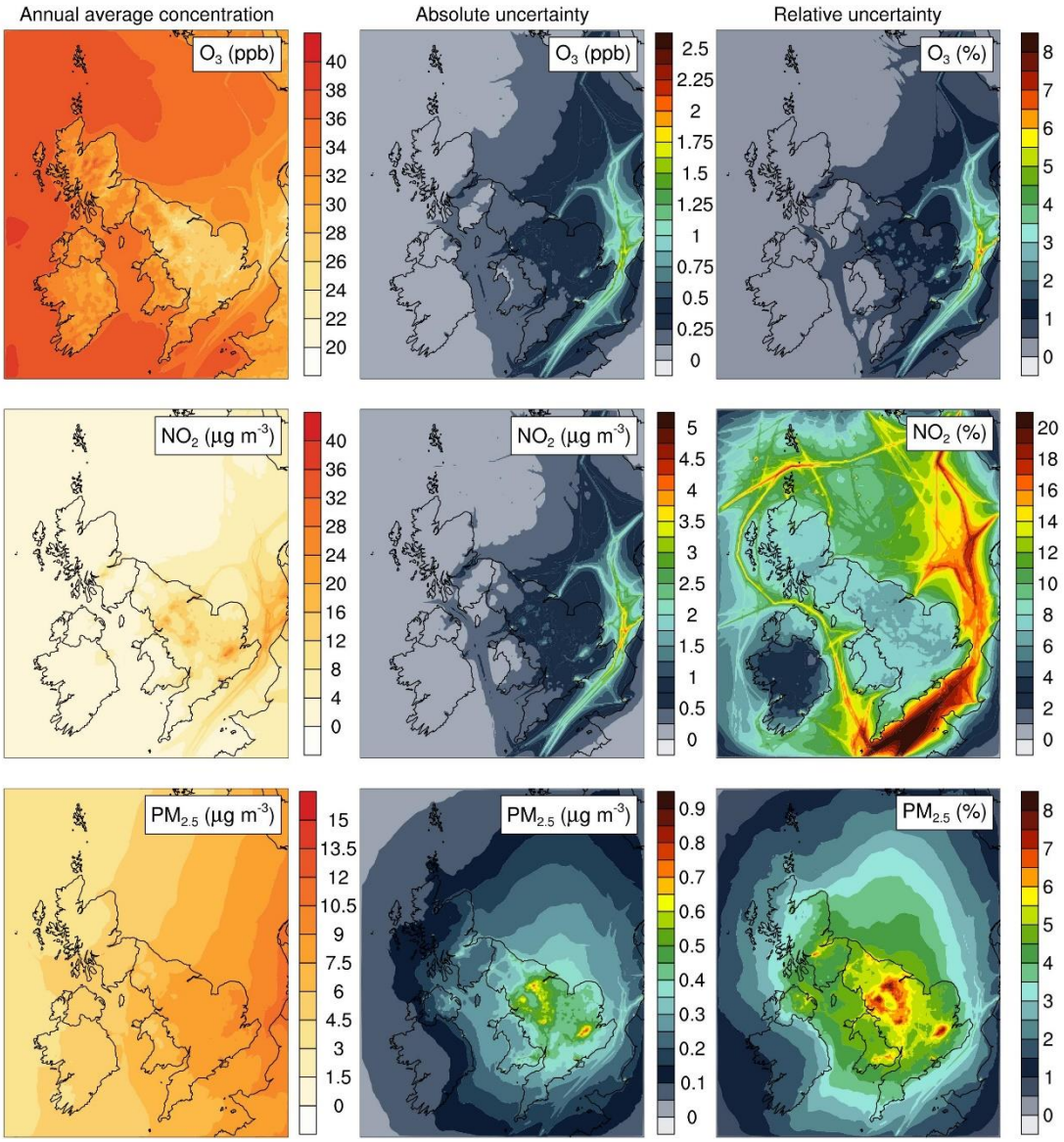

Figure 5.2 Baseline surface concentrations of O_3, NO_2, and $PM_{2.5}$, and their respective spatial distributions of the absolute and relative uncertainties (at the 5 km × 5 km model grid resolution, year 2012) for the specified uncertainties in UK emissions. The uncertainty values are represented as a range of ± the baseline value and represent the 95% confidence interval. Note, the same colour scheme is used to represent values with different ranges and units.

For O_3 and NO_2 the areas with the highest uncertainty coincide with the location of the shipping lanes. This is due to assigning all shipping emissions an uncertainty of ± 30%, which causes high variability in the corresponding NO_x emissions. The uncertainty in O_3 surface concentrations for the land-based grid cells is generally low (median

relative uncertainty is ± 0.6%) with values of uncertainty up to ± 7% or ± 1.4 ppb occurring in the grid cells containing major UK cities. The overall low uncertainty in the modelled O_3 concentrations can be attributed to the combination of a low uncertainty in precursor emissions and the substantial contribution of hemispheric background O_3 to UK ambient concentrations, the concentrations of which are not part of this analysis of uncertainty with respect to the UK-only emissions.

The relative uncertainty of NO_2 has a homogeneous spatial pattern (median relative uncertainty for all land-based grid cells is ± 7.4%) while absolute uncertainty is found to be higher (up to ± 3.5 μg m^{-3} or ± 9%) in the areas with the major UK cities. The magnitude of uncertainty in NO_2 is determined by the combination of two factors: i) NO_2 uncertainty is driven by NO_x emission inputs which have low levels of uncertainty associated with them; ii) low overall variation in O_3 surface concentrations affects the reactions between NO, NO_2 and O_3 that are linked through the photolysis of NO_2 to give NO and the reaction of NO with O_3 to produce NO_2.

The spatial pattern of $PM_{2.5}$ surface concentrations and the corresponding absolute and relative uncertainties differ from those for O_3 and NO_2. The concentration gradient indicates the presence of transboundary $PM_{2.5}$ transport into the UK. This is consistent with findings reported by Air Quality Expert Group (AQEG, 2013) that only about half of the $PM_{2.5}$ annual average concentrations have a UK origin. The spatial pattern of uncertainty in $PM_{2.5}$ concentrations shows higher uncertainty, both relative and absolute, in the grid cells with major cities; median relative uncertainty for all land-based grid cells is ± 4.6% with up to ± 9% (± 0.9 μg m^{-3}) in the grid cells with major cities. The surface concentrations of $PM_{2.5}$ are dominantly comprised of primary $PM_{2.5}$ emissions and inorganic aerosols resulting from chemical reactions between SO_2, NO_x, and NH_3. Hence the spatial pattern of uncertainty can be explained by the fact that the main contribution to primary $PM_{2.5}$ comes from emissions from sources such as stationary combustion (e.g. residential heating) and road transport. The pattern of decreasing uncertainty from the land-based grid cells (centre) towards the edges of the domain indicates the change in variation due to the transport of $PM_{2.5}$ away from the sources of emitted pollutants.

The overall uncertainty in the output variables (O_3, NO_2, and $PM_{2.5}$) was found to be lower compared to the uncertainty of the model input emissions. This can be explained by the overall weak response of surface concentrations to changes in the emission originating from the UK which leads to the conclusion that the surface concentrations are affected by the transport of pollutants from elsewhere. Another explanation is the 'compensation of errors' whereby a positive effect of one or multiple input variables on the output is compensated by a negative effect of another input variable(s). This leads to the narrower confidence intervals associated with the EMEP4UK outputs.

An important observation from this uncertainty analysis is that the areas with the highest uncertainty coincide with the most populated areas. Given that O_3, NO_2, and $PM_{2.5}$ are associated with adverse health effects, it is particularly important to have an estimate for the confidence level of the modelled values in the more densely-populated regions. This work has shown that the highest uncertainty is precisely in these regions. The reason for the increased levels of uncertainty in the grid cells coinciding with urban areas is discussed below.

5.3.2 Sensitivity analysis

In addition to quantitative uncertainty estimates, it is of interest to know how the uncertainty of each input contributes to the overall uncertainty and whether there are interactions between inputs that potentially affect the magnitude of overall uncertainty. This was achieved by conducting a variance-based sensitivity analysis.

Figures 5.3, 5.4, and 5.5 show the spatial distribution of the first-order sensitivity indices that represent the fractional contribution of the uncertainty of each input variable to the overall uncertainty in the output. Only the variables with $S_i > 0.03$ are presented here. First-order indices with values less than 0.03 were omitted as the method used for computation of sensitivity indices is prone to numerical errors when the analytical sensitivity index values are close to zero (Saltelli et al., 2006). The threshold was estimated by examining the noise in first-order sensitivity indices calculated for unimportant input variables. Excluding $S_i < 0.03$ does not have an effect

on the results presented because a relative contribution of less than 3% to the overall uncertainty can be considered negligible.

Difference between total and first-order sensitivity is used to highlight interactions between variable *Xi* and all other input variables. For the sensitivity coefficients computed for the annual-averaged model outputs, there was no substantial difference found between first and total- order sensitivity indices, hence no between-input interactions were identified on the annual timescale (Fig. C.2)

Figure 5.3 shows the spatial distribution of first-order sensitivity indices for the input variables affecting modelled O_3 concentrations. It is predominantly the NO_x input emissions that drive the uncertainty in modelled O_3 surface concentrations.

The greatest contribution to O_3 surface concentration uncertainty in the areas with higher levels of overall uncertainty is from the input variable NO_x_O, which represents NO_x emissions from all the other SNAP sectors apart from SNAP 1 (combustion in energy and transformation industries) and SNAP 7 (road transport). The NO_x emissions combined into this input variable account for 27% of total NO_x emissions and the uncertainty range for this variable is ± 19%. The input variable NO_x_D1 (emissions from combustion in energy and transformation industries) does not contribute substantially to output uncertainty despite making up 41% of total NO_x emissions, with a relative uncertainty of ± 7%.

This is explained by the height at which these emissions occur; the emissions are injected into the vertical layers at heights of >184 m above ground level. This leads to NO_x being dispersed and transported away from these elevated sources without affecting ground-level O_3 concentrations locally. The NO_x emissions from input variable NO_x_D2 (road transport) account for the remaining 32% of total NO_x emissions. The spatial distribution of corresponding sensitivity indices indicates that uncertainty in road transport emissions affects overall uncertainty in O_3 surface concentrations in the grid cells closest to the emission sources (i.e. major roads). A large proportion (>80%) of overall uncertainty in O_3 concentrations in areas adjacent to the south and south-east coasts of England is apportioned to the uncertainty in shipping emissions.

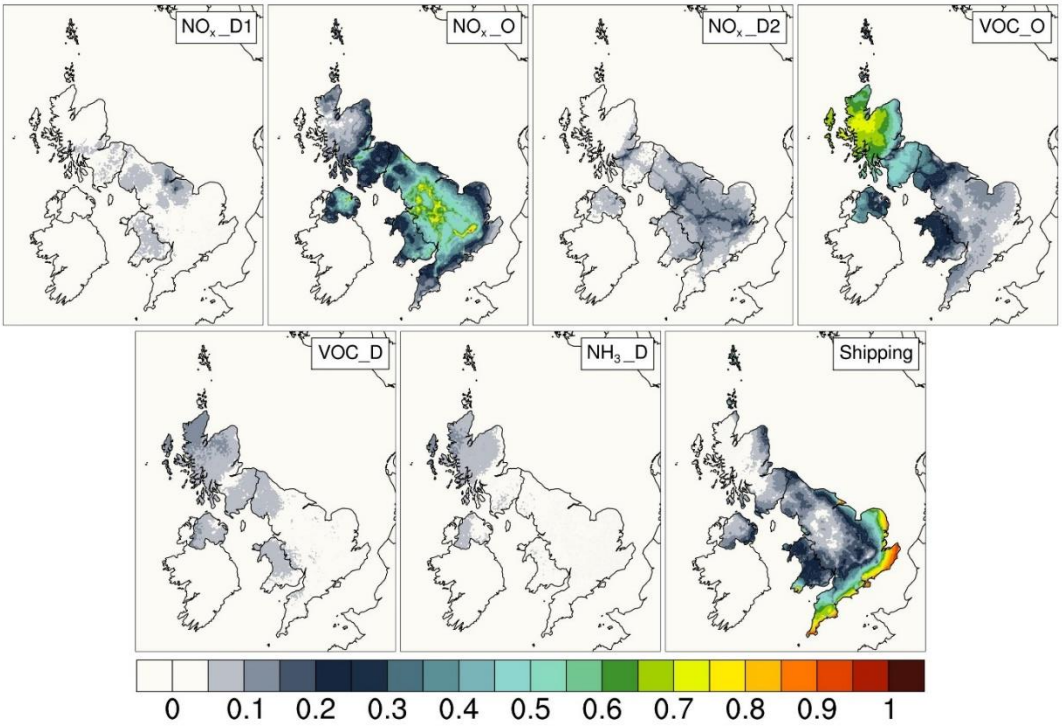

Figure 5.3 Spatial distributions (at the 5km×5km model grid resolution) of the first-order sensitivity indices for modelled surface concentrations of O_3. D indicates emissions from a dominant sector and O indicates grouped emissions from the rest of the sectors. For NO_x emissions dominant sectors are energy production (D1) and road transport (D2), for VOC emissions – solvent use, and for NH_3 – agriculture. Shipping emissions variable combines emissions of all relevant pollutants.

In Scotland, most of the overall uncertainty in O_3 surface concentration is apportioned to the variables VOC_D and VOC_O that respectively represent VOC input emissions from the dominant VOC source sector (solvent and other product use) and emissions from the rest of the source sectors grouped into a single input. A small proportion is apportioned to the variable NH_3_D that represents NH_3 emissions from agricultural sources. The effect of these input variables manifests in Scotland because of low levels of locally-emitted NO_x. The overall uncertainty in this area is very low.

In summary, the uncertainty in modelled surface concentrations of O_3 in the densely populated areas can be apportioned to the uncertainty in NO_x emissions from non-dominant sources and uncertainty in shipping emissions.

The uncertainty in surface concentration of NO_2 was found to be driven mostly by uncertainty in NO_x emissions (variables NO_x_D1, NO_x_D2, NO_x_O) and shipping emissions (Fig. 5.4). Similarly to O_3, NO_2 is most sensitive to NO_x emissions combined from all SNAP sectors apart from SNAP 1 (combustion in energy and transformation industries) and SNAP 7 (road transport). There is almost no sensitivity to NO_x emissions from SNAP 1, for the same reason given above that these are elevated emissions. The sensitivity to NO_x emissions from SNAP 7 is most pronounced close to the source of emissions (i.e. major roads and cities).

The similarity in spatial distribution of sensitivity indices for O_3 and NO_2 model outputs results from the concentrations of these pollutants being inversely correlated, as their chemical transformation reactions are interlinked. In the same way as for O_3, uncertainty in the NO_2 concentrations along the south and south-east coasts of England is mostly driven by the uncertainty in the shipping emissions. In fact, uncertainty in shipping emissions contributes approximately 30% of uncertainty in NO_2 concentrations even well inland, in areas away from major roads and cities.

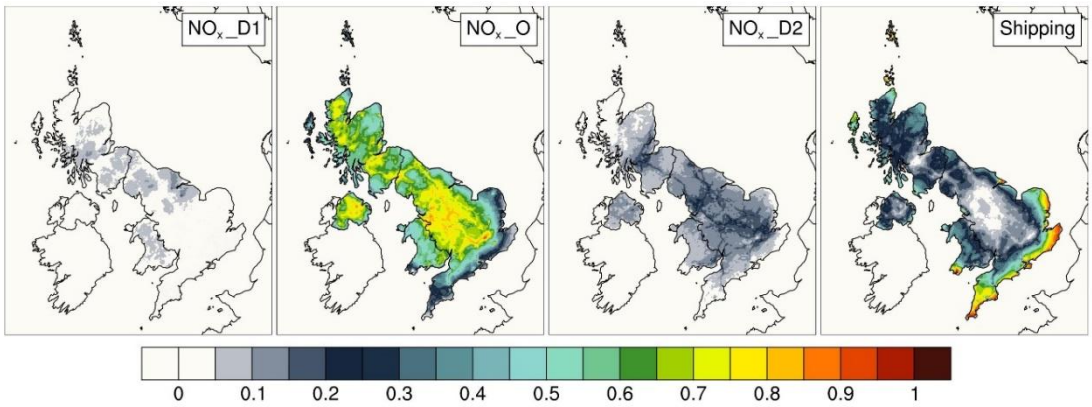

Figure 5.4 Spatial distributions (at the 5km×5km model grid resolution) of the first-order sensitivity indices for modelled surface concentrations of NO_2. D indicates emissions from a dominant sector and O indicates grouped emissions from the rest of the sectors. For NO_x emissions dominant sectors are energy production (D1) and road transport (D2). Shipping emissions variable combines emissions of all relevant pollutants.

Figure 5.5 shows the spatial distribution of first-order sensitivity indexes for the model inputs that contribute to the uncertainty in modelled surface concentrations of $PM_{2.5}$. Modelled $PM_{2.5}$ is sensitive to all emissions of NH_3 (dominant sector is agriculture) and to primary $PM_{2.5}$ (dominant sectors D1 is residential combustion and D2 is road transport), and to shipping emissions. In the areas with lower surface $PM_{2.5}$ concentrations such as Scotland, Wales, northern England and south-west England the uncertainty is mainly driven by NH_3 emissions from agriculture (NH_3_D). The spatial pattern of emissions sensitivity indices for $PM_{2.5}$ mirrors the spatial distribution of $PM_{2.5}$ emission sources. From Figure 5.2 and Figure 5.5 it can be seen that in the areas with the highest levels of uncertainty the model output is most sensitive to the emissions of primary $PM_{2.5}$. Similar to the results for O_3 and NO_2, the areas with the highest uncertainty coincide with the most populated areas.

The pattern in calculated sensitivity indices partially agrees with a previous study of changes in $PM_{2.5}$ surface concentrations in response to 30% reduction in emissions of $PM_{2.5}$, NH_3, SO_x, NO_x, and VOC by Vieno et al. (2016). In the study by Vieno et al. (2016) surface concentrations of $PM_{2.5}$ were found to be sensitive to reductions in each of the five pollutants individually (the same reduction was applied to a pollutant's emissions from all SNAP sectors simultaneously), with highest sensitivity to NH_3 and $PM_{2.5}$ emissions (up to ~6% reduction in surface concentration in response to 30% reduction in emissions). In comparison, in this study the uncertainty in $PM_{2.5}$ surface concentrations is not affected by the perturbations of SO_x, NO_x, and VOC. This is likely to be due to i) the difference in ranges of variation (i.e. uncertainty ranges) in this study (SO_x, NO_x and VOC input variables have narrower ranges of variation compared to $PM_{2.5}$ and NH_3), and ii) the presence of non-additivity and non-linearity in the model response to perturbations in the inputs. In the presence of non-linearity in the model response, the sensitivity value estimated using the OAT method becomes dependent on the range of perturbation chosen for the input. The interactions present in non-additive models lead to the discrepancy between the sensitivity values calculated by perturbing inputs one-at-a-time and perturbing the same inputs simultaneously.

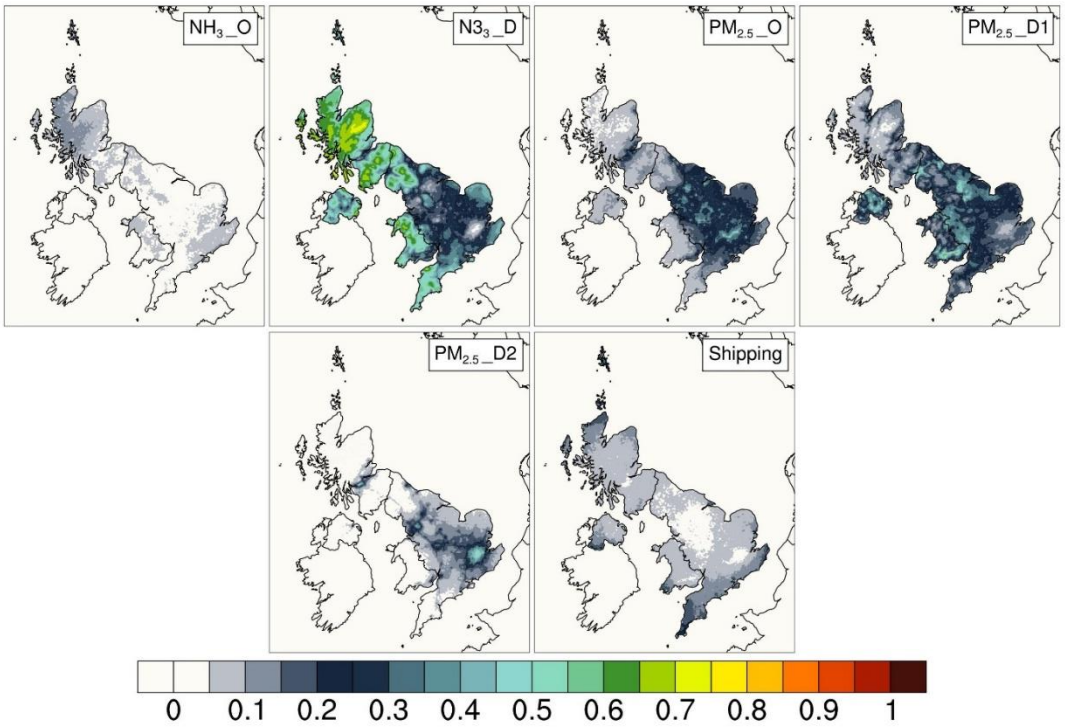

Figure 5.5 Spatial distributions (at the 5km×5km model grid resolution) of the first-order sensitivity indices for modelled surface concentrations of $PM_{2.5}$. D indicates emissions from a dominant sector and O indicates grouped emissions from the rest of the sectors. For NH_3 emissions dominant sector is agriculture, for $PM_{2.5}$ dominant sectors are residential and non-industrial combustion (D1) and road transport (D2). Shipping emissions variable combines emissions of all relevant pollutants.

5.3.3 Uncertainty propagation and sensitivity analysis for monthly averaged model outputs

The uncertainty assessment and sensitivity analysis for monthly averaged surface concentrations of NO_2, O_3, and $PM_{2.5}$ were performed for five different grid cells that were assigned the following environment types based on the national-network monitoring site within that grid cell: Auchencorth Moss and Harwell - rural background, Birmingham Acocks Green and London N. Kensington - urban background, and London Marylebone Road - urban traffic.

Monthly average concentrations with error bars representing the absolute uncertainty values (as a 95% CI) are presented in Figure 5.6. Figure 5.7 shows corresponding values of the relative uncertainty. Figure 5.8 shows how the magnitude of first-order sensitivity indices estimated for five different grid cells changes on a monthly

timescale. If all first-order sensitivity coefficients add up to 1 then there are no interactions between inputs and all model variance can be apportioned to the variance in the individual inputs.

The NO_2 surface concentrations show a seasonal trend of lower concentrations occurring during summer months with the exception of the Auchencorth Moss grid cell where NO_2 concentrations are low throughout the year. The magnitude of uncertainty in NO_2 is proportional to the modelled concentration and changes relative to the concentration, which can be seen from the monthly relative uncertainty values (Fig. 5.7). The first-order sensitivity indices for NO_2 show that only NO_x emissions (across all sectors) and shipping emissions influence the modelled surface NO_2 concentrations. Hence it can be concluded that the uncertainty in modelled concentrations of NO_2 directly depends on the uncertainty in NO_x emissions and is not affected by the uncertainties in the emissions of any other pollutant. The change in the magnitude of sensitivity coefficients for the Harwell grid cell indicates increasing influence of shipping emissions on NO_2 concentrations during the summer months. Potential explanation for this is seasonal change in the wind direction which results in more NO_x from shipping emissions being transported to the grid cell during the summer months.

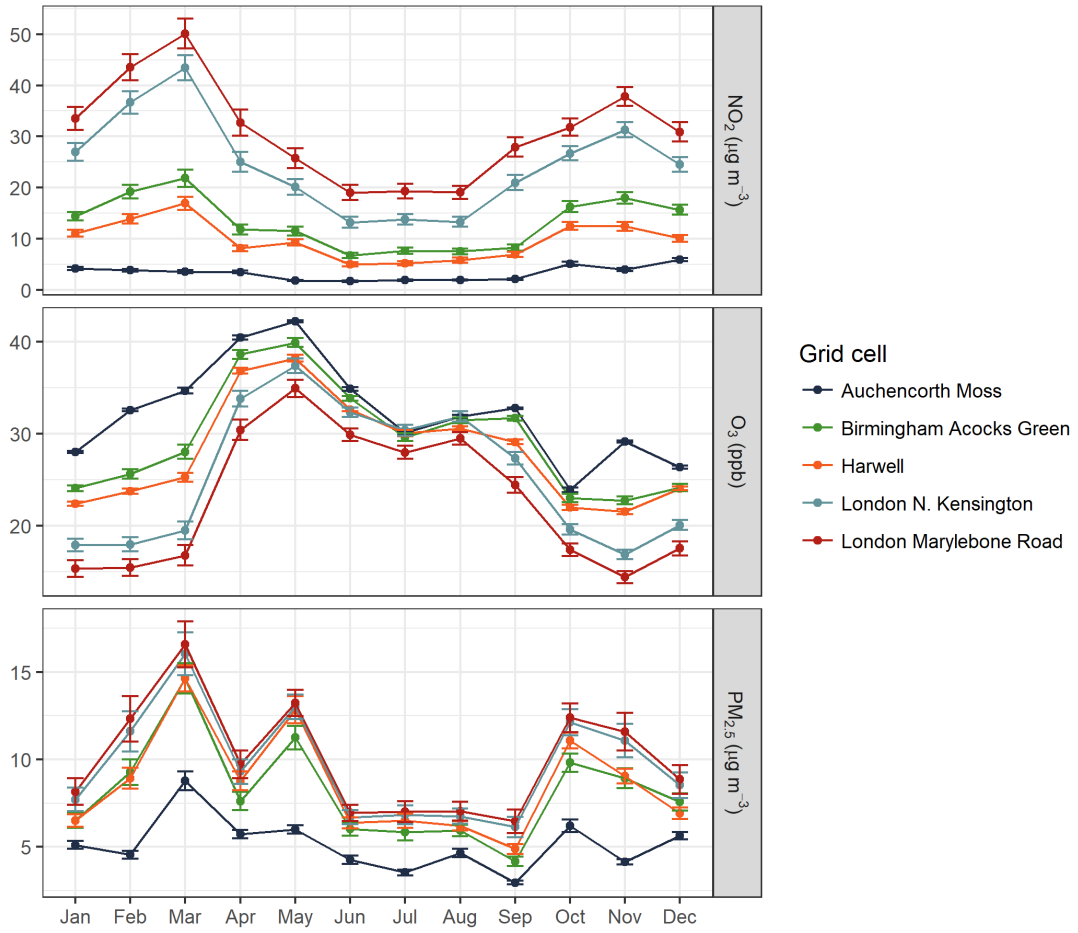

Figure 5.6 Monthly average surface concentrations of NO_2, O_3 and $PM_{2.5}$ with error bars showing (absolute) uncertainty, for five grid cells across the UK representing a spread of geographical locations and environment types. The environment types are assigned as follows: Auchencorth Moss and Harwell - rural background, Birmingham Acocks Green and London N. Kensington - urban background, and London Marylebone Road - urban traffic.

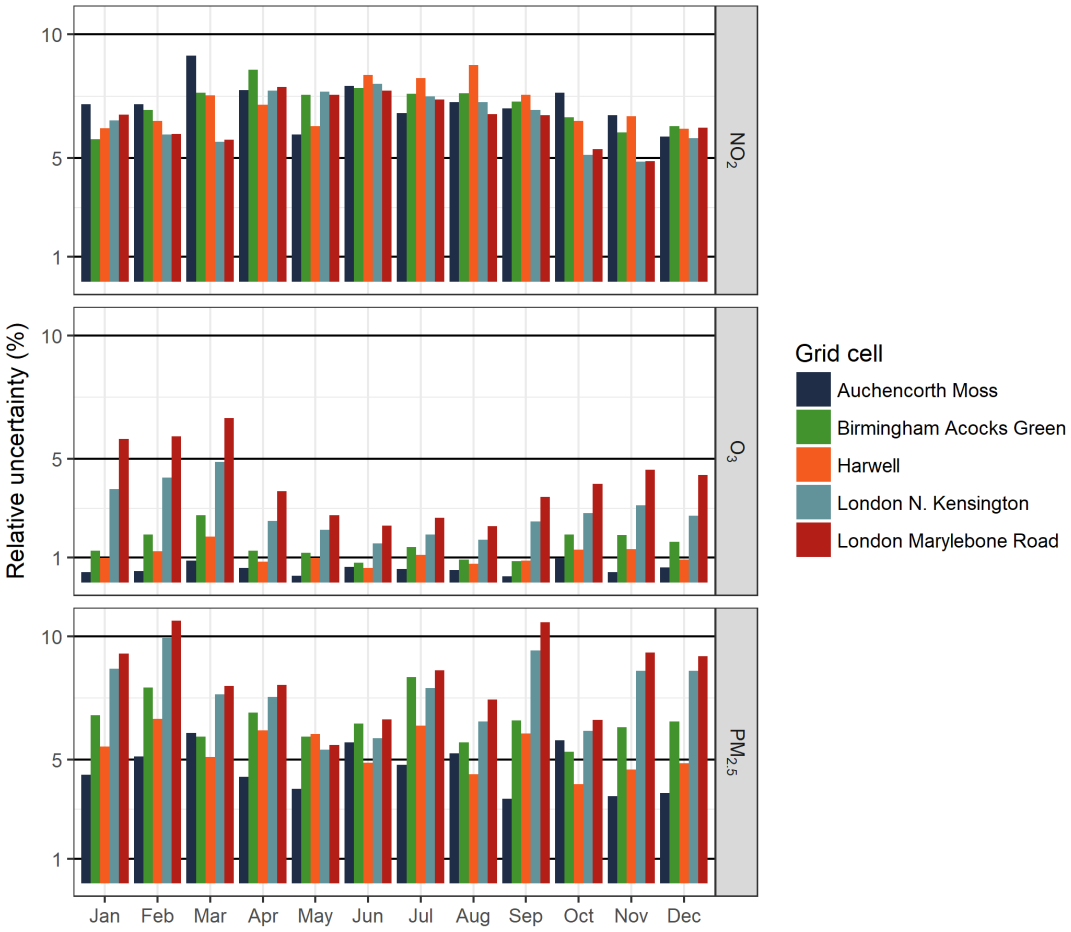

Figure 5.7 Magnitude of relative uncertainty in monthly average surface concentrations of NO_2, O_3, and $PM_{2.5}$ for five grid cells across the UK representing a spread of geographical locations and environment types. The environment types are assigned as follows: Auchencorth Moss and Harwell - rural background, Birmingham Acocks Green and London N. Kensington - urban background, and London Marylebone Road - urban traffic.

The uncertainties in the O_3 modelled surface concentrations show an inverse seasonal trend compared to the uncertainties in modelled NO_2. Unlike the uncertainty in NO_2 concentration, the uncertainty in O_3 concentration is influenced by the grid cell environment type; the highest level of uncertainty is observed for the London Marylebone Road grid cell (urban traffic). The relative uncertainty in O_3 concentrations for the Auchencorth Moss grid cell (rural background) is small and close to the median relative uncertainty in O_3 for annual average concentrations, which

as discussed above is ± 0.6%. This indicates that perturbations in the input emissions do not substantially affect O_3 concentration in this grid cell. Although the magnitude of uncertainty in O_3 is very small in this grid cell, the inputs that drive it differ noticeably throughout the year; during May-August the variance is mostly explained by VOC emissions (explains 77% of uncertainty for July) and during November-February NO_x emissions drive the uncertainty. The magnitude of O_3 concentrations and corresponding uncertainties in the Birmingham Acocks Green and Harwell grid cells are very similar. The trends in sensitivity indices are also similar; during the April-September period some variance in the model output is explained by uncertainty in VOC emissions. However, in the Harwell grid cell shipping emissions play a more important role. For the London-based grid cells, the level of uncertainty is the highest and it is mainly driven by the uncertainty in NO_x and shipping emissions.

For the $PM_{2.5}$ monthly average concentrations, London-based grid cells show the highest values of absolute uncertainty and Auchencorth Moss - the lowest. The relative uncertainty in London based grid cells is also the highest. From Figure 5.8 it can be seen that the contribution to the overall uncertainty from the uncertainty due to NH_3 emissions for these grid cells is not as important as for other three, the majority of uncertainty is explained by the uncertainty in the primary $PM_{2.5}$ emissions with $PM_{2.5}$ from road transport being the dominating variable. In Birmingham Acocks Green and Harwell, the effect of NH_3 emissions from agricultural sources is more pronounced; from 30% to 70% of overall uncertainty in $PM_{2.5}$ can be apportioned to uncertainty coming from agricultural emissions of NH_3 during spring and summer months.

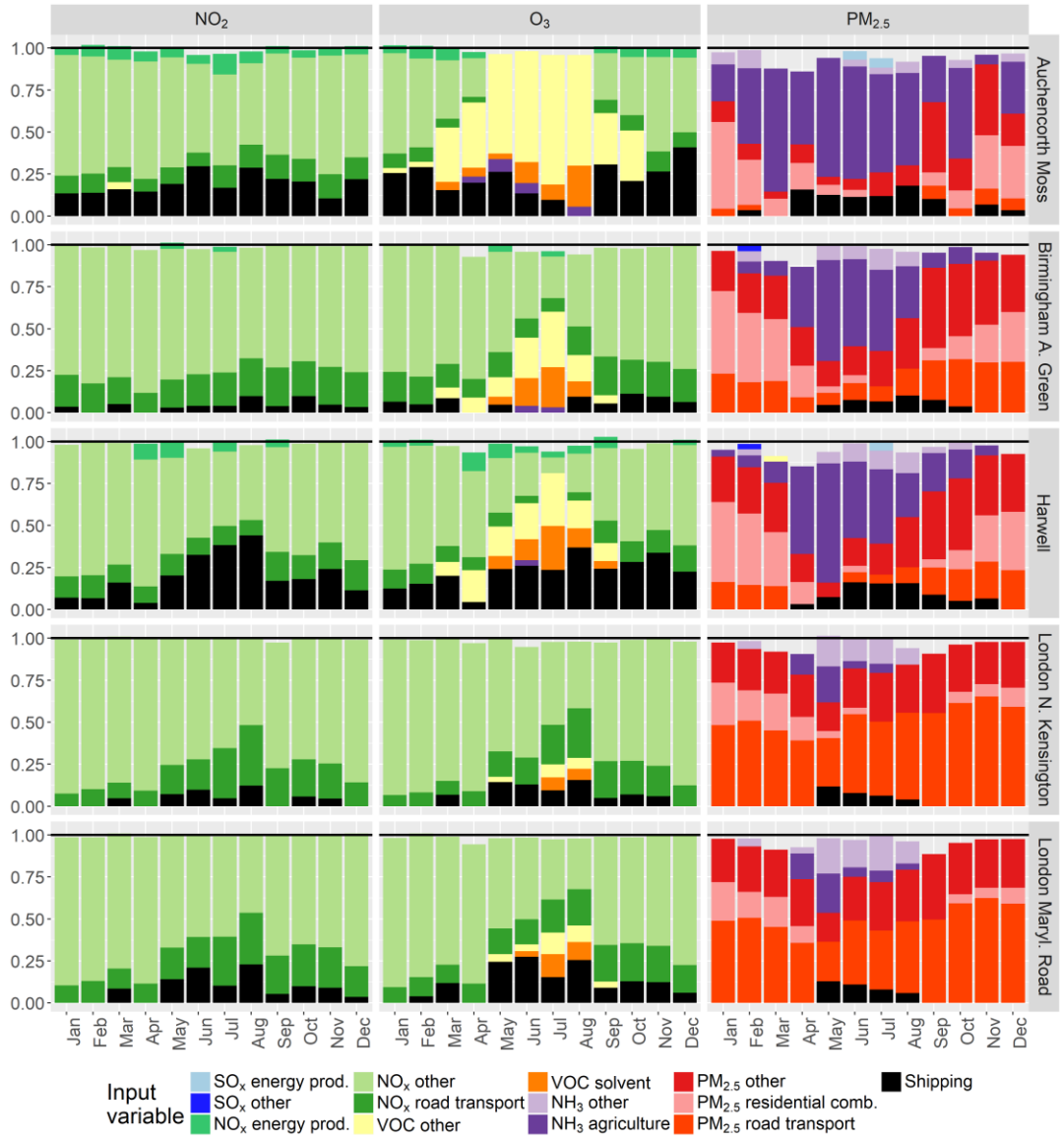

Figure 5.8 Monthly variation in the first-order sensitivity indices for five grid cells across the UK representing a spread of geographical locations and environment types. Based on the monitoring station classification grid squares are assigned the following environment types: Auchencorth Moss and Harwell - rural background, Birmingham Acocks Green and London N. Kensington - urban background, and London Marylebone Road - urban traffic.

5.3.4 Wider implications of this study

There are published studies that apply global sampling-based uncertainty and sensitivity analyses as well as derivative based methods (methods that do not have limitations of local OAT, i.e. linearity assumption) to ACTMs. However, the results reported by these studies are mostly of use for model development and calibration purposes and not the assessment of confidence in the model predictions/outputs. This is mainly because the simulations are performed for a short period ranging from days (Beddows et al., 2017; Chen and Brune, 2012; Rodriguez et al., 2007) to weeks (Cohan et al., 2010; Shrivastava et al., 2016).

Additionally, in some studies, commercial software or packages with a graphical user interface (GUI) are used for global sensitivity and uncertainty analysis (Chen and Brune, 2012; Christian et al., 2017; Lee et al., 2011). These tools are well designed for a specific purpose but lack the option to scale up and to automate the analysis, i.e. ability to calculate sensitivity indices and uncertainty ranges for thousands of grid squares automatically.

The study addresses both of the shortcomings. The study demonstrates sensitivity and uncertainty analyses for the ACTM for a whole year for the UK domain as well as investigate variations in sensitivity and uncertainty on the monthly timescale for multiple locations with different environmental characteristics. Additionally, the package used to create Gaussian process emulators and to conduct uncertainty and sensitivity calculations is fully customisable and can be adapted for any application.

The model runs generated for the global sensitivity and uncertainty analysis can be utilised for other purposes provided that the sampling range for all inputs of interest is wide enough. For example, in this study the training points for the Gaussian emulator were selected to cover a wider range of input perturbations compared to the corresponding uncertainty range (Table 5.2). For all input emissions of SO_x, NO_x, VOC, and NH_3 the ranges of variation for the LHS design were set to ± 40% of their baseline value, for primary $PM_{2.5}$ emissions the range was set to ± 75% and for shipping emissions from – 40% to + 100%. Hence the emulators created in this study using the model runs within the aforementioned input space can be used to investigate

other scenarios of the model response to input emission perturbations with no extra computational cost. Hence, alternative ranges and probability distributions can be assigned to the model inputs to estimate the resulting output uncertainty or the emulator can be used for various emission reduction scenario analyses.

Finally, in this study the overall model output uncertainty is likely to be lower than the theoretical total model output uncertainty, as in addition to the input emissions there is a variety of other uncertain model inputs. Assessing the effect of variation in every model input and parameter on the model output is a laborious task, hence ideally sensitivity analysis should be incorporated as a part of the model development process. By using this approach, the effect of all uncertain inputs and parameters could be assessed without having to do it retrospectively.

5.4 Conclusions

In this study, global sensitivity and uncertainty analyses have been conducted for the EMEP4UK Eulerian atmospheric chemistry transport model to quantify the uncertainty in surface concentrations of O_3, NO_2, and $PM_{2.5}$ and to identify the input emission variables that contribute the most to the uncertainty in each of the outputs. The uncertainty for model outputs was estimated from the uncertainties assigned to the UK emissions of SO_2, NO_x, NH_3, VOC, and primary $PM_{2.5}$ and documented in the UK National Atmospheric Emissions Inventory. The benefit of conducting global sensitivity analysis in addition to uncertainty assessment is that it allows to determine how a model responds to the input perturbations within the ranges set by the input uncertainty estimates and consequently to identify the inputs which cause the variation in the model outputs (i.e. drive the uncertainty). The median values of the overall uncertainty calculated for the UK land-based grid cells for annual average surface concentrations of O_3, NO_2, and $PM_{2.5}$ were found to be in the ranges of ± 0.6%, ± 7.4%, and ± 4.6% respectively. This indicates that the variation in the input data (i.e. emissions) does not cause a substantial variation in the outputs. The results indicate, that this can likely be explained by variations in the other model input parameters such as chemical reaction rates, deposition velocities or physical constant values which

might cause more variation in the model outputs. Alternatively, surface concentrations of the modelled pollutants in the UK may be dominated by the precursor emissions and long-range transport from outside the UK and are therefore relatively insensitive to changes in the UK emissions.

As a consequence, the results can provide more clarity about the confidence in modelled surface concentrations of pollutants that affect human health, especially in densely-populated urban areas. The results of the analysis indicate that modelled surface concentrations of O_3, NO_2, and $PM_{2.5}$ have the highest level of uncertainty in the grid cells comprising dense urban areas. The uncertainties of O_3, NO_2, and $PM_{2.5}$ in these grid cells reach ± 7%, ± 9%, and ± 9% respectively.

In addition to obtaining a quantitative estimate of the overall uncertainty, the input emissions that have the greatest influence on the uncertainty in the modelled outputs were identified by performing a global variance-based sensitivity analysis. It was found that in urban areas uncertainty in $PM_{2.5}$ concentrations are driven by the uncertainty in primary $PM_{2.5}$ emissions. In contrast, in more remote areas NH_3 emissions had a stronger influence. Emissions of NO_x combined from non-dominant sectors (i.e. all sectors excluding energy production and road transport) were found to contribute the most to the uncertainty in both O_3 and NO_2 surface concentrations. Along the south and east coasts of England the uncertainty in shipping emissions contributed the most to the overall uncertainty in O_3 and NO_2 concentrations.

The comparison between first and total-order sensitivity indices did not indicate substantial interactions between the input variables for the model response on the annual timescale.

In this study it was also demonstrated how the degree of uncertainty changes throughout the year by calculating uncertainty ranges for monthly-averaged surface concentrations of O_3, NO_2, and $PM_{2.5}$ for five selected grid cells. The global sensitivity conducted for monthly-averaged values showed seasonal trends in the type of input emissions that drive uncertainty in the surface concentrations.

The ability to estimate uncertainty in the predictions produced by a model is vital, because even low levels of uncertainty could be important in areas where the model yields predictions of surface concentrations that are close to limit values. This can lead to instances of exceedance due to the binary nature of limit value exceedance calculations, i.e. concentration is either over or under the limit. The sensitivity analysis should be an integral part of the assessment process applied *ex-ante* for the implementation of policy interventions, as it is also important to know which of the inputs contribute to the uncertainty in model outputs the most.

This work has demonstrated a global sensitivity and uncertainty analyses application for a Eulerian ACTM. The emulator-based approach used here is applicable to any other complex model and any type of model inputs such as emissions, physical constants or chemical reaction rate constants. The results of the analyses provide useful insights into the level of confidence in modelled predictions. Additionally, the Gaussian process emulators created for this analysis can be used with very little computational cost for any other scenario exploration purposes or assessment of overall uncertainty given different uncertainty ranges and probability distributions assigned to the model inputs.

Chapter 6

Comparative analysis of uncertainty and sensitivity for the FRAME and EMEP4UK models and investigation of an alternative sensitivity measure

6.1 Introduction

The model evaluation guidelines by the US Environmental Protection Agency (EPA, 2009) and the European Environment Agency (EEA, 2011) recommend the implementation of both uncertainty assessment and sensitivity analysis. Nevertheless, for ACTMs model performance evaluation is still carried out mainly by comparing model predictions with historic data. Methods for model evaluation that include uncertainty in both modelled and measured data have been discussed by Monteiro et al. (2018) and Thunis et al. (2012). However, the authors suggest assigning constant relative uncertainty values to model outputs that simply reflect the measurement uncertainty in the corresponding pollutants. This practice of assigning constant relative uncertainty values to the model outputs could result in misleading conclusions when comparing model outputs to the measurement data. Additionally, it is not correct to assume that in different ACTMs, uncertainty from model inputs propagates similarly and results in the same levels of output uncertainty.

This chapter presents the results of comparing the uncertainty ranges calculated for the EMEP4UK model outputs with those calculated for the FRAME model. The model simulations are performed for the year 2012 with the same uncertainty ranges applied to the input emissions. This comparison highlights the difference in the estimated

uncertainty ranges for the outputs of two different models given the same level of uncertainty assigned to the inputs of both models.

Additionally, the uncertainty ranges for the EMEP4UK outputs were calculated using the recent emission uncertainty range estimates from the UK Informative Inventory Report (Wakeling et al., 2017) and the first-order variance based sensitivity coefficients were used to apportion the overall uncertainty. The magnitude and the spatial distribution of the first-order sensitivity indices for EMEP4UK model outputs presented in this chapter were compared to the values for FRAME model outputs presented in Chapter 4 to highlight the differences in the uncertainty apportionment.

Finally, the use of Pearson product-moment correlation coefficients as the sensitivity measure is investigated and discussed. The Pearson product-moment correlation coefficients were estimated for the EMEP4UK model from the re-sampled data obtained using the emulator, which is described in Chapter 5.

6.2 Methods

6.2.1 Uncertainty propagation and first order sensitivity indices

The uncertainty propagation methods used in this chapter for the EMEP4UK output variables are described in Chapter 5. The overall uncertainty in the model outputs was calculated with two separate sets of uncertainty ranges assigned to the inputs. The first set of input uncertainties contained the ranges for 13 model inputs as listed in Table 5.2. In the second set all SO_x input emissions were assigned an uncertainty of ± 4%, and all NO_x and all NH_3 emissions were assigned uncertainties of ± 10%, and ± 20% respectively. The VOC and $PM_{2.5}$ input emissions were set to their baseline value and the shipping emissions were assigned an uncertainty of ± 10%. A uniform distribution was assumed for all aforementioned input variables to match the methods of uncertainty propagation used for the FRAME model (Chapter 4). This was done to

allow direct comparison between the predicted uncertainty ranges for the EMEP4UK and FRAME model output variables.

The first-order sensitivity indices presented in this chapter were calculated as described in Chapter 5; Table 5.2 lists the variation ranges for the input variables included the calculation.

6.2.2 Pearson correlation coefficients

The EMEP4UK simulation data (i.e. the input samples and the corresponding model outputs described in Chapter 5) was used to investigate the suitability of Pearson correlation coefficient as a sensitivity measure for the model sensitivity analysis. For this purpose, the range of variation for all 13 EMEP4UK input variables was set to ± 40%. The Pearson correlation coefficient values were estimated using the UQLab module (Marelli and Sudret, 2014) by creating an emulator based on the simulation input-output EMEP4UK data and subsequently re-sampling the input space and estimating model predictions at the new sampling points.

6.3 Results and discussion

6.3.1 Uncertainty ranges

Figure 6.1 summarises the distributions of relative uncertainty ranges across all model land-based grid cells for each EMEP4UK output with a corresponding FRAME output when SO_x, NO_x, and NH_3 input emissions for both models were assigned the same uncertainty ranges. In contrast, Figure 6.2 illustrates the distribution of relative uncertainty values cross all model land-based grid cells for EMEP4UK outputs when uncertainties in the emissions of all of SO_x, NO_x, VOC, NH_3, and $PM_{2.5}$ are taken into account (ranges listed in Table 5.2). To aid the comparison, the median values of the distributions presented in the box plots are summarised in Table 6.1.

Figure 6.1 shows that for most output variables, EMEP4UK distributions of relative uncertainty values across all land-based grid cells display lower median values and

narrower interquartile ranges compared to those for FRAME. The exception is the surface concentration of NH_3; for this output, both models estimate a median uncertainty of 19.8% and those from EMEP4UK display a wider variation of uncertainty values. Additionally, the relative uncertainty for wet and dry deposition of reduced nitrogen (NH_x) from the EMEP4UK model has a noticeably wider spread of values than from the FRAME model.

The spatial distribution of relative uncertainty values for surface concentrations of NH_4^+, SO_4^{2-}, NO_3^-, and dry and wet deposition of oxidised sulfur (SO_y), for the EMEP4UK model is presented in Figure 6.3. The relative uncertainty ranges in Figure 6.3 are plotted on the same scale and with the same colour scheme as the uncertainty ranges for the FRAME model outputs in Figure 4.5, which allows the direct comparison of the spatial distribution of the ranges estimated for the two models.

The spatial variability pattern for the relative uncertainty for NH_4^+ and NO^{3-} was found to be similar for both the EMEP4UK and FRAME models (Figs. 4.5 and 6.3); the lowest levels of relative uncertainty were found in the south-east England area. The uncertainty ranges for SO_4^{2-} concentrations estimated with EMEP4UK were less spatially variable and did not display the increase seen in the FRAME output for the Scotland area. Additionally, the relative uncertainty for the dry and wet deposition of SO_y modelled with EMEP4UK was found to have greater spatial variability with the higher relative uncertainty values occurring close to the location of SO_2 emission point sources (especially pronounced in Figure 6.3(b)).

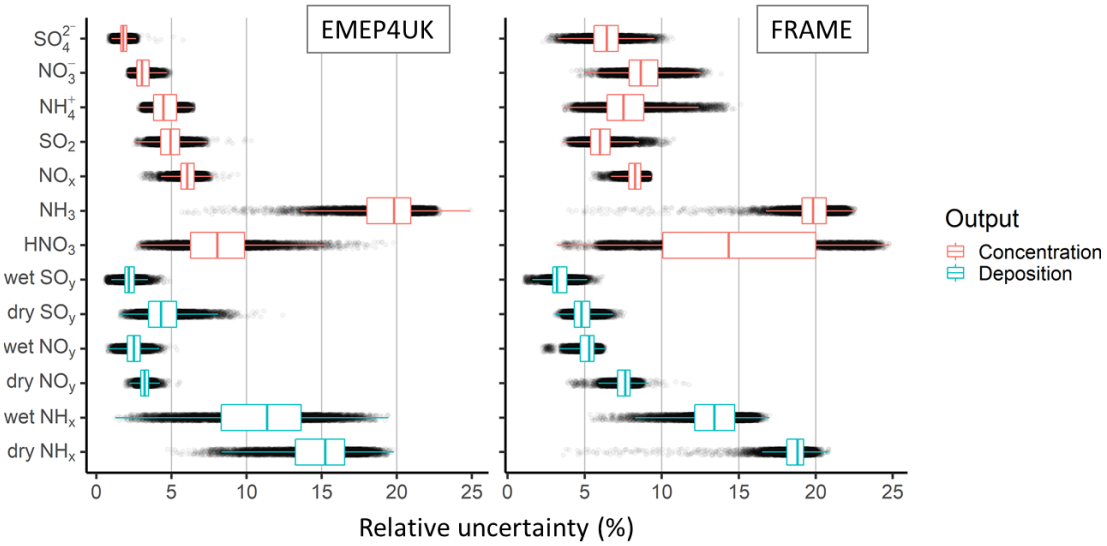

Figure 6.1 Box plots illustrating the distribution of relative uncertainty values calculated for all land-based grid cells for EMEP4UK and FRAME model outputs. The input uncertainty ranges are ± 4%, ± 10%, and ± 20% for the emissions of SO_x, NO_x, and NH_3 respectively. The boxplot represents median and first and third quartiles; the whiskers extend to 1.5 times the interquartile range.

Figures 6.2 and 6.3(b) demonstrate the distribution of the uncertainty ranges for EMEP4UK model outputs for the case when the model inputs were assigned the uncertainty ranges listed in Table 5.2. These uncertainty ranges were estimated from the latest UK Informative Inventory Report (IIR) (Wakeling et al., 2017) and are on average higher than the uncertainty ranges used for the study with the FRAME model, which were obtained from an earlier version of the IIR report (Misra et al., 2015). The increase in the input uncertainty caused the shift towards higher relative uncertainty values for the EMEP4UK model outputs (Fig. 6.2) but did not have a noticeable effect on the spatial distribution of the relative uncertainty (Fig. 6.3).

The difference in the median values and the distributions of the uncertainty ranges predicted for the FRAME and EMEP4UK models is most likely to be due to different representation of physical and chemical processes in the model. For example, changes in meteorological parameters such as wind speed and direction or rainfall can have a dramatic effect on pollutant transport and removal processes.

After considering possible differences in how pollutants are transformed and transported in the EMEP4UK and FRAME models the difference in the overall uncertainty estimated for the outputs of the two models remains unexplained. However, this is a clear demonstration of how uncertainty in complex models cannot be readily predicted and consequently of the need for quantitative uncertainty analysis for any model that is used.

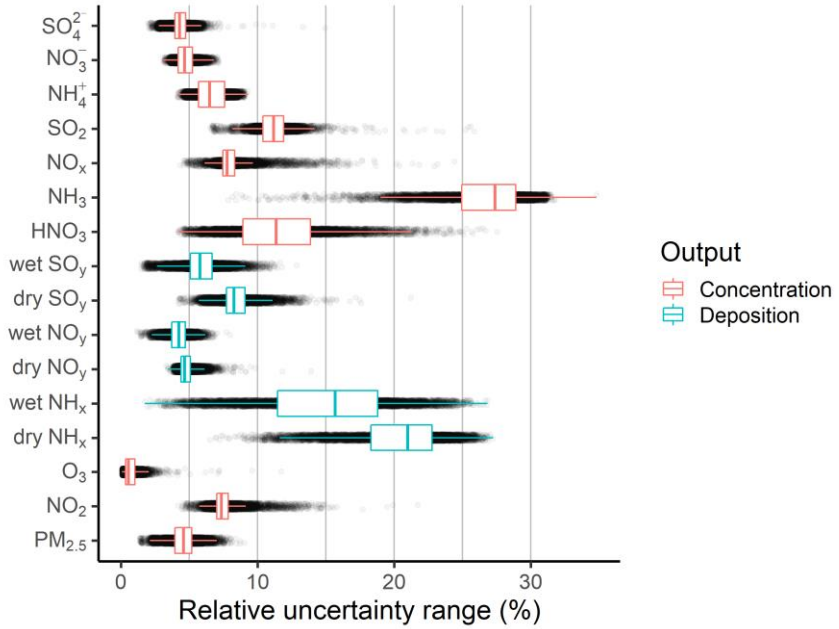

Figure 6.2 Box plots illustrating the distribution of relative uncertainty values calculated for all land-based grid cells for EMEP4UK model outputs. The uncertainty ranges for the input emissions of SO_x, NO_x, NH_3, VOC, and $PM_{2.5}$ split by source sector are reported in Table 5.2. The boxplot represents median and first and third quartiles; the whiskers extend to 1.5 times the interquartile range.

Table 6.1 Median values of uncertainty ranges across all land-based grid cells for FRAME and EMEP4UK model outputs (common output variables).

Variable	Median uncertainty for FRAME from Fig. 6.1 / %	Median uncertainty for EMEP4UK from Fig. 6.1 / %	Median uncertainty for EMEP4UK from Fig. 6.2 / %
SO_4^{2-}	6.4	1.8	4.3
NO_3^-	8.6	3.0	4.7
NH_4^+	7.5	4.5	6.5
SO_2	6.0	4.9	11.2
NO_x	8.3	6.1	7.8
NH_3	19.8	19.8	27.4
HNO_3	14.4	8.1	11.3
Wet SO_y	3.2	2.2	5.8
Dry SO_y	4.8	4.3	8.3
Wet NO_y	5.3	2.5	4.2
Dry NO_y	7.6	3.2	4.7
Wet NH_x	13.4	11.4	15.7
Dry NH_x	18.8	15.2	21.0

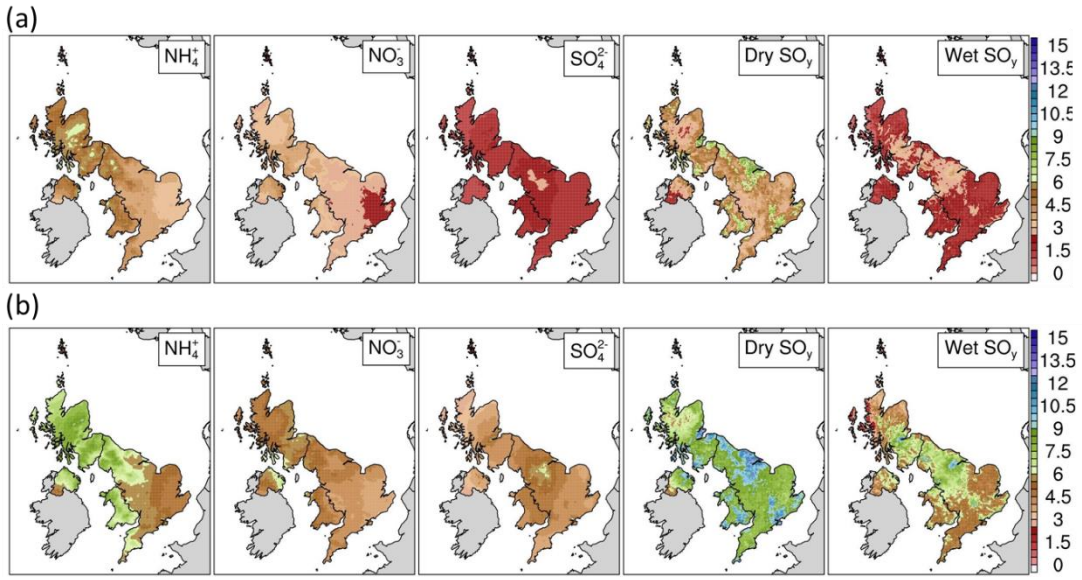

Figure 6.3 Spatial distribution of the relative uncertainty ranges at the 5 km × 5 km grid resolution for the EMEP4UK model outputs. Scale bar in %. Panel (a) illustrates the uncertainties propagated from the uncertainty ranges of ± 4%, ± 10%, and ± 20% for the input emissions of SO_x, NO_x, and NH_3 respectively. Panel (b) illustrates the uncertainties propagated from the input emissions of SO_x, NO_x, NH_3, VOC, and $PM_{2.5}$ split by source sector as reported in Table 5.2.

6.3.2 Uncertainty apportionment

The first-order sensitivity indices discussed in this section represent the fractional contribution of the uncertainty in the input emissions (the input variables and corresponding ranges are listed in Table 5.2) to the overall uncertainty in the EMEP4UK model outputs illustrated in Figures 6.2 and 6.3(b).

Figures 6.4 and 6.5 summarise the distribution of first-order sensitivity indices calculated for the concentration and deposition output variables, for land-based grid cells. These boxplots were used to identify the inputs that contribute most to the uncertainty of a given output and to assess the magnitude of that contribution. Figures 6.6 and 6.7 show the spatial distribution of the first-order sensitivity indices for the

surface concentrations of particulate NH_4^+, NO_3^-, and SO_4^{2-}, as well as for the wet and dry deposition of SO_y.

The magnitudes of the first-order sensitivity indices estimated for the EMEP4UK model cannot be directly compared to those estimated for the FRAME model (FRAME sensitivity indices are presented in Chapter 4) because the input emissions for the EMEP4UK model were split not only by pollutant species but also by source sector. Additionally, the uncertainty ranges assigned to the EMEP4UK inputs were generally higher. However, the spatial distribution of the contribution of the uncertainty in different pollutant species to the overall uncertainty can be compared for the two models.

As for the FRAME model, uncertainty in NH_4^+ output from the EMEP4UK model is mainly driven by the uncertainty in NH_3 emissions (Figs. 4.6 and 6.6). The sensitivity index maps in Figure 6.6 show that for NH_4^+ ammonia emissions from non-agricultural sources (NH_3_O) show the greatest effect on the uncertainty in the London area. Likewise, uncertainty in the surface concentrations of NH_3 and NO_x is affected by the uncertainty in the emissions of corresponding pollutants.

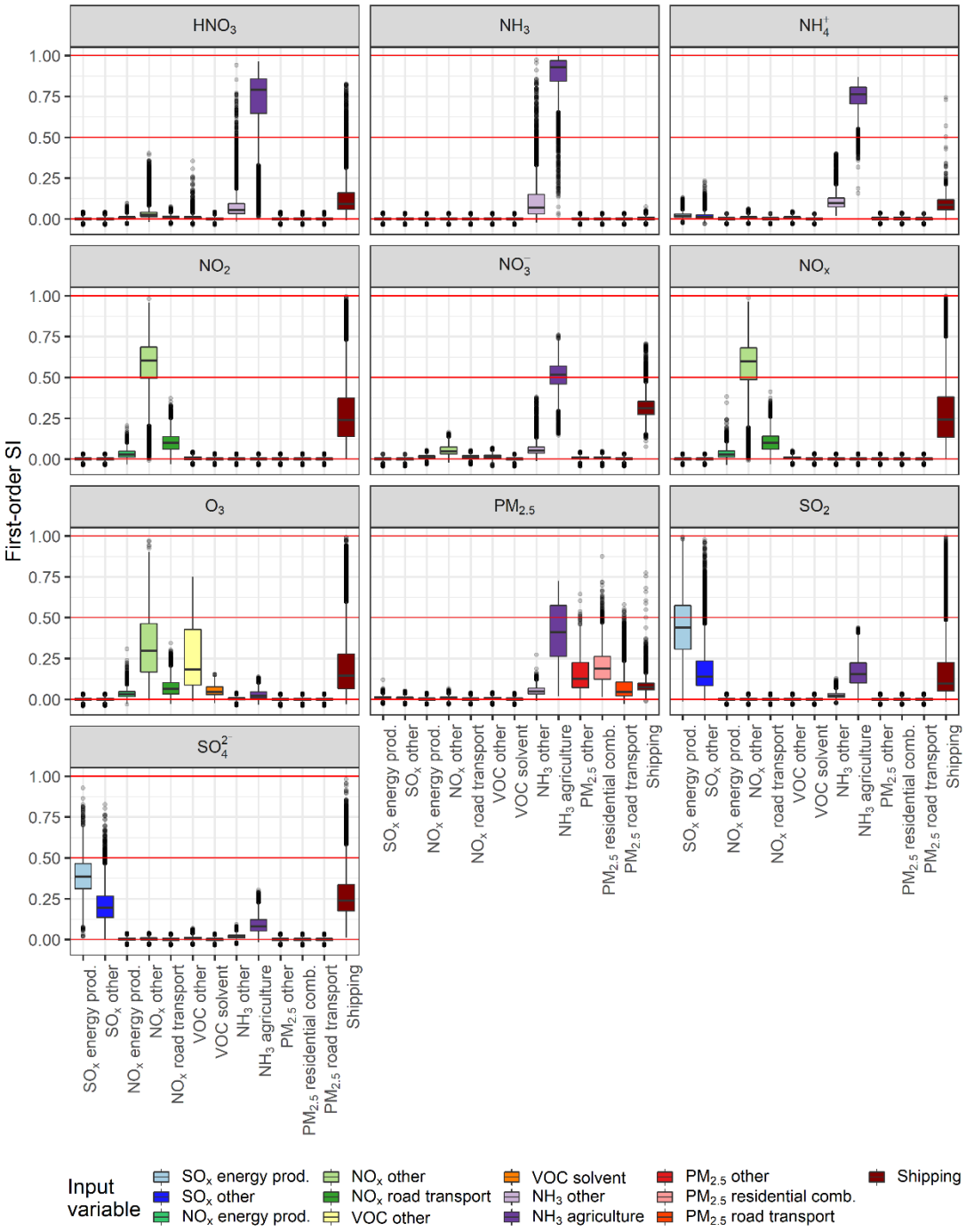

Figure 6.4 Box plots of first-order sensitivity indices for the EMEP4UK surface concentration output variables. Boxes represent median and lower and upper quartiles; the whiskers extend to 1.5 times the interquartile range.

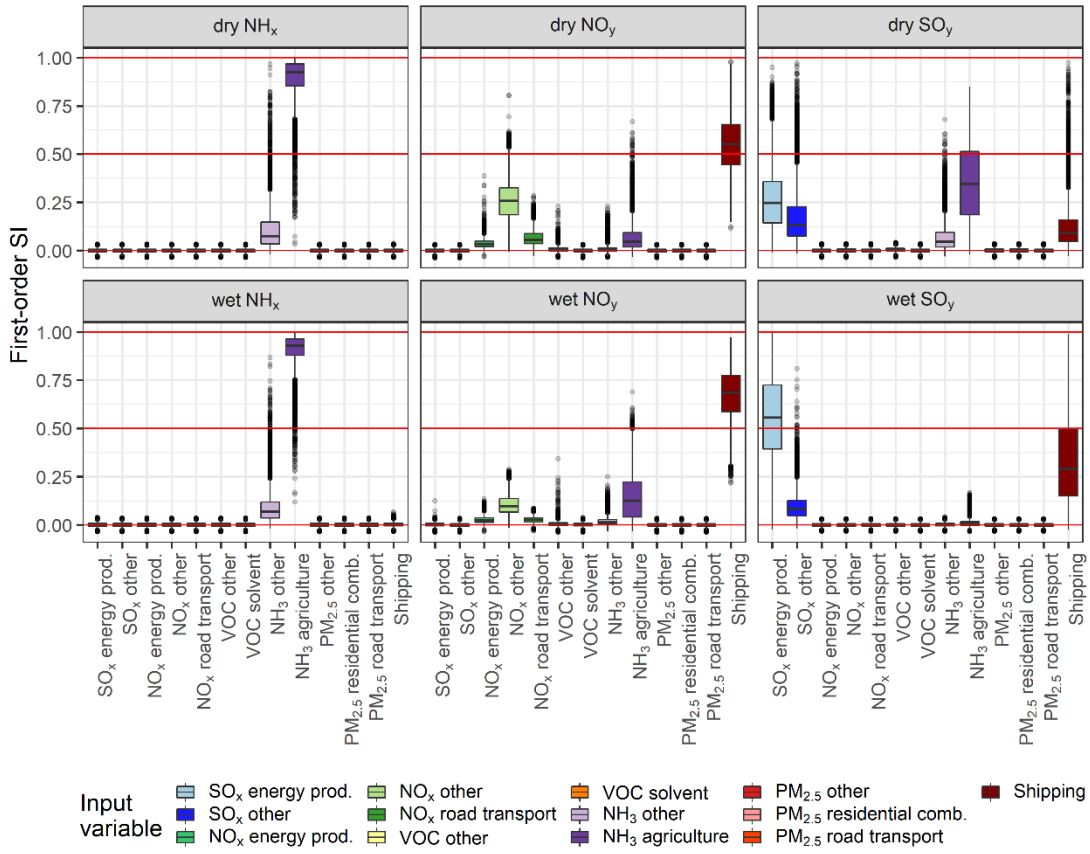

Figure 6.5 Box plots of first-order sensitivity indices for the EMEP4UK deposition output variables. Boxes represent median and lower and upper quartiles; the whiskers extend to 1.5 times the interquartile range.

Unlike in the FRAME model results, uncertainty in SO_4^{2-} is affected but not dominated by the uncertainty in NH_3 emissions. The reason for this could be the wider uncertainty range assigned to the SO_x input emissions in the EMEP4UK model: ± 12% for SO_x from energy production and ± 17% for SO_x from other sources, compared to ± 4% uncertainty range for SO_x emissions in the FRAME model. The uncertainty in NO_3^- for the EMEP4UK model was found to be mainly driven by the uncertainty in the agricultural emissions of NH_3 and not by NO_x emissions (Figs. 4.6 and 6.6). This can be the result of increased uncertainty levels assigned to the EMEP4UK NH_3 input emissions (± 33% for agricultural and ± 35% for non-agricultural emissions compared to ± 20% for all NH_3 emissions in FRAME) combined with the difference between the description of the NO_3^- formation chemistry in the models. Additionally, uncertainty

in NH_3 emissions was not found to have a strong impact on the wet SO_y deposition, in contrast to the FRAME model (Figs. 4.7 and 6.7).

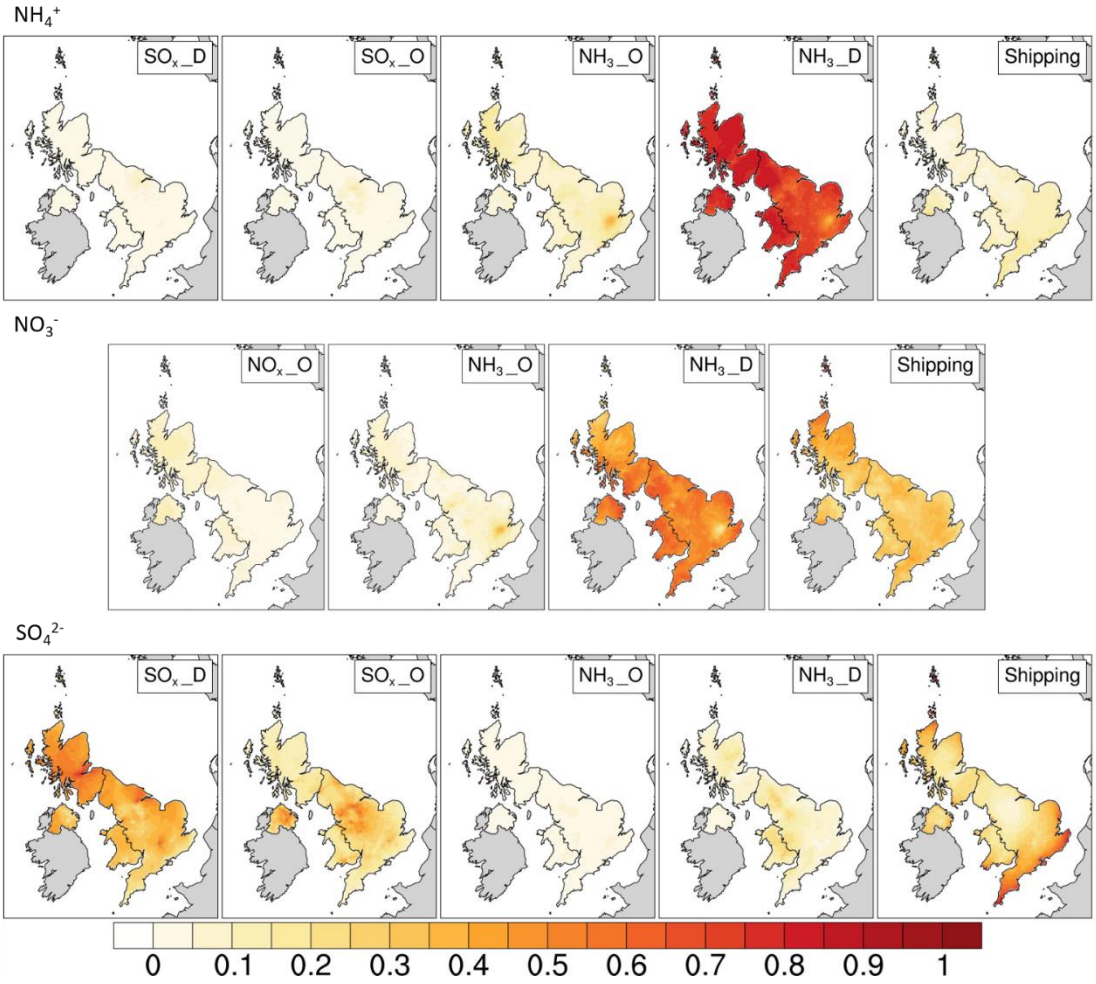

Figure 6.6 Spatial distributions from the EMEP4UK model of the first-order sensitivity indices that represent fractional contribution of the uncertainty in the given input emissions to the overall uncertainty in the surface concentrations of particulate NH_4^+, NO_3^-, and SO_4^{2-}. Input emission variable definitions are presented in Table 5.2.

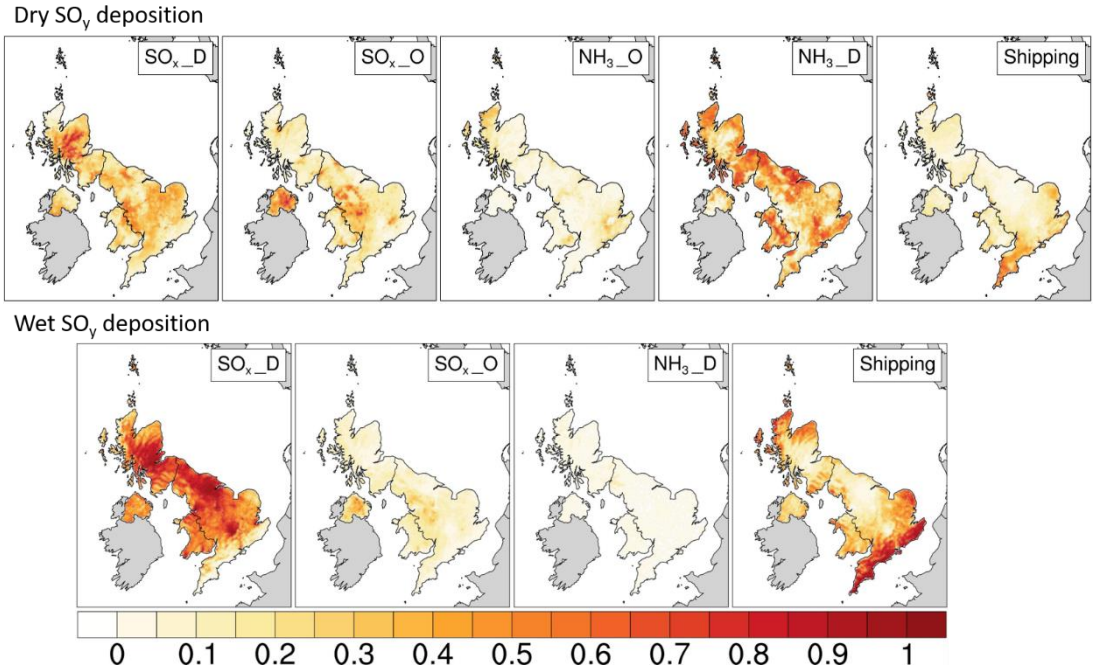

Figure 6.7 Spatial distributions from the EMEP4UK model of the first-order sensitivity indices that represent fractional contribution of the uncertainty in the given input emissions to the overall uncertainty in the wet and dry deposition of SO_y. Input emission variable definitions are presented in Table 5.2.

6.3.3 Pearson correlation coefficient

The Pearson product-moment correlation coefficient is still widely used as an sensitivity measure for estimating the sensitivity of model outputs to the variations in inputs (Borgonovo, 2006; Borgonovo and Plischke, 2016; Gan et al., 2014; Iooss and Lemaître, 2015). It can be seen as an indicator of goodness of linear fit between the input variable X_j and output variable Y. However, it only identifies the strength of linear relationship between the input and output variables and not the strength of the actual response of the output to changes in the input.

Figures 6.8 and 6.9 display the summary box plots for Pearson correlation coefficients calculated for various EMEP4UK output variables. The data presented in the figures indicates that only a few output variables have a strong linear relationship with one or

more inputs, i.e. surface concentrations of NH_3 and NH_3 emissions from agricultural sources or surface concentrations of SO_2 and SO_x emissions from the energy production industry. In addition to the strength of the linear relationship, Pearson correlation coefficients indicate the direction of the relationship.

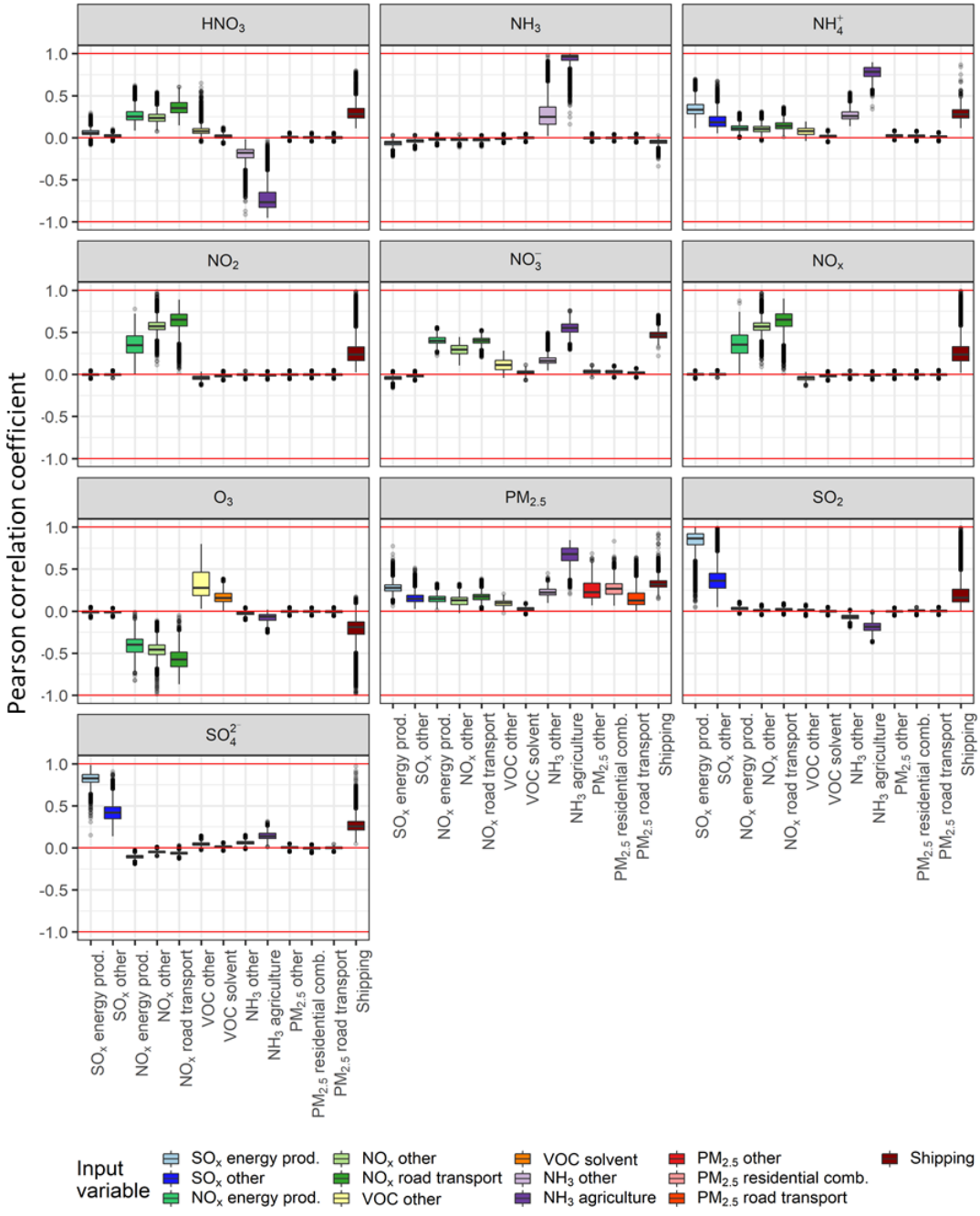

Figure 6.8 Box plots summarising the Pearson correlation coefficients for the EMEP4UK surface concentration output variables. Boxes represent median and lower and upper quartiles; the whiskers extend to 1.5 times the interquartile range.

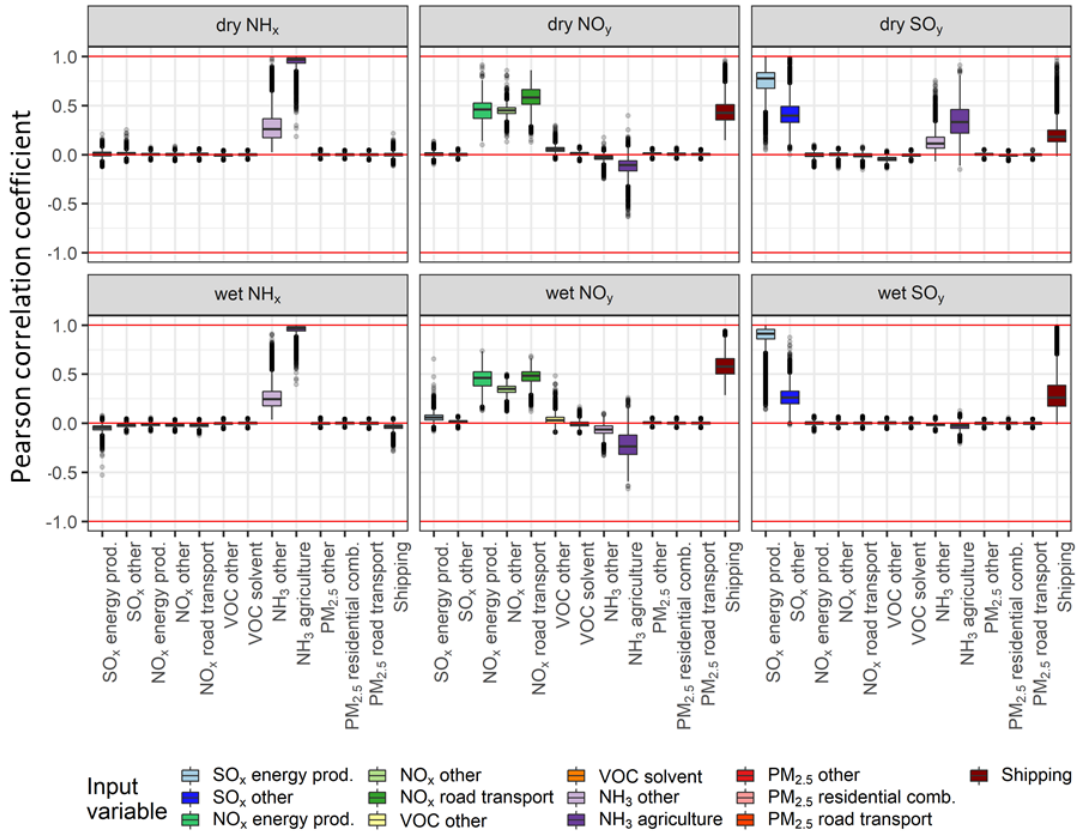

Figure 6.9 Box plots summarising the Pearson correlation coefficients for the EMEP4UK deposition output variables. Boxes represent median and lower and upper quartiles; the whiskers extend to 1.5 times the interquartile range.

Using only Pearson correlation coefficients as a sensitivity measure can result in misleading conclusions. The main reason for this is that the strength of the response is not taken into account. Figure 6.10 illustrates the spatial distribution of the Pearson correlation coefficients calculated for the surface concentration of O_3 modelled with EMEP4UK. The maps indicate the presence of strong inverse linear relationships between O_3 concentrations and NO_x emissions in most areas as well as between O_3 concentrations and shipping emissions along the coast in south England. However, Figure 6.11 shows the spatial distribution of regression coefficients (RCs) that represent the relative effect of changing an input X_i on the output Y (the detailed description of RCs and their interpretation is provided in Chapters 3 and 4). From these plots it can be concluded that although the surface concentrations of O_3 have a strong

linear relationship with NO_x emissions, the magnitude of the O_3 response is relatively low (RC = -0.1 indicates a 3% decrease in O_3 concentration in response to 30% decrease ion NO_x emissions).

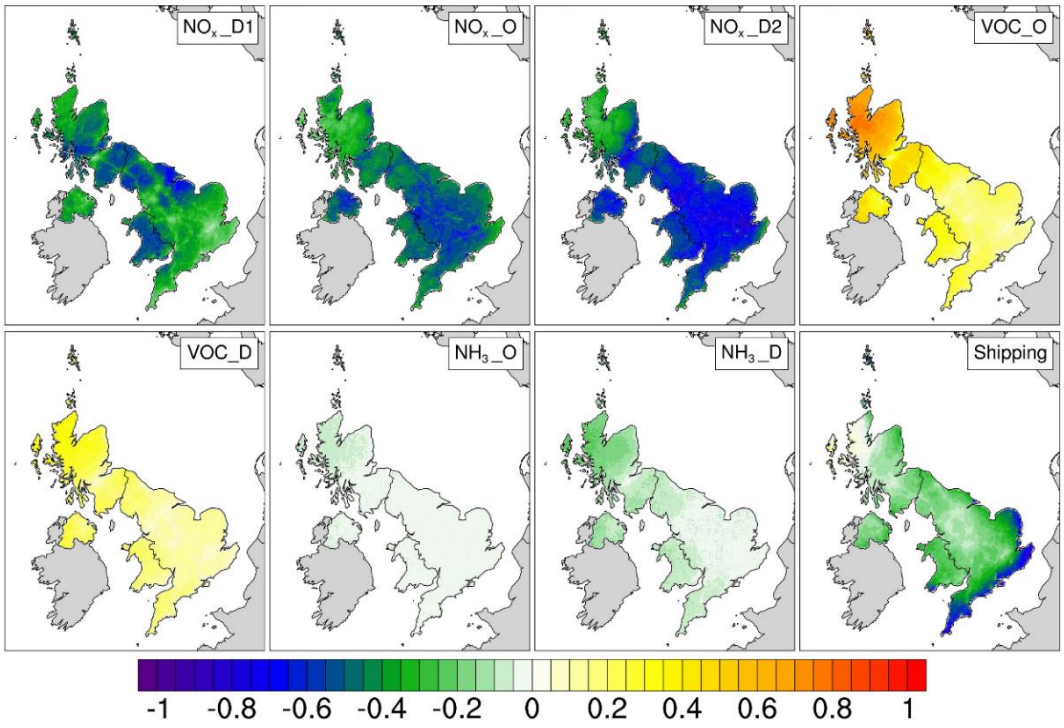

Figure 6.10 Spatial distributions of the Pearson correlation coefficients for the surface concentration of O_3 modelled with EMEP4UK (input variable definitions are presented in Table 5.2).

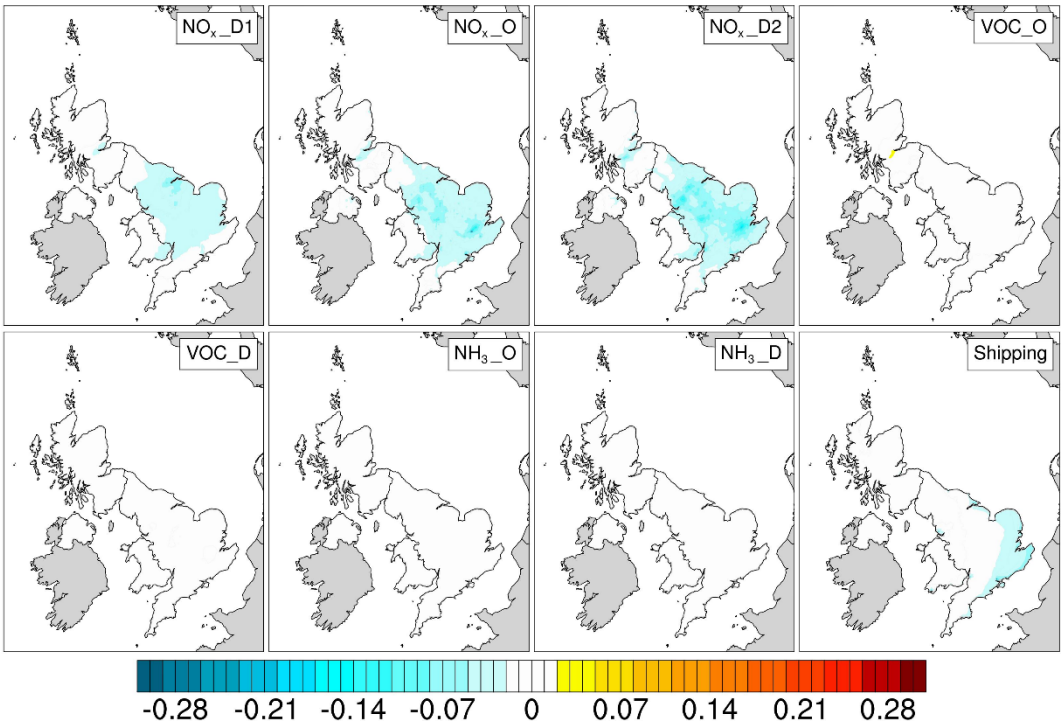

Figure 6.11 Spatial distributions of the regression coefficient (RC) values for the surface concentrations of O_3 modelled with EMEP4UK (detailed description of how RCs are estimated and interpreted can be found in Chapters 3 and 4). The RC values represent the relative effect of varying a specific input on the surface concentration of O_3 (input variable definitions are presented in Table 5.2).

6.4 Conclusions

The comparison between the magnitude and spatial distribution of the relative uncertainty values for the EMEP4UK and FRAME models presented in this Chapter demonstrates that similar levels of uncertainty assigned to the input emissions of the two models do not result in similar ranges of uncertainty for the outputs. On average, the median values of uncertainty ranges for different model outputs calculated for the land-based grid cells of the EME4UK model domain were found to be lower compared to the median values for the corresponding FRAME model outputs. No specific explanation was found for this observed difference. This leads to the conclusion that ranges of uncertainty for different model outputs are model specific and results obtained for one model cannot be directly transferred to another.

Analysis of first-order sensitivity indices for the EMEP4UK model indicated that the overall uncertainty in FRAME and EMEP4UK is not always driven by the uncertainty in the emissions of the same pollutants. For example, the uncertainty in NO_3^- for the EMEP4UK model was found to be driven by the uncertainty in the agricultural emissions of NH_3 and not NO_x emissions as was identified for the FRAME model. The reason for the differences observed for the two models can range from the conceptually different representation of physical and chemical processes in the models, to finer detail such as exact emission input definition and differences in the uncertainty ranges assigned to the input emissions. It is not possible to identify the specific reasons for the discrepancies without fully exploring the effect of the variation in different chemical and physical processes on the model outputs.

Finally, the applicability of the Pearson product-moment correlation coefficient as a sensitivity measure for ACTMs was assessed. Despite the fact that the Pearson correlation coefficient is applicable only in the presence of linear input-output relationships (and that some level of non-linearity is expected in the response of ACTM outputs to changes in the inputs), its ease of calculation and interpretation make it a worthwhile measure for model input-output relationship assessment in conjunction with other sensitivity measures.

Chapter 7

Conclusions and future work

This work has demonstrated the application of uncertainty assessment and global sensitivity analysis to complex atmospheric chemistry transport models (ACTMs), using the FRAME and EMEP4UK models as examples. Unlike commonly-used one-at-a-time sensitivity analysis, global sensitivity analysis does not require an assumption of linearity and additivity in model responses to input perturbations and can hence be used to identify the presence of interactions between input data. For complex models such as ACTMs, for which input-output mapping is not analytically tractable, these characteristics make global sensitivity analysis a valuable tool for investigating model behaviour.

The main disadvantage of the Monte Carlo based uncertainty propagation methods and global sensitivity analysis is that they require a large number of model simulations to be performed, which is too computationally expensive for most ACTMs. In order to overcome this impediment, an emulation-based approach to sensitivity analysis and uncertainty assessment was investigated and implemented in this study.

Although the sensitivity and uncertainty results presented in this thesis are model-specific, the methodologies demonstrated here can inform similar studies and be applied to other ACTMs.

7.1 Summary of the results

7.1.1 FRAME

The response of the FRAME model outputs to the perturbations in the input emissions of three pollutants, SO_2, NO_x, and NH_3, within a ± 40% range was investigated. No substantial deviations from linearity or presence of interactions between the model input variables were identified for the model in response to the described range of input emission perturbations.

The FRAME model responses were shown to be close to linear over the perturbation range investigated, which means that the regression coefficients (RCs) obtained from the multiple linear regression performed on FRAME input-output data relationships can be used as a useful model response indicator. The RC represents the relative effect of changing a single input on the model output of interest given that all other inputs are allowed to vary and acts as a scaling factor, i.e. RC = 0.5 indicates there is a 15 % reduction in the output in response to a 30 % reduction in the input.

In the FRAME model, the sensitivity of surface concentrations of the primary trace gases (SO_2, NO_x and NH_3) and of deposition of S and N was dominated by the emissions of a single corresponding pollutant. In contrast, the sensitivities of secondary species (HNO_3, SO_4^{2-}, NO_3^- and NH_4^+) to pollutant emissions were more complex, as well as spatially variable. Overall the dry deposition output variables showed stronger response to changes in the emissions compared to wet deposition.

Additionally, the uncertainty ranges for all FRAME model output variables were estimated from the uncertainty ranges attributed to the official UK emissions of SO_2, NO_x and NH_3 (± 4 %, ± 10 % and ± 20 % respectively) by the UK National Atmospheric Emissions Inventory. The spatial distribution of the relative uncertainty ranges estimated for FRAME output variables was found to be affected both by the sensitivity of the model output to variations in the inputs and the magnitude of this variation (i.e. the input uncertainty range).

The analysis of FRAME input-output relationships demonstrated that although the response to emission perturbations was found to be linear in the ± 40 % range, the geographical pattern of sensitivity and uncertainty cannot be predicted without conducting global uncertainty and sensitivity analyses.

7.1.2 EMEP4UK

For investigation of the EMEP4UK model the range of uncertainty in input emissions was increased. In total, 13 input variables representing anthropogenic emissions of SO_2, NO_x, NH_3, VOC, primary $PM_{2.5}$, and shipping emissions were perturbed. The study concentrated on quantifying uncertainty in the surface concentrations of pollutants relevant to human health: O_3, NO_2, and $PM_{2.5}$. The input emission variables that contribute the most to the uncertainty in each of the outputs were also identified. Lastly, the comparison of first-order and total sensitivity indices led to the conclusion that there were no significant interactions between the input variables.

The median values of the overall uncertainty calculated for the UK land-based grid cells for annual average surface concentrations of O_3, NO_2, and $PM_{2.5}$ were found to be relatively low (± 0.6 %, ± 7.4 %, and ± 4.6 % respectively). This was an unexpected result given that primary $PM_{2.5}$ emissions have a ± 58 % uncertainty, and that O_3 and NO_2 precursor variables (NOx and VOC emission variables) were assigned uncertainty ranges between ± 7 % and ± 24 %. This indicates that the variation in the input data (i.e. emissions) does not cause a substantial variation in the outputs.

A plausible explanation for this is that variations in the other model input parameters such as chemical reaction rates, deposition velocities or physical constant values might contribute more to the variation in the model outputs. Alternatively, surface concentrations of the modelled pollutants in the UK may be dominated by precursor emissions and formation of secondary pollutants outside of the UK, which are then transported to the UK, and are therefore relatively insensitive to changes in the UK emissions.

The highest levels of uncertainty for O_3, NO_2, and $PM_{2.5}$ surface concentrations were found in the grid cells comprising dense urban areas. The uncertainties in these grid cells for the three pollutants reached ± 7%, ± 9%, and ± 9% respectively.

The inputs that contribute the most to the estimated uncertainty were determined by performing a global variance-based sensitivity analysis. In urban areas uncertainty in $PM_{2.5}$ concentrations was found to be driven by the uncertainty in primary $PM_{2.5}$ emissions. In comparison, NH_3 emissions had a stronger influence in more remote rural areas. Emissions of NO_x combined from non-dominant sectors (i.e. all sectors excluding energy production and road transport) were found to contribute the most to the uncertainty in both O_3 and NO_2 surface concentrations.

7.1.3 Comparison results

The comparison between the magnitude and spatial distribution of the relative uncertainty values for the EMEP4UK and FRAME models leads to the conclusion that results obtained for one model cannot be directly transferred to another. In a case where the same uncertainty ranges were assigned to the input emission variables, the output species modelled by both the EMEP4UK and FRAME models were found to have substantially different estimated uncertainty. Additionally, differences in the main inputs driving the uncertainty were identified. For example, the uncertainty in NO_3^- from the EMEP4UK model was driven by the uncertainty in the agricultural emissions of NH_3 whilst uncertainty in the same output from the FRAME model was driven by the NO_x emissions.

It was concluded that the differences observed for the two models could stem from the conceptually different representation of physical and chemical processes in the model and hence sensitivity analysis should be conducted for a wider range of uncertain model parameters and inputs.

7.2 Future work

The global sensitivity analysis and uncertainty assessment presented in this thesis concentrates on the relationships between model input emissions and model outputs. The methods and results discussed provide useful insights into model behaviour. However, in addition to the uncertainties in the emission data that are being directly used as input to an ACTM, there are a large number of other uncertain parameters, such as chemical reaction rates, land-cover data, or deposition parameters, that could potentially be investigated. For example the study by Beddows et al. (2017) which utilised the Community Multiscale Air Quality model concludes that O_3 concentrations are most sensitive to the changes in boundary conditions and changes in NO_2 photolysis reaction rate.

The data quality objectives for ambient air quality assessment specified by the European commission (EC Directive, 2008) requires uncertainty in $PM_{2.5}$ measurements not to exceed ± 25 % for more than 10 % of measurements. Measurement of $PM_{2.5}$ is likely not to strictly meet this objective and Thunis et al. (2012) suggest it is appropriate to assign the ± 25 % uncertainty to both the observational data and model predictions for model performance evaluation purposes.

Figure 7.1 illustrates a short time series of measured and modelled concentrations of $PM_{2.5}$ for two different locations in the UK. In this figure observations are assigned ± 25 % uncertainty and EMEP4UK model outputs are reported with the relative uncertainty calculated given the input emissions uncertainty described in Chapter 5 (Table 5.2). The uncertainty in model predictions shown in the figure is very low. This result indicates that accounting only for the uncertainty in the input emissions might not be sufficient and that other uncertain model parameters should be investigated.

There are various reasons for the discrepancies between modelled and measured data points. In ACTMs concentration and deposition outputs are calculated as spatially averaged values; for the EMEP4UK model the outputs are averaged over a 5 km × 5 km grid square with a vertical layer height of ~90 m. The best practice in model performance assessment up to date is to compare these averaged values to the

measurements obtained at a single point in space. This in itself is an issue as a single point might not be representative of a whole model grid volume. This conventional way of evaluating model performance (Fig. 7.1) does not provide model developers and users with the information about what drives the model and whether there is a potentially misrepresented process or a conceptual error present in the model. Therefore, methods that concentrate more on exploring model response to various uncertain inputs and parameters should be included as an essential part of the model assessment, development, and evaluation processes.

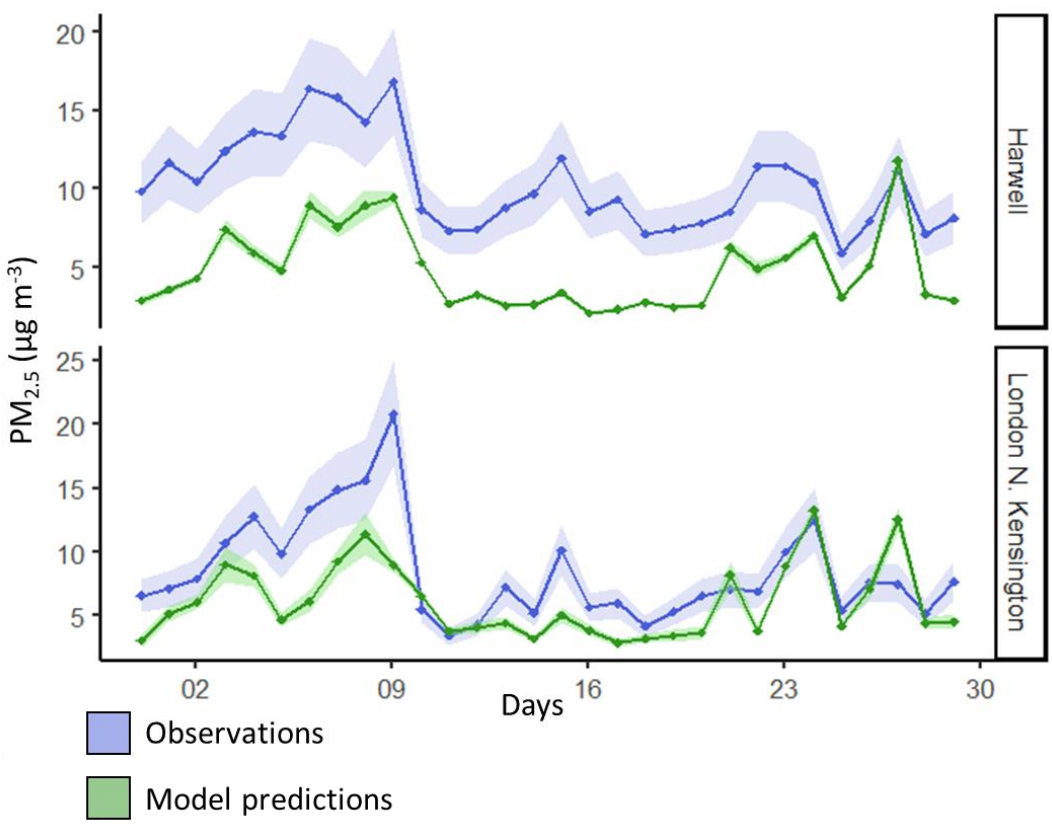

Figure 7.1 Example of comparison of modelled (EMEP4UK) and measured values of $PM_{2.5}$ for a single month (September 2012). The coloured area represents uncertainty. The uncertainty in the measurement data is set to a constant value ± 25%, the uncertainty in modelled values is propagated from the uncertainty in the input emissions.

In order to make sensitivity and uncertainty analysis more accessible for both ACTM developers and users further work on development of suitable emulators is required.

For example, the efficiency of the emulation approach described in Chapter 5 can be improved by treating the whole modelled domain as a continuous spatial field. This approach results in a single emulator for the whole domain instead of a separate emulators for each grid square, which in turn improves the computational efficiency related to the application of the emulator for the sensitivity and uncertainty analyses. However, due to the high spatial variability in the pollutant concentrations modelled with ACTMs, the creation of a single well-performing emulator is difficult. In conclusion the sensitivity and uncertainty analysis methods described and applied in this thesis have been shown to provide valuable information for both atmospheric chemistry transport model developers and users. It has been demonstrated that uncertainty estimation is integral for any model that is used to support a decision-making process. In addition, it was shown that model uncertainty ranges and their spatial distributions are not transferable to other models that runs over the same domain. Combined together uncertainty and sensitivity analysis help to achieve better understanding of how model outputs are driven by various inputs and if a model is performing adequately. Although uncertainty propagation and sensitivity analysis remain time and resource intensive, the current and future developments in high performance computing and emulation techniques are making them more accessible.

References

Air Quality Expert Group: Mitigation of United Kingdom PM 2.5 Concentrations. [online] Available from: https://uk-air.defra.gov.uk/assets/documents/reports/cat11/1508060903_DEF-PB14161_Mitigation_of_UK_PM25.pdf (Accessed 15 May 2018), 2013.

Anderson, J. O., Thundiyil, J. G. and Stolbach, A.: Clearing the Air: A Review of the Effects of Particulate Matter Air Pollution on Human Health, J. Med. Toxicol., 8(2), 166–175, doi:10.1007/s13181-011-0203-1, 2012.

Anenberg, S. C., Horowitz, L. W., Tong, D. Q. and West, J. J.: An Estimate of the Global Burden of Anthropogenic Ozone and Fine Particulate Matter on Premature Human Mortality Using Atmospheric Modeling, Environ. Health Perspect., 118(9), 1189–1195, doi:10.1289/ehp.0901220, 2010.

Appel, K. W., Gilliland, A. B., Sarwar, G. and Gilliam, R. C.: Evaluation of the Community Multiscale Air Quality (CMAQ) model version 4.5: Sensitivities impacting model performance, Atmos. Environ., 41(40), 9603–9615, doi:10.1016/j.atmosenv.2007.08.044, 2007.

Asher, M. J., Croke, B. F. W., Jakeman, A. J. and Peeters, L. J. M.: A review of surrogate models and their application to groundwater modeling, Water Resour. Res., 51(8), 5957–5973, doi:10.1002/2015WR016967, 2015.

Bastos, L. S. and O'Hagan, A.: Diagnostics for Gaussian Process Emulators, Technometrics, 51(4), 425–438, 2009.

Beddows, A. V., Kitwiroon, N., Williams, M. L. and Beevers, S. D.: Emulation and Sensitivity Analysis of the Community Multiscale Air Quality Model for a UK Ozone Pollution Episode, Environ. Sci. Technol., 51(11), 6229–6236, doi:10.1021/acs.est.6b05873, 2017.

Benton, J., Fuhrer, J., Gimeno, B. S., Skärby, L., Palmer-Brown, D., Ball, G., Roadknight, C. and Mills, G.: An international cooperative programme indicates the widespread occurrence of ozone injury on crops, Agric. Ecosyst. Environ., 78(1), 19–30, doi:10.1016/S0167-8809(99)00107-3, 2000.

Berge, E. and Jakobsen, H. A.: A regional scale multilayer model for the calculation of long-term transport and deposition of air pollution in Europe, Tellus B Chem. Phys. Meteorol., 50(3), 205–223, doi:10.3402/tellusb.v50i3.16097, 1998.

Bergin, M. S. and Milford, J. B.: Application of Bayesian Monte Carlo analysis to a Lagrangian photochemical air quality model, Atmos. Environ., 34(5), 781–792, doi:10.1016/S1352-2310(99)00346-5, 2000.

Bergin, M. S., Noblet, G. S., Petrini, K., Dhieux, J. R., Milford, J. B. and Harley, R. A.: Formal Uncertainty Analysis of a Lagrangian Photochemical Air Pollution Model, Environ. Sci. Technol., 33(7), 1116–1126, doi:10.1021/es980749y, 1999.

Bergström, R., Denier Van Der Gon, H. A. C., Prévôt, A. S. H., Yttri, K. E. and Simpson, D.: Modelling of organic aerosols over Europe (2002-2007) using a volatility basis set (VBS) framework: Application of different assumptions regarding the formation of secondary organic aerosol, Atmos. Chem. Phys., 12(18), 8499–8527, doi:10.5194/acp-12-8499-2012, 2012.

Bertrand, I., Alexandre, J. and Gilles, P.: Package “sensitivity”. Global sensitivity analysis of model outputs, , 1–76 [online] Available from: https://cran.r-project.org/web/packages/sensitivity/sensitivity.pdf (Accessed 23 August 2018), 2018.

Binkowski, F. S. and Shankar, U.: The Regional Particulate Matter Model: 1. Model description and preliminary results, J. Geophys. Res., 100(D12), 26191, doi:10.1029/95JD02093, 1995.

Blatman, G. and Sudret, B.: A comparison of three metamodel-based methods for global sensitivity analysis: GP modelling, HDMR and LAR-gPC, Procedia - Soc. Behav. Sci., 2(6), 7613–7614, doi:10.1016/j.sbspro.2010.05.143, 2010.

Bobbink, R., Hornung, M. and Roelofs, J. G. M.: The effects of air-borne nitrogen pollutants on species diversity in natural and semi-natural European vegetation, J. Ecol., 86(5), 717–738, doi:10.1046/j.1365-2745.1998.8650717.x, 1998.

Boldo, E., Linares, C., Lumbreras, J., Borge, R., Narros, A., García-Pérez, J., Fernández-Navarro, P., Pérez-Gómez, B., Aragonés, N., Ramis, R., Pollán, M., Moreno, T., Karanasiou, A. and López-Abente, G.: Health impact assessment of a reduction in ambient PM2.5 levels in Spain, Environ. Int., 37(2), 342–348, doi:10.1016/j.envint.2010.10.004, 2011.

Borge, R., Alexandrov, V., José del Vas, J., Lumbreras, J. and Rodríguez, E.: A comprehensive sensitivity analysis of the WRF model for air quality applications over the Iberian Peninsula, Atmos. Environ., 42(37), 8560–8574, doi:10.1016/j.atmosenv.2008.08.032, 2008.

Borgonovo, E.: Measuring uncertainty importance: Investigation and comparison of alternative approaches, Risk Anal., 26(5), 1349–1361, doi:10.1111/j.1539-6924.2006.00806.x, 2006.

Borgonovo, E. and Plischke, E.: Sensitivity analysis: A review of recent advances, Eur. J. Oper. Res., 248(3), 869–887, doi:10.1016/j.ejor.2015.06.032, 2016.

Bouwman, A. F., Van Vuuren, D. P., Derwent, R. G. and Posch, M.: A Global Analysis of Acidification and Eutrophication of Terrestrial Ecosystems, Water. Air. Soil Pollut., 141(1/4), 349–382, doi:10.1023/A:1021398008726, 2002.

Box, G. E. P. and Hunter, J. S.: The 2 k-p Fractional Factorial Designs Part I, Technometrics, 3(3), 311–351, doi:10.2307/1266725, 1961.

Boylan, J. W. and Russell, A. G.: PM and light extinction model performance metrics, goals, and criteria for three-dimensional air quality models, Atmos. Environ., 40(26), 4946–4959, doi:10.1016/j.atmosenv.2005.09.087, 2006.

Breuer, L., Huisman, J. A., Willems, P., Bormann, H., Bronstert, A., Croke, B. F. W., Frede, H.-G., Gräff, T., Hubrechts, L., Jakeman, A. J., Kite, G., Lanini, J., Leavesley, G., Lettenmaier, D. P., Lindström, G., Seibert, J., Sivapalan, M. and Viney, N. R.:

Assessing the impact of land use change on hydrology by ensemble modeling (LUCHEM). I: Model intercomparison with current land use, Adv. Water Resour., 32, 129–146, doi:10.1016/j.advwatres.2008.10.003, 2009.

Brown, J. D.: Knowledge, uncertainty and physical geography: Towards the development of methodologies for questioning belief, Trans. Inst. Br. Geogr., 29(3), 367–381, doi:10.1111/j.0020-2754.2004.00342.x, 2004.

Bücker, M., Corliss, G., Naumann, U., Hovland, P. and Norris, B.: Automatic Differentiation: Applications, Theory, and Implementations. Lecture Notes in Computational Science and Engineering, Springer Berlin Heidelberg., 2006.

Canepa, E. and Ratto, C. F.: SAFE_AIR Algorithms to simulate the transport of pollutant elements: a model validation exercise and sensitivity analysis, Environ. Model. Softw., 18(4), 365–372, doi:10.1016/S1364-8152(02)00105-6, 2003.

Capaldo, K. P. and Pandis, S. N.: Dimethylsulfide chemistry in the remote marine atmosphere: Evaluation and sensitivity analysis of available mechanisms, J. Geophys. Res.-Atmos., 102(D19), 23251–23267, doi:10.1029/97JD01807, 1997.

Carnell, R.: lhs: Latin Hypercube Samples, [online] Available from: https://cran.r-project.org/package=lhs, 2016.

Carslaw, D. and Ropkins, K.: openair: Tools for the Analysis of Air Pollution Data, [online] Available from: https://cran.r-project.org/web/packages/openair/openair.pdf, 2018.

Carslaw, K. S., Lee, L. A., Reddington, C. L., Pringle, K. J., Rap, A., Forster, P. M., Mann, G. W., Spracklen, D. V., Woodhouse, M. T., Regayre, L. A. and Pierce, J. R.: Large contribution of natural aerosols to uncertainty in indirect forcing, Nature, 503(7474), 67–71, doi:10.1038/nature12674, 2013.

Castelletti, A., Galelli, S., Ratto, M., Soncini-Sessa, R. and Young, P. C.: A general framework for Dynamic Emulation Modelling in environmental problems, Environ. Model. Softw., 34, 5–18, doi:10.1016/j.envsoft.2012.01.002, 2012.

Chen, S. and Brune, W. H.: Global sensitivity analysis of ozone production and O3–NOx–VOC limitation based on field data, Atmos. Environ., 55, 288–296, doi:10.1016/j.atmosenv.2012.03.061, 2012.

Chen, S., Brune, W. H., Oluwole, O. O., Kolb, C. E., Bacon, F., Li, G. and Rabitz, H.: Global Sensitivity Analysis of the Regional Atmospheric Chemical Mechanism: An Application of Random Sampling-High Dimensional Model Representation to Urban Oxidation Chemistry, Environ. Sci. Technol., 46(20), 11162–11170, doi:10.1021/es301565w, 2012.

Chen, S., Brune, W. H., Lambe, A. T., Davidovits, P. and Onasch, T. B.: Modeling organic aerosol from the oxidation of α-pinene in a Potential Aerosol Mass (PAM) chamber, Atmos. Chem. Phys., 13(9), 5017–5031, doi:10.5194/acp-13-5017-2013, 2013.

Chen, T.-M., Kuschner, W. G., Gokhale, J. and Shofer, S.: Outdoor Air Pollution: Nitrogen Dioxide, Sulfur Dioxide, and Carbon Monoxide Health Effects, Am. J. Med. Sci., 333(4), 249–256, doi:10.1097/MAJ.0b013e31803b900f, 2007.

Christian, K. E., Brune, W. H. and Mao, J.: Global sensitivity analysis of the GEOS-Chem chemical transport model: ozone and hydrogen oxides during ARCTAS (2008), Atmos. Chem. Phys., 17(5), 3769–3784, doi:10.5194/acp-17-3769-2017, 2017.

Cohan, D. S., Koo, B. and Yarwood, G.: Influence of uncertain reaction rates on ozone sensitivity to emissions, Atmos. Environ., 44(26), 3101–3109, doi:10.1016/j.atmosenv.2010.05.034, 2010.

Corbett, J. J.: Updated emissions from ocean shipping, J. Geophys. Res., 108(D20), 4650, doi:10.1029/2003JD003751, 2003.

Crippa, M., Janssens-Maenhout, G., Dentener, F., Guizzardi, D., Sindelarova, K., Muntean, M., Van Dingenen, R. and Granier, C.: Forty years of improvements in European air quality: regional policy-industry interactions with global impacts, Atmos. Chem. Phys., 16(6), 3825–3841, doi:10.5194/acp-16-3825-2016, 2016.

Cukier, R. ., Levine, H. . and Shuler, K. .: Nonlinear sensitivity analysis of

multiparameter model systems, J. Comput. Phys., 26(1), 1–42, doi:10.1016/0021-9991(78)90097-9, 1978.

Cukier, R. I., Fortuin, C. M., Shuler, K. E., Petschek, A. G. and Schaibly, J. H.: Study of the sensitivity of coupled reaction systems to uncertainties in rate coefficients. I Theory, J. Chem. Phys., 59(8), 3873–3878, doi:10.1063/1.1680571, 1973.

Dean, A., Morris, M., Stufken, J. and Bingham, D.: Handbook of Design and Analysis of Experiments, Chapman and Hall/CRC, New York., 2015.

Defra: UK AIR, Air Information Resource, [online] Available from: https://uk-air.defra.gov.uk/, 2018.

Dennis, R., Fox, T., Fuentes, M., Gilliland, A., Hanna, S., Hogrefe, C., Irwin, J., Rao, S. T., Scheffe, R., Schere, K., Steyn, D. and Venkatram, A.: A framework for evaluating regional-scale numerical photochemical modeling systems, Environ. Fluid Mech., 10(4), 471–489, doi:10.1007/s10652-009-9163-2, 2010.

Derwent, R. G.: Treating uncertainty in models of the atmospheric chemistry of nitrogen compounds, Atmos. Environ., 21(6), 1445–1454, doi:10.1016/0004-6981(88)90095-9, 1987.

Dore, A. J., Kryza, M., Hall, J. R., Hallsworth, S., Keller, V. J. D., Vieno, M. and Sutton, M. a.: The influence of model grid resolution on estimation of national scale nitrogen deposition and exceedance of critical loads, Biogeosciences, 9(5), 1597–1609, doi:10.5194/bg-9-1597-2012, 2012.

Dore, A. J., Carslaw, D. C., Braban, C., Cain, M., Chemel, C., Conolly, C., Derwent, R. G., Griffiths, S. J., Hall, J., Hayman, G., Lawrence, S., Metcalfe, S. E., Redington, A., Simpson, D., Sutton, M. A., Sutton, P., Tang, Y. S., Vieno, M., Werner, M. and Whyatt, J. D.: Evaluation of the performance of different atmospheric chemical transport models and inter-comparison of nitrogen and sulphur deposition estimates for the UK, Atmos. Environ., 119(606), 131–143, doi:10.1016/j.atmosenv.2015.08.008, 2015.

Dunker, A. M., Yarwood, G., Ortmann, J. P. and Wilson, G. M.: The Decoupled Direct

Method for Sensitivity Analysis in a Three-Dimensional Air Quality Model Implementation, Accuracy, and Efficiency, Environ. Sci. Technol., 36(13), 2965–2976, doi:10.1021/es0112691, 2002.

EC: Impact assessment guidelines. [online] Available from: http://ec.europa.eu/smart-regulation/impact/commission_guidelines/docs/iag_2009_en.pdf (Accessed 21 June 2018), 2009.

EC Directive: Directive 2008/50/EC of the European Parliament and of the Council of 21 May 2008 on ambient air quality and cleaner air for Europe, [online] Available from: https://eur-lex.europa.eu/legal-content/EN/TXT/HTML/?uri=CELEX:32008L0050&from=en (Accessed 1 May 2018), 2008.

Entec: Quantification of emissions from ships associated with ship movements between ports in the European Community. [online] Available from: http://ec.europa.eu/environment/air/pdf/chapter2_ship_emissions.pdf (Accessed 2 May 2018), 2002.

Entec: UK Ship Emissions Inventory. [online] Available from: http://uk-air.defra.gov.uk/reports/cat15/1012131459_21897_Final_Report_291110.pdf (Accessed 1 July 2018), 2010.

EPA: Guidance on the Development, Evaluation, and Application of Environmental Models. [online] Available from: https://www.epa.gov/measurements-modeling/guidance-document-development-evaluation-and-application-environmental-models (Accessed 10 February 2017), 2009.

EPA NCEE: Working Paper Series The Role of Scenario Uncertainty in Estimating the Benefits of Carbon Mitigation The Role of Scenario Uncertainty in Estimating the Benefits of Carbon Mitigation The Role of Scenario Uncertainty in Estimating the Benefits of Carbon Mitigation, [online] Available from: http://www.epa.gov/economics (Accessed 12 July 2018), 2014.

European Environment Agency: The application of models under the European

Union’s Air Quality Directive: A technical reference guide., 2011.

Eurostat: NAMEA for Air Emissions Compilation Guide., 2004.

Exbrayat, J.-F., Viney, N. R., Seibert, J., Wrede, S., Frede, H.-G. and Breuer, L.: Ensemble modelling of nitrogen fluxes: data fusion for a Swedish meso-scale catchment, Earth Syst. Sci, 145194(10), 2383–2397, doi:10.5194/hess-14-2383-2010, 2010.

Ferretti, F., Saltelli, A. and Tarantola, S.: Trends in sensitivity analysis practice in the last decade, Sci. Total Environ., 568, 666–670, doi:10.1016/j.scitotenv.2016.02.133, 2015.

Finlayson-Pitts, B. J. and Pitts, J. N.: Chemistry of the Upper and Lower Atmosphere, in Chemistry of the Upper and Lower Atmosphere, pp. 1–14, Elsevier., 2000.

Fournier, N., Pais, V. . A., Sutton, M. . A., Weston, K. . J., Dragosits, U., Tang, S. . Y. and Aherne, J.: Parallelisation and application of a multi-layer atmospheric transport model to quantify dispersion and deposition of ammonia over the British Isles, Environ. Pollut., 116(1), 95–107, doi:10.1016/S0269-7491(01)00146-4, 2002.

Fournier, N., Dore, a. J., Vieno, M., Weston, K. J., Dragosits, U. and Sutton, M. a.: Modelling the deposition of atmospheric oxidised nitrogen and sulphur to the United Kingdom using a multi-layer long-range transport model, Atmos. Environ., 38(5), 683–694, doi:10.1016/j.atmosenv.2003.10.028, 2004.

Fournier, N., Weston, K. J., Dore, A. J. and Sutton, M. A.: Modelling the wet deposition of reduced nitrogen over the British Isles using a Lagrangian multi-layer atmospheric transport model, Q. J. R. Meteorol. Soc., 131(606), 703–722, doi:10.1256/qj.04.76, 2005.

Gan, Y., Duan, Q., Gong, W., Tong, C., Sun, Y., Chu, W., Ye, A., Miao, C. and Di, Z.: A comprehensive evaluation of various sensitivity analysis methods: A case study with a hydrological model, Environ. Model. Softw., 51(2014), 269–285, doi:10.1016/j.envsoft.2013.09.031, 2014.

Ghanem, R., Higdon, D. and Owhadi, H.: Handbook of Uncertainty Quantification, edited by R. Ghanem, D. Higdon, and H. Owhadi, Springer International Publishing., 2017.

Gladish, D. W., Pagendam, D. E., Peeters, L. J. M., Kuhnert, P. M. and Vaze, J.: Emulation Engines: Choice and Quantification of Uncertainty for Complex Hydrological Models, J. Agric. Biol. Environ. Stat., 23(1), 39–62, doi:10.1007/s13253-017-0308-3, 2017.

Halton, J. H.: On the efficiency of certain quasi-random sequences of points in evaluating multi-dimensional integrals, Numer. Math., 2(1), 84–90, doi:10.1007/BF01386213, 1960.

Hanna, S. R., Lu, Z., Frey, H. C., Wheeler, N., Vukovich, J., Arunachalam, S., Fernau, M. and Hansen, D. A.: Uncertainties in predicted ozone concentrations due to input uncertainties for the UAM-V photochemical grid model applied to the July 1995 OTAG domain, Atmos. Environ., 35(5), 891–903, doi:10.1016/S1352-2310(00)00367-8, 2001.

Hanna, S. R., Paine, R., Heinold, D., Kintigh, E. and Baker, D.: Uncertainties in air toxics calculated by the dispersion models AERMOD and ISCST3 in the Houston ship channel area, J. Appl. Meteorol. Climatol., 46(9), 1372–1382, doi:10.1175/JAM2540.1, 2007.

Hannaa, S. R., Changa, J. C. and Fernaua, M. E.: Monte carlo estimates of uncertainties in predictions by a photochemical grid model (UAM-IV) due to uncertainties in input variables, Atmos. Environ., 32(21), 3619–3628, doi:10.1016/S1352-2310(97)00419-6, 1998.

Heal, M. R., Kumar, P. and Harrison, R. M.: Particles, air quality, policy and health, Chem. Soc. Rev., 41(19), 6606–30, doi:10.1039/c2cs35076a, 2012.

Heal, M. R., Heaviside, C., Doherty, R. M., Vieno, M., Stevenson, D. S. and Vardoulakis, S.: Health burdens of surface ozone in the UK for a range of future scenarios, Environ. Int., 61, 36–44, doi:10.1016/j.envint.2013.09.010, 2013.

Hellsten, S., Dragosits, U., Place, C. J., Vieno, M., Dore, A. J., Misselbrook, T. H., Tang, Y. S. and Sutton, M. A.: Modelling the spatial distribution of ammonia emissions in the UK, Environ. Pollut., 154(3), 370–379, doi:10.1016/j.envpol.2008.02.017, 2008.

Helton, J. C., Johnson, J. D., Sallaberry, C. J. and Storlie, C. B.: Survey of sampling-based methods for uncertainty and sensitivity analysis, Reliab. Eng. Syst. Saf., 91(10–11), 1175–1209, doi:10.1016/j.ress.2005.11.017, 2006.

Hoek, G., Krishnan, R. M., Beelen, R., Peters, A., Ostro, B., Brunekreef, B. and Kaufman, J. D.: Long-term air pollution exposure and cardio- respiratory mortality: a review, Environ. Heal., 12(1), 43, doi:10.1186/1476-069X-12-43, 2013.

Holmes, N. S. and Morawska, L.: A review of dispersion modelling and its application to the dispersion of particles: An overview of different dispersion models available, Atmos. Environ., 40(30), 5902–5928, doi:10.1016/j.atmosenv.2006.06.003, 2006.

Homma, T. and Saltelli, A.: Importance measures in global sensitivity analysis of nonlinear models, Reliab. Eng. Syst. Saf., 52(1), 1–17, doi:10.1016/0951-8320(96)00002-6, 1996.

Im, U., Brandt, J., Geels, C., Hansen, K. M., Christensen, J. H., Andersen, M. S., Solazzo, E., Kioutsioukis, I., Alyuz, U., Balzarini, A., Baro, R., Bellasio, R., Bianconi, R., Bieser, J., Colette, A., Curci, G., Farrow, A., Flemming, J., Fraser, A., Jimenez-Guerrero, P., Kitwiroon, N., Liang, C.-K., Nopmongcol, U., Pirovano, G., Pozzoli, L., Prank, M., Rose, R., Sokhi, R., Tuccella, P., Unal, A., Vivanco, M. G., West, J., Yarwood, G., Hogrefe, C. and Galmarini, S.: Assessment and economic valuation of air pollution impacts on human health over Europe and the United States as calculated by a multi-model ensemble in the framework of AQMEII3, Atmos. Chem. Phys., 18(8), 5967–5989, doi:10.5194/acp-18-5967-2018, 2018.

Iooss, B. and Lemaître, P.: A Review on Global Sensitivity Analysis Methods, in Uncertainty management in Simulation-Optimization of Complex Systems: Algorithms and Applications, pp. 101–122, Springer US., 2015.

IPCC: Good Practice Guidance and Uncertainty Management in National Greenhouse Gas Inventories (Quantifying Uncertantiesin Practice). [online] Available from: http://www.ipcc-nggip.iges.or.jp/public/gp/english/, 2000.

IPCC: IPCC Guidelines for National Greenhouse Gas Inventories, General Guidance and Reporting. [online] Available from: https://www.ipcc-nggip.iges.or.jp/public/2006gl/pdf/1_Volume1/V1_3_Ch3_Uncertainties.pdf (Accessed 2 February 2018), 2006.

IPCC: Climate Change 2013: The Physical Science Basis. Contribution of Working Group I to the Fifth Assessment Report of the Intergovernmental Panel on Climate Change, Cambridge, United Kingdom and New York, NY, USA,., 2013.

Janon, A., Klein, T., Lagnoux, A., Nodet, M. and Prieur, C.: Asymptotic normality and efficiency of two Sobol index estimators, ESAIM Probab. Stat., 18, 342–364, doi:10.1051/ps/2013040, 2014.

Jansen, M. J. W.: Analysis of variance designs for model output, Comput. Phys. Commun., 117(1), 35–43, doi:10.1016/S0010-4655(98)00154-4, 1999.

Jimenez, L. O. and Landgrebe, D.: Supervised classification in high-dimensional space: geometrical, statistical, and asymptotical properties of multivariate data, IEEE Trans. Syst. Man Cybern. Part C, 28(1), 39–54, doi:10.1109/5326.661089, 1998.

Johnson, M. E., Moore, L. M. and Ylvisaker, D.: Minimax and maximin distance designs, J. Stat. Plan. Inference, 26(2), 131–148, doi:10.1016/0378-3758(90)90122-B, 1990.

Jolliff, J. K., Kindle, J. C., Shulman, I., Penta, B., Friedrichs, M. A. M., Helber, R. and Arnone, R. A.: Summary diagrams for coupled hydrodynamic-ecosystem model skill assessment, J. Mar. Syst., 76(1–2), 64–82, doi:10.1016/j.jmarsys.2008.05.014, 2009.

Jones, B. and Johnson, R. T.: Design and analysis for the Gaussian process model, Qual. Reliab. Eng. Int., 25(5), 515–524, doi:10.1002/qre.1044, 2009.

Kampa, M. and Castanas, E.: Human health effects of air pollution., Environ. Pollut.,

151(2), 362–7, doi:10.1016/j.envpol.2007.06.012, 2008.

Kennedy, M.: Description of the Gaussian process model used in GEM-SA., 2004.

Kennedy, M. C. and O'Hagan, A.: Bayesian calibration of computer models, J. R. Stat. Soc. Ser. B (Statistical Methodol., 63(3), 425–464, doi:10.1111/1467-9868.00294, 2001.

Kleijnen, J. P. C. and Helton, J. C.: Statistical analyses of scatterplots to identify important factors in large-scale simulations, 1: Review and comparison of techniques, Reliab. Eng. Syst. Saf., 65(2), 147–185, doi:10.1016/S0951-8320(98)00091-X, 1999.

Konda, U., Singh, T., Singla, P. and Scott, P.: Uncertainty propagation in puff-based dispersion models using polynomial chaos, Environ. Model. Softw., 25(12), 1608–1618, doi:10.1016/j.envsoft.2010.04.005, 2010.

Koo, B., Dunker, A. M. and Yarwood, G.: Implementing the Decoupled Direct Method for Sensitivity Analysis in a Particulate Matter Air Quality Model, Environ. Sci. Technol., 41(8), 2847–2854, doi:10.1021/es0619962, 2007.

Krupa, S. V.: Effects of atmospheric ammonia (NH3) on terrestrial vegetation: A review, Environ. Pollut., 124(2), 179–221, doi:10.1016/S0269-7491(02)00434-7, 2003.

Krupnick, A., Morgenstern, R., Batz, M., Nelson, P., Burtraw, D., Shih, J. and McWilliams, M.: RFF: Not a Sure Thing: Making Regulatory Choices under Uncertainty. [online] Available from: http://citeseerx.ist.psu.edu/viewdoc/download?doi=10.1.1.114.3396&rep=rep1&type=pdf (Accessed 1 December 2014), 2006.

Kryza, M., Mill, W., Dore, A. J., Werner, M. and Błaś, M.: Calculation of Sulphur and Nitrogen Deposition with the Frame Model and Assessment of the Exceedance of Critical Loads in Poland, Ecol. Chem. Eng. S, 20(2), 279–290, doi:10.2478/eces-2013-0020, 2013.

Labrador, L. J., von Kuhlmann, R. and Lawrence, M. G.: The effects of lightning-

produced NO_x and its vertical distribution on atmospheric chemistry: sensitivity simulations with MATCH-MPIC, Atmos. Chem. Phys., 5(7), 1815–1834, doi:10.5194/acp-5-1815-2005, 2005.

Lagerwall, G., Kiker, G., Muñoz-Carpena, R. and Wang, N.: Global uncertainty and sensitivity analysis of a spatially distributed ecological model, Ecol. Modell., 275, 22–30, doi:10.1016/j.ecolmodel.2013.12.010, 2014.

Lataniotis, C., Marelli, S. and Sudret, B.: Gaussian process modelling using UQLab, [online] Available from: http://arxiv.org/abs/1709.09382, 2017.

Lauer, A., Eyring, V., Hendricks, J., Jöckel, P. and Lohmann, U.: Global model simulations of the impact of ocean-going ships on aerosols, clouds, and the radiation budget, Atmos. Chem. Phys., 7(19), 5061–5079, doi:10.5194/acp-7-5061-2007, 2007.

Lee, L. A., Carslaw, K. S., Pringle, K. J., Mann, G. W. and Spracklen, D. V.: Emulation of a complex global aerosol model to quantify sensitivity to uncertain parameters, Atmos. Chem. Phys., 11(23), 12253–12273, doi:10.5194/acp-11-12253-2011, 2011.

Lee, L. A., Carslaw, K. S., Pringle, K. J. and Mann, G. W.: Mapping the uncertainty in global CCN using emulation, Atmos. Chem. Phys., 12(20), 9739–9751, doi:10.5194/acp-12-9739-2012, 2012.

Lee, L. A., Pringle, K. J., Reddington, C. L., Mann, G. W., Stier, P., Spracklen, D. V, Pierce, J. R. and Carslaw, K. S.: The magnitude and causes of uncertainty in global model simulations of cloud condensation nuclei, Atmos. Chem. Phys., 13(17), 8879–8914, doi:10.5194/acp-13-8879-2013, 2013.

Lin, C., Heal, M. R., Vieno, M., MacKenzie, I. A., Armstrong, B. G., Butland, B. K., Milojevic, A., Chalabi, Z., Atkinson, R. W., Stevenson, D. S., Doherty, R. M. and Wilkinson, P.: Spatiotemporal evaluation of EMEP4UK-WRF v4.3 atmospheric chemistry transport simulations of health-related metrics for NO2, O3, and PM10 for 2001-2010, Geosci. Model Dev., 10(4), 1767–1787, doi:10.5194/gmd-10-1767-2017, 2017.

Lin, J., Brunner, D., Gerbig, C., Stohl, A., Luhar, A. and Webley, P.: Lagrangian

Modeling of the Atmosphere, American Geophysical Union., 2012.

Luo, Z., Wang, E., Bryan, B. A., King, D., Zhao, G., Pan, X. and Bende-Michl, U.: Meta-modeling soil organic carbon sequestration potential and its application at regional scale, Ecol. Appl., 23(2), 408–420, doi:10.1890/12-0672.1, 2013.

Makar, P. A., Moran, M. D., Zheng, Q., Cousineau, S., Sassi, M., Duhamel, A., Besner, M., Davignon, D., Crevier, L.-P. and Bouchet, V. S.: Modelling the impacts of ammonia emissions reductions on North American air quality, Atmos. Chem. Phys., 9(18), 7183–7212, doi:10.5194/acp-9-7183-2009, 2009.

Makler-Pick, V., Gal, G., Gorfine, M., Hipsey, M. R. and Carmel, Y.: Sensitivity analysis for complex ecological models – A new approach, Environ. Model. Softw., 26(2), 124–134, doi:10.1016/j.envsoft.2010.06.010, 2011.

Marelli, S. and Sudret, B.: UQLab: A Framework for Uncertainty Quantification in Matlab, in Vulnerability, Uncertainty, and Risk, pp. 2554–2563, American Society of Civil Engineers, Reston, VA., 2014.

Marrel, A., Iooss, B., Laurent, B. and Roustant, O.: Calculations of Sobol indices for the Gaussian process metamodel, Reliab. Eng. Syst. Saf., 94(3), 742–751, doi:10.1016/j.ress.2008.07.008, 2009.

Matejko, M., Dore, A. J., Hall, J., Dore, C. J., Błaś, M., Kryza, M., Smith, R. and Fowler, D.: The influence of long term trends in pollutant emissions on deposition of sulphur and nitrogen and exceedance of critical loads in the United Kingdom, Environ. Sci. Policy, 12(7), 882–896, doi:10.1016/j.envsci.2009.08.005, 2009.

McKay, M. D., Beckman, R. J. and Conover, W. J.: Comparison of Three Methods for Selecting Values of Input Variables in the Analysis of Output from a Computer Code, Technometrics, 21(2), 239–245, doi:10.1080/00401706.1979.10489755, 1979.

Misra, A., Passant, N. R., Murrells, T. P., Pang, Y., Thistlethwaite, G., Walker, C., Broomfield, M., Wakeling, D., del Vento, S., Pearson, B., Hobson, M., Misselbrook, T. and Dragosits, U.: UK Informative Inventory Report (1990 to 2013). [online] Available from: http://naei.beis.gov.uk/reports/reports?report_id=809, 2015.

Monteiro, A., Durka, P., Flandorfer, C., Georgieva, E., Guerreiro, C., Kushta, J., Malherbe, L., Maiheu, B., Miranda, A. I., Santos, G., Stocker, J., Trimpeneers, E., Tognet, F., Stortini, M., Wesseling, J., Janssen, S. and Thunis, P.: Strengths and weaknesses of the FAIRMODE benchmarking methodology for the evaluation of air quality models, Air Qual. Atmos. Heal., doi:10.1007/s11869-018-0554-8, 2018.

Moreno-Gutiérrez, J., Calderay, F., Saborido, N., Boile, M., Rodríguez Valero, R. and Durán-Grados, V.: Methodologies for estimating shipping emissions and energy consumption: A comparative analysis of current methods, Energy, 86, 603–616, doi:10.1016/j.energy.2015.04.083, 2015.

Morris, D. E., Oakley, J. E. and Crowe, J. a.: A web-based tool for eliciting probability distributions from experts, Environ. Model. Softw., 52, 1–4, doi:10.1016/j.envsoft.2013.10.010, 2014.

Morris, M. D. and Mitchell, T. J.: Exploratory designs for computational experiments, J. Stat. Plan. Inference, 43(3), 381–402, doi:10.1016/0378-3758(94)00035-T, 1995.

NCEP: NCEP FNL Operational Model Global Tropospheric Analyses, continuing from July 1999. Research Data Archive at the National Center for Atmospheric Research, Computational and Information Systems Laboratory, Boulder, CO., 2000.

O'Hagan, A.: Bayesian analysis of computer code outputs: A tutorial, Reliab. Eng. Syst. Saf., 91(10–11), 1290–1300, doi:10.1016/j.ress.2005.11.025, 2006.

Oakley, J. and O'Hagan, A.: Bayesian inference for the uncertainty distribution of computer model outputs, Biometrika, 89(4), 769–784, 2002.

Oakley, J. E. and O'Hagan, A.: Probabilistic sensitivity analysis of complex models: A Bayesian approach, J. R. Stat. Soc. Ser. B Stat. Methodol., 66(3), 751–769, doi:10.1111/j.1467-9868.2004.05304.x, 2004.

Oxley, T., Apsimon, H., Dore, A., Sutton, M., Hall, J., Heywood, E., Gonzales Del Campo, T. and Warren, R.: The UK Integrated Assessment Model , UKIAM : A National Scale Approach to the Analysis of Strategies for Abatement of Atmospheric Pollutants Under the Convention on Long-Range Transboundary Air Pollution, Integr.

Assess., 4(4), 236–249, doi:10.1080/1389517049051538, 2003.

Oxley, T., Dore, A. J., ApSimon, H., Hall, J. and Kryza, M.: Modelling future impacts of air pollution using the multi-scale UK Integrated Assessment Model (UKIAM)., Environ. Int., 61, 17–35, doi:10.1016/j.envint.2013.09.009, 2013.

Park, J. S.: Optimal Latin-hypercube designs for computer experiments, J. Stat. Plan. Inference, 39(1), 95–111, doi:10.1016/0378-3758(94)90115-5, 1994.

Parker, W. S.: Ensemble modeling, uncertainty and robust predictions, Wiley Interdiscip. Rev. Clim. Chang., 4(3), 213–223, doi:10.1002/wcc.220, 2013.

Parry, H. R., Topping, C. J., Kennedy, M. C., Boatman, N. D. and Murray, A. W. A.: A Bayesian sensitivity analysis applied to an Agent-based model of bird population response to landscape change, Environ. Model. Softw., 45, 104–115, doi:10.1016/j.envsoft.2012.08.006, 2013.

Passant, N. R., Murrells, T. P., Pang, Y., Thistlethwaite, G., Venfield, H. L., Whiting, R. and Walker, C.: UK Informative Inventory Report (1980 to 2012), , (March), 210, 2013.

Petersen, A. C., Janssen, P. H. M., van der Sluijs, J. P., Risbey, J. S., Ravetz, J. R., Wardekker, J. A. and Martinson Hughes, H.: Guidance for uncertainty assessment and communication. [online] Available from: www.pbl.nl/en (Accessed 12 July 2018), 2013.

Pulles, T. and Kuenen, J.: EMEP/EEA air pollutant emission inventory guidebook. [online] Available from: https://www.eea.europa.eu/publications/emep-eea-guidebook-2016, 2016.

Qian, S. S., Stow, C. a. and Borsuk, M. E.: On Monte Carlo methods for Bayesian inference, Ecol. Modell., 159(2–3), 269–277, doi:10.1016/S0304-3800(02)00299-5, 2003.

Rabitz, H.: Systems analysis at the molecular scale, Science (80-.)., 246(4927), 221–226, doi:10.1126/science.246.4927.221, 1989.

Rabitz, H. and Alış, Ö. F.: General foundations of high-dimensional model representations, J. Math. Chem., 25(2–3), 197–233, doi:10.1023/A:1019188517934, 1999.

Rasmussen, C. E. and Williams, C. K. I.: Gaussian Processes for Machine Learning, University Press Group Limited., 2006.

Ratto, M., Castelletti, A. and Pagano, A.: Emulation techniques for the reduction and sensitivity analysis of complex environmental models, Environ. Model. Softw., 34, 1–4, doi:10.1016/j.envsoft.2011.11.003, 2012.

Refsgaard, J. C., van der Sluijs, J. P., Højberg, A. L. and Vanrolleghem, P. a.: Uncertainty in the environmental modelling process – A framework and guidance, Environ. Model. Softw., 22(11), 1543–1556, doi:10.1016/j.envsoft.2007.02.004, 2007.

Rodriguez, M. A., Brouwer, J., Samuelsen, G. S. and Dabdub, D.: Air quality impacts of distributed power generation in the South Coast Air Basin of California 2: Model uncertainty and sensitivity analysis, Atmos. Environ., 41(27), 5618–5635, doi:10.1016/j.atmosenv.2007.02.049, 2007.

Roustant, O., Ginsbourger, D. and Deville, Y.: DiceKriging , DiceOptim : Two R Packages for the Analysis of Computer Experiments by Kriging-Based Metamodeling and Optimization, J. Stat. Softw., 51(1), doi:10.18637/jss.v051.i01, 2012.

Ryan, E., Wild, O., O'Connor, F., Voulgarakis, A. and Lee, L.: Fast sensitivity analysis methods for computationally expensive models with multidimensional output, Geosci. Model Dev. Discuss., 44(November), 1–35, doi:10.5194/gmd-2017-271, 2017.

Ryan, E., Wild, O., Voulgarakis, A. and Lee, L.: Fast sensitivity analysis methods for computationally expensive models with multi-dimensional output, Geosci. Model Dev., 11(8), 3131–3146, doi:10.5194/gmd-11-3131-2018, 2018.

Saltelli, a, Tarantola, S. and Chan, K. P.-S.: A Quantitative Model-Independent Method for Global Sensitivity Analysis of Model Output, Technometrics, 41(1), 39–

56, doi:10.1080/00401706.1999.10485594, 1999.

Saltelli, A.: Making best use of model evaluations to compute sensitivity indices, Comput. Phys. Commun., 145, 280–297, doi:10.1016/S0010-4655(02)00280-1, 2002.

Saltelli, A. and Annoni, P.: How to avoid a perfunctory sensitivity analysis, Environ. Model. Softw., 25(12), 1508–1517, doi:10.1016/j.envsoft.2010.04.012, 2010.

Saltelli, A., Chan, K. and Scott, E. M.: Sensitivity Analysis, edited by A. Saltelli, K. Chan, and E. M. Scott, Wiley, Chichester, UK., 2000.

Saltelli, A., Ratto, M., Tarantola, S. and Campolongo, F.: Sensitivity analysis practice: A guide to scientific models., 2006.

Saltelli, A., Ratto, M., Andres, T., Campolongo, F., Cariboni, J., Gatelli, D., Saisana, M. and Tarantola, S.: Global Sensitivity Analysis. The Primer, John Wiley & Sons, Ltd, Chichester, UK., 2008.

Saltelli, A., Annoni, P., Azzini, I., Campolongo, F., Ratto, M. and Tarantola, S.: Variance based sensitivity analysis of model output. Design and estimator for the total sensitivity index, Comput. Phys. Commun., 181(2), 259–270, doi:10.1016/j.cpc.2009.09.018, 2010.

Sax, T. and Isakov, V.: A case study for assessing uncertainty in local-scale regulatory air quality modeling applications, Atmos. Environ., 37(25), 3481–3489, doi:10.1016/S1352-2310(03)00411-4, 2003.

Scarbrough, T., Tsagatakis, I., Smith, K., Wakeling, D., Smith, T., Hauerhoff, E. and Murrells, T.: A review of the NAEI shipping emissions methodology. [online] Available from: https://uk-air.defra.gov.uk/assets/documents/reports/cat07/1712140936_ED61406_NAEI_shipping_report_12Dec2017.pdf (Accessed 15 March 2018), 2017.

Schindler, D. W.: Effects of Acid Rain on Freshwater Ecosystems, Science (80-.)., 239(4836), 149–157, doi:10.1126/science.239.4836.149, 1988.

Shahsavani, D. and Grimvall, A.: Variance-based sensitivity analysis of model outputs using surrogate models, Environ. Model. Softw., 26(6), 723–730, doi:10.1016/j.envsoft.2011.01.002, 2011.

Sheikholeslami, R. and Razavi, S.: Progressive Latin Hypercube Sampling: An efficient approach for robust sampling-based analysis of environmental models, Environ. Model. Softw., 93(2017), 109–126, doi:10.1016/j.envsoft.2017.03.010, 2017.

Shin, M. J., Guillaume, J. H. A., Croke, B. F. W. and Jakeman, A. J.: Addressing ten questions about conceptual rainfall-runoff models with global sensitivity analyses in R, J. Hydrol., 503(2013), 135–152, doi:10.1016/j.jhydrol.2013.08.047, 2013.

Shrivastava, M., Zhao, C., Easter, R. C., Qian, Y., Zelenyuk, A., Fast, J. D., Liu, Y., Zhang, Q. and Guenther, A.: Sensitivity analysis of simulated SOA loadings using a variance-based statistical approach, J. Adv. Model. Earth Syst., 8(2), 499–519, doi:10.1002/2015MS000554, 2016.

De Simone, F., Gencarelli, C. N., Hedgecock, I. M. and Pirrone, N.: Global atmospheric cycle of mercury: A model study on the impact of oxidation mechanisms, Environ. Sci. Pollut. Res., 21(6), 4110–4123, doi:10.1007/s11356-013-2451-x, 2014.

Simpson, D., Tuovinen, J. P., Emberson, L. and Ashmore, M. R.: Characteristics of an ozone deposition module II: Sensitivity analysis, Water. Air. Soil Pollut., 143(1–4), 123–137, doi:10.1023/A:1022890603066, 2003.

Simpson, D., Benedictow, a., Berge, H., Bergström, R., Emberson, L. D., Fagerli, H., Flechard, C. R., Hayman, G. D., Gauss, M., Jonson, J. E., Jenkin, M. E., Nyíri, a., Richter, C., Semeena, V. S., Tsyro, S., Tuovinen, J.-P., Valdebenito, Á. and Wind, P.: The EMEP MSC-W chemical transport model – technical description, Atmos. Chem. Phys., 12(16), 7825–7865, doi:10.5194/acp-12-7825-2012, 2012.

Singles, R., Sutton, M. A. and Weston, K. J.: A multi-layer model to describe the atmospheric transport and deposition of ammonia in Great Britain, Atmos. Environ., 32(3), 393–399, doi:10.1016/S1352-2310(97)83467-X, 1998.

Skamarock, W., Klemp, J., Dudhia, J., Gill, D., Barker, D., Duda, M., Huang, X., Wang, W. and Powers, J.: A Description of the Advanced Research WRF Version 3. NCAR technical note NCAR/TN-475+STR., 2008.

van der Sluijs, J. P., Craye, M., Funtowicz, S., Kloprogge, P., Ravetz, J. and Risbey, J.: Combining quantitative and qualitative measures of uncertainty in model-based environmental assessment: the NUSAP system., Risk Anal., 25(2), 481–492, doi:10.1111/j.1539-6924.2005.00604.x, 2005.

Smith, R. I., Fowler, D., Sutton, M. A., Flechard, C. and Coyle, M.: Regional estimation of pollutant gas dry deposition in the UK: model description, sensitivity analyses and outputs, Atmos. Environ., 34(22), 3757–3777, doi:10.1016/S1352-2310(99)00517-8, 2000.

Sobol, I. .: Global sensitivity indices for nonlinear mathematical models and their Monte Carlo estimates, Math. Comput. Simul., 55(1–3), 271–280, doi:10.1016/S0378-4754(00)00270-6, 2001.

Sobol, I. M.: On the distribution of points in a cube and the approximate evaluation of integrals, USSR Comput. Math. Math. Phys., 7(4), 86–112, doi:10.1016/0041-5553(67)90144-9, 1967.

Sobol, I. M.: Uniformly distributed sequences with an additional uniform property, USSR Comput. Math. Math. Phys., 16(5), 236–242, doi:10.1016/0041-5553(76)90154-3, 1976.

Sobol, I. M.: Sensitivity estimates for nonlinear mathematical models, Math. Model. Comput. Exp., 1(4), 407–414, 1993.

Sobol, I. M. and Levitan, Y. L.: A pseudo-random number generator for personal computers, Comput. Math. with Appl., 37(4–5), 33–40, doi:10.1016/S0898-1221(99)00057-7, 1999.

Song, X., Bryan, B. A., Paul, K. I. and Zhao, G.: Variance-based sensitivity analysis of a forest growth model, Ecol. Modell., 247, 135–143, doi:10.1016/j.ecolmodel.2012.08.005, 2012.

Stevenson, D. S., Young, P. J., Naik, V., Lamarque, J. F., Shindell, D. T., Voulgarakis, A., Skeie, R. B., Dalsoren, S. B., Myhre, G., Berntsen, T. K., Folberth, G. A., Rumbold, S. T., Collins, W. J., MacKenzie, I. A., Doherty, R. M., Zeng, G., Van Noije, T. P. C., Strunk, A., Bergmann, D., Cameron-Smith, P., Plummer, D. A., Strode, S. A., Horowitz, L., Lee, Y. H., Szopa, S., Sudo, K., Nagashima, T., Josse, B., Cionni, I., Righi, M., Eyring, V., Conley, A., Bowman, K. W., Wild, O. and Archibald, A.: Tropospheric ozone changes, radiative forcing and attribution to emissions in the Atmospheric Chemistry and Climate Model Intercomparison Project (ACCMIP), Atmos. Chem. Phys., 13(6), 3063–3085, doi:10.5194/acp-13-3063-2013, 2013.

Storlie, C. B. and Helton, J. C.: Multiple predictor smoothing methods for sensitivity analysis: Description of techniques, Reliab. Eng. Syst. Saf., 93(1), 28–54, doi:10.1016/J.RESS.2006.10.012, 2008.

Storlie, C. B., Swiler, L. P., Helton, J. C. and Sallaberry, C. J.: Implementation and evaluation of nonparametric regression procedures for sensitivity analysis of computationally demanding models, Reliab. Eng. Syst. Saf., 94(11), 1735–1763, doi:10.1016/j.ress.2009.05.007, 2009.

Sudret, B.: Global sensitivity analysis using polynomial chaos expansions, Reliab. Eng. Syst. Saf., 93(7), 964–979, doi:10.1016/j.ress.2007.04.002, 2008.

Taylor, K. E.: Summarizing multiple aspects of model performance in a single diagram, J. Geophys. Res., 106(D7), 7183, doi:10.1029/2000JD900719, 2001.

Tebaldi, C. and Knutti, R.: The use of the multi-model ensemble in probabilistic climate projections, Philos. Trans. R. Soc. A Math. Phys. Eng. Sci., 365(1857), 2053–2075, doi:10.1098/rsta.2007.2076, 2007.

Teixeira, E., Fischer, G., van Velthuizen, H., van Dingenen, R., Dentener, F., Mills, G., Walter, C. and Ewert, F.: Limited potential of crop management for mitigating surface ozone impacts on global food supply, Atmos. Environ., 45(15), 2569–2576, doi:10.1016/j.atmosenv.2011.02.002, 2011.

Thompson, T. M. and Selin, N. E.: Influence of air quality model resolution on

uncertainty associated with health impacts, Atmos. Chem. Phys., 12(20), 9753–9762, doi:10.5194/acp-12-9753-2012, 2012.

Thunis, P., Pederzoli, A. and Pernigotti, D.: Performance criteria to evaluate air quality modeling applications, Atmos. Environ., 59, 476–482, doi:10.1016/j.atmosenv.2012.05.043, 2012.

Tuet, W. Y., Chen, Y., Fok, S., Champion, J. A. and Ng, N. L.: Inflammatory responses to secondary organic aerosols (SOA) generated from biogenic and anthropogenic precursors, , (18), 11423–11440, doi:10.5194/acp-17-11423-2017, 2017.

Turanyi, T. ': Sensitivity analysis of complex kinetic systems. Tools and applications, J. Math. Chem., 5, 203–248 [online] Available from: https://link.springer.com/content/pdf/10.1007%2FBF01166355.pdf (Accessed 13 July 2018), 1990.

United Nations Economic Commission for Europe: Guidelines for Reporting Emissions and Projections Data under the Convention on Long-range Transboundary Air Pollution. [online] Available from: https://www.unece.org/fileadmin/DAM/env/documents/2015/AIR/EB/English.pdf, 2015.

Urban, N. M. and Fricker, T. E.: A comparison of Latin hypercube and grid ensemble designs for the multivariate emulation of an Earth system model, Comput. Geosci., 36(6), 746–755, doi:10.1016/j.cageo.2009.11.004, 2010.

Vieno, M., Dore, a. J., Stevenson, D. S., Doherty, R., Heal, M. R., Reis, S., Hallsworth, S., Tarrason, L., Wind, P., Fowler, D., Simpson, D. and Sutton, M. a.: Modelling surface ozone during the 2003 heat-wave in the UK, Atmos. Chem. Phys., 10(16), 7963–7978, doi:10.5194/acp-10-7963-2010, 2010.

Vieno, M., Heal, M. R., Hallsworth, S., Famulari, D., Doherty, R. M., Dore, a. J., Tang, Y. S., Braban, C. F., Leaver, D., Sutton, M. a. and Reis, S.: The role of long-range transport and domestic emissions in determining atmospheric secondary inorganic particle concentrations across the UK, Atmos. Chem. Phys., 14(16), 8435–

8447, doi:10.5194/acp-14-8435-2014, 2014.

Vieno, M., Heal, M. R., Williams, M. L., Carnell, E. J., Nemitz, E., Stedman, J. R. and Reis, S.: The sensitivities of emissions reductions for the mitigation of UK PM2.5, Atmos. Chem. Phys., 16(1), 265–276, doi:10.5194/acp-16-265-2016, 2016a.

Vieno, M., Heal, M. R., Twigg, M. M., MacKenzie, I. A., Braban, C. F., Lingard, J. J. N., Ritchie, S., Beck, R. C., Móring, A., Ots, R., Di Marco, C. F., Nemitz, E., Sutton, M. A. and Reis, S.: The UK particulate matter air pollution episode of March–April 2014: more than Saharan dust, Environ. Res. Lett., 11(4), 044004, doi:10.1088/1748-9326/11/4/044004, 2016b.

Wakeling, D., Passant, N. R., Murrells, T. P., Pang, Y., Thistlethwaite, G., Walker, C., Garcia, J. M. R., Webb, J., Brown, P., Vento, S. del, Misra, A., Hobson, M., Pridmore, A., Dore, C. and Misselbrook, T.: UK Informative Inventory Report (1990 to 2014), 2016.

Wakeling, D., Passant, N., Murrells, T., Pang, Y., Thistlethwaite, G., Walker, C., Brown, P., Vento, S. del, Hunter, R., Wiltshire, J., Broomfield, M., Watterson, J., Pearson, B., Rushton, K., Hobson, M., Smith, H. and Misselbrook, T.: UK Informative Inventory Report (1990 to 2015)., 2017.

Walker, W. E., Harremoës, P., Rotmans, J., van der Sluijs, J. P., van Asselt, M. B. a., Janssen, P. and Krayer von Krauss, M. P.: Defining Uncertainty: A Conceptual Basis for Uncertainty Management in Model-Based Decision Support, Integr. Assess., 4(1), 5–17, doi:10.1076/iaij.4.1.5.16466, 2003.

WHO: Air quality guidelines. Global update 2005. Particulate matter, ozone, nitrogen dioxide and sulfur dioxide, World Health Organisation Regional Office for Europe, Copenhagen., 2006.

WHO: Health risks of air pollution in Europe – HRAPIE project, Copenhagen. [online] Available from: http://www.euro.who.int/__data/assets/pdf_file/0017/234026/e96933.pdf?ua=1 (Accessed 2 December 2017), 2013.

WHO: Air pollution, [online] Available from: http://www.who.int/topics/air_pollution/en/ (Accessed 20 June 2015), 2015.

Xing, J., Wang, S. X., Chatani, S., Zhang, C. Y., Wei, W., Hao, J. M., Klimont, Z., Cofala, J. and Amann, M.: Projections of air pollutant emissions and its impacts on regional air quality in China in 2020, Atmos. Chem. Phys., 11(7), 3119–3136, doi:10.5194/acp-11-3119-2011, 2011.

Yang, J.: Convergence and uncertainty analyses in Monte-Carlo based sensitivity analysis, Environ. Model. Softw., 26(4), 444–457, doi:10.1016/j.envsoft.2010.10.007, 2011.

Yatheendradas, S., Wagener, T., Gupta, H., Unkrich, C., Goodrich, D., Schaffner, M. and Stewart, A.: Understanding uncertainty in distributed flash flood forecasting for semiarid regions, Water Resour. Res., 44(5), doi:10.1029/2007WR005940, 2008.

Zhang, Y., Liu, X.-H., Olsen, K. M., Wang, W.-X., Do, B. A. and Bridgers, G. M.: Responses of future air quality to emission controls over North Carolina, Part II: Analyses of future-year predictions and their policy implications, Atmos. Environ., 44(23), 2767–2779, doi:10.1016/j.atmosenv.2010.03.022, 2010.

Zhou, Y., Zhao, Y., Mao, P., Zhang, Q., Zhang, J., Qiu, L. and Yang, Y.: Development of a high-resolution emission inventory and its evaluation and application through air quality modeling for Jiangsu Province, China, Atmos. Chem. Phys., 17(1), 211–233, doi:10.5194/acp-17-211-2017, 2017.

Zhu, Z., Bai, H. and Zhu, T.: An inquiry into the potential of scenario analysis for dealing with uncertainty in strategic environmental assessment in China, Environ. Impact Assess. Rev., 31(6), 538–548, doi:10.1016/J.EIAR.2010.02.001, 2011.

Ziehn, T. and Tomlin, A. S.: GUI–HDMR – A software tool for global sensitivity analysis of complex models, Environ. Model. Softw., 24(7), 775–785, doi:10.1016/j.envsoft.2008.12.002, 2009.

Appendix A

Publications included in the systematic overview of the application of sensitivity analysis in atmospheric chemistry transport modelling

Table A.1 presents the list of publications discussed in the Section 2.4 of the thesis. Table A.2 shows the results of the overview of the publications in Table A.1; the publication details and the overview results in the two tables are linked via the index.

Table 0.1 List of publications used for the systematic overview of the application of sensitivity analysis in atmospheric chemistry transport modelling discussed in Sect. 2.4.

Index	Authors	Title	Year	Source title	No of citations
1	Giovannoni J.-M.	Modeling of SO2, Pb and Cd atmospheric deposition over a one-year period	1993	Atmospheric Environment Part A, General Topics	2
2	Van Dop H., et al.	Changing trends in tropospheric methane and carbon monoxide: A sensitivity analysis of the OH-radical	1996	Journal of Atmospheric Chemistry	9
3	Yang Y.-J., et al.	Fast, direct sensitivity analysis of multidimensional photochemical models	1997	Environmental Science and Technology	125
4	Van Jaarsveld J.A., et al.	Modelling transport and deposition of persistent organic pollutants in the European region	1997	Atmospheric Environment	81
5	He S., et al.	Sensitivity of photolysis rates and ozone production in the troposphere to aerosol properties	1999	Journal of Geophysical Research Atmospheres	63
6	Smith R.I., et al.	Regional estimation of pollutant gas dry deposition in the UK: Model description, sensitivity analyses and outputs	2000	Atmospheric Environment	174

Index	Authors	Title	Year	Source title	No of citations
7	He S., et al.	Application of ADIFOR for air pollution model sensitivity studies	2000	Environmental Modelling & Software	15
8	Mendoza-Dominguez A., et al.	Estimation of emission adjustments from the application of four-dimensional data assimilation to photochemical air quality modeling	2001	Atmospheric Environment	43
9	Kang D., et al.	Nonmethane hydrocarbons and ozone in three rural southeast United States national parks: A model sensitivity analysis and comparison to measurements	2003	Journal of Geophysical Research D: Atmospheres	18
10	Canepa E., et al.	SAFE_AIR Algorithms to simulate the transport of pollutant elements: a model validation exercise and sensitivity analysis	2003	Environmental Modelling & Software	16
11	Han Z., et al.	Model study of the impact of biogenic emission on regional ozone and the effectiveness of emission reduction scenarios over eastern China	2005	Tellus, Series B: Chemical and Physical Meteorology	21
12	Lin C.-J., et al.	Sensitivity analysis of ground-level ozone concentration to emission changes in two urban regions of southeast Texas	2005	Journal of Environmental Management	16
13	Cohan D.S., et al.	Dependence of ozone sensitivity analysis on grid resolution	2006	Atmospheric Environment	49
14	Kindap T., et al.	Long-range aerosol transport from Europe to Istanbul, Turkey	2006	Atmospheric Environment	39
15	Toro M.V., et al.	Relationship between VOC and NOx emissions and chemical production of tropospheric ozone in the Aburrá Valley (Colombia)	2006	Chemosphere	18
16	Lauer A., et al.	Global model simulations of the impact of ocean-going ships on aerosols, clouds, and the radiation budget	2007	Atmospheric Chemistry and Physics	171
17	de Meij A.	Model evaluation and scale issues in chemical and optical aerosol properties over the greater Milan area (Italy), for June 2001	2007	Atmospheric Research	17
18	Odman M.T., et al.	Determining the sources of regional haze in the southeastern United States using the CMAQ model	2007	Journal of Applied Meteorology and Climatology	8
19	Rodriguez M.A., et al.	Air quality impacts of distributed power generation in the South Coast Air Basin of California 2: Model uncertainty and sensitivity analysis	2007	Atmospheric Environment	7
20	Yu Y., et al.	Performance characteristics of MM5-SMOKE-CMAQ for a summer photochemical episode in southeast England, United Kingdom	2008	Atmospheric Environment	27
21	Yarwood G., et al.	Modeling weekday to weekend changes in emissions and ozone in the Los Angeles basin for 1997 and 2010	2008	Atmospheric Environment	23

Index	Authors	Title	Year	Source title	No of citations
22	Jin L., et al.	Sensitivity analysis of ozone formation and transport for a central California air pollution episode	2008	Environmental Science and Technology	19
23	Henze D.K., et al.	Inverse modeling and mapping US air quality influences of inorganic PM 2.5 precursor emissions using the adjoint of GEOS-Chem	2009	Atmospheric Chemistry and Physics	102
24	Zavala M., et al.	Modeled and observed ozone sensitivity to mobile-source emissions in Mexico City	2009	Atmospheric Chemistry and Physics	24
25	Odman M.T., et al.	Quantifying the sources of ozone, fine particulate matter, and regional haze in the Southeastern United States	2009	Journal of Environmental Management	18
26	Chaxel E.	Ozone production from Grenoble city during the August 2003 heat wave	2009	Atmospheric Environment	12
27	Cohan D.S., et al.	Influence of uncertain reaction rates on ozone sensitivity to emissions	2010	Atmospheric Environment	18
28	Xing J.,et al	Projections of air pollutant emissions and its impacts on regional air quality in China in 2020	2011	Atmospheric Chemistry and Physics	64
29	Lee L.A., et al.	Emulation of a complex global aerosol model to quantify sensitivity to uncertain parameters	2011	Atmospheric Chemistry and Physics	48
30	Soulhac L., et al.	The model SIRANE for atmospheric urban pollutant dispersion; PART II, validation of the model on a real case study	2012	Atmospheric Environment	25
31	Walker T.W., et al.	Impacts of midlatitude precursor emissions and local photochemistry on ozone abundances in the Arctic	2012	Journal of Geophysical Research Atmospheres	23
32	Chen S., et al	Global sensitivity analysis of ozone production and O-3-NOx-VOC limitation based on field data	2012	Atmospheric Environment	17
33	Gao Y., et al.	Sensitivity analysis of surface ozone to emission controls in Beijing and its neighboring area during the 2008 Olympic Games	2012	Journal of Environmental Sciences	12
34	Chen S., et al	Global Sensitivity Analysis of the Regional Atmospheric Chemical Mechanism: An Application of Random Sampling-High Dimensional Model Representation to Urban Oxidation Chemistry	2012	Environmental Science and Technology	11
35	Muntaseer Billah Ibn Azkar M.A., et al.	Simulation of urban and regional air pollution in Bangladesh	2012	Journal of Geophysical Research Atmospheres	9
36	Galloway M.M., et al.	Observations and modeling of formaldehyde at the PROPHET mixed hardwood forest site in 2008	2012	Atmospheric Environment	5

Index	Authors	Title	Year	Source title	No of citations
37	Carslaw K.S., et al.	Large contribution of natural aerosols to uncertainty in indirect forcing	2013	Nature	209
38	Lam S.H.M., et al.	Modelling VOC source impacts on high ozone episode days observed at a mountain summit in Hong Kong under the influence of mountain-valley breezes	2013	Atmospheric Environment	21
39	Menut L., et al.	On the impact of the vertical resolution on chemistry-transport modelling	2013	Atmospheric Environment	17
40	Ghannam K., et al.	A framework for emissions source apportionment in industrial areas: MM5/CALPUFF in a near-field application	2013	Journal of the Air & Waste Management Association	16
41	Huang M., et al.	Impacts of transported background pollutants on summertime western US air quality: Model evaluation, sensitivity analysis and data assimilation	2013	Atmospheric Chemistry and Physics	15
42	Jin L., et al.	Role of meteorological processes in ozone responses to emission controls in California's San Joaquin Valley	2013	Journal of Geophysical Research Atmospheres	2
43	Wang S., et al.	Effectiveness of national air pollution control policies on the air quality in metropolitan areas of China	2014	Journal of Environmental Sciences (China)	43
44	Ikeda K., et al.	Sensitivity analysis of source regions to PM2.5 concentration at Fukue Island, Japan	2014	Journal of the Air & Waste Management Association	22
45	Lapina K., et al.	Assessment of source contributions to seasonal vegetative exposure to ozone in the U.S	2014	Journal of Geophysical Research	22
46	Shimadera H., et al.	Sensitivity analyses of factors influencing CMAQ performance for fine particulate nitrate	2014	Journal of the Air and Waste Management Association	12
47	Itahashi S., et al.	Modeling investigation of controlling factors in the increasing ratio of nitrate to non-seasalt sulfate in precipitation over Japan	2014	Atmospheric Environment	8
48	Q Y.	Effects of NO (x) and VOCs from five emission sources on summer surface O-3 over the Beijing-Tianjin-Hebei region	2014	ADVANCES IN ATMOSPHERIC SCIENCES	6
49	Choi K.-C., et al.	Assessment of transboundary ozone contribution toward South Korea using multiple source-receptor modeling techniques	2014	Atmospheric Environment	4
50	Garcia-Menendez F., et al.	Simulating smoke transport from wildland fires with a regional-scale air quality model: Sensitivity to spatiotemporal allocation of fire emissions	2014	Science of the Total Environment	4

Index	Authors	Title	Year	Source title	No of citations
51	Hou X., et al.	Contributions of regional air pollutant emissions to ozone and fine particulate matter-related mortalities in eastern US urban areas	2015	Environmental Research	14
52	Itahashi S., et al.	Comprehensive study of emission source contributions for tropospheric ozone formation over East Asia	2015	Journal of Geophysical Research	5
53	Itahashi S., et al.	Variation of the ratio of nitrate to non-seasalt sulfate in precipitation over East Asia with emissions from China	2015	Atmospheric Environment	2
54	Calkins C., et al.	Effects of meteorological conditions on sulfur dioxide air pollution in the North China plain during winters of 2006–2015	2016	Atmospheric Environment	9
55	Sharma S., et al.	Sensitivity analysis of ground level ozone in India using WRF-CMAQ models	2016	Atmospheric Environment	7
56	Rea G., et al.	Impact of the New South Wales fires during October 2013 on regional air quality in eastern Australia	2016	Atmospheric Environment	4
57	Markakis K., et al.	Mid-21st century air quality at the urban scale under the influence of changed climate and emissions-case studies for Paris and Stockholm	2016	Atmospheric Chemistry and Physics	3
58	Shrivastava M., et al.	Sensitivity analysis of simulated SOA loadings using a variance-based statistical approach	2016	Journal of Advances in Modeling Earth Systems	3
59	Archer-Nicholls S., et al.	The regional impacts of cooking and heating emissions on ambient air quality and disease burden in China	2016	Environmental Science and Technology	3
60	Chang C.-Y., et al.	Investigating ambient ozone formation regimes in neighboring cities of shale plays in the Northeast United States using photochemical modeling and satellite retrievals	2016	Atmospheric Environment	2
61	Zhou Y., et al.	Development of a high-resolution emission inventory and its evaluation and application through air quality modeling for Jiangsu Province, China	2017	Atmospheric Chemistry and Physics	5
62	Beddows A.V.,et al.	Emulation and Sensitivity Analysis of the Community Multiscale Air Quality Model for a UK Ozone Pollution Episode	2017	Environmental Science and Technology	0
63	Lee H-M., et al.	PM2.5 source attribution for Seoul in May from 2009 to 2013 using GEOS-Chem and its adjoint model	2017	Environmental Pollution	0

Table 0.2 Overview of the publications listed in Table A.1. Indices 0 and 1 indicate the absence or presence respectively of a sensitivity or uncertainty analysis in the reviewed study. In some publications the number of model inputs perturbed, and the number of model simulations performed were not clearly stated; “Not clear” is used to indicate this.

Index	Local SA	Global SA	Other type	Sensitivity analysis type	Sensitivity measure	Uncertainty analysis	Model type	Model outputs investigated	Model inputs perturbed	No of inputs	No of model runs
1	1	0	0	OAT, Partial derivatives	variation factor	0	Gaussian plume, first order chemistry	Deposition of SO_2	Emissions, wind, deposition	Not clear	Not clear
2	1	0	0	OAT	Change relative to BL	0	1D CTM	CH_4 and CO concentrations	Fluxes, emissions, cloud cover, reaction rate	4	5
3	1	0	1	DDM	ppb	0	CIT, 3D photochemical model	O_3	Wind, emissions, deposition velocity, background conc. of O_3	8	Not clear
4	1	0	1	Fractional factorial design	Comparison between results	1	Persistent organic pollutant transport and deposition model	B(a)P, HCH	Conversion rate, particle size, deposition velocity, scavenging ratio	4	19
5	0	0	1	ADIFOR automatic differentiation for FORTRAN	Derivative	0	1D CTM	NO_2 photolysis rates, O_3 production	Aerosol types, profiles, relative humidity, NOx emissions	Not clear	Not clear
6	1	0	1	Factorial design	Percentage change in output to percentage change in input	1	Dry deposition model	Dry deposition of SO_2, NO_2, NH_3 and HNO_3	Precursor gas conc., temperature, solar radiation, wind speed	5	25

Index	Local SA	Global SA	Other type	Sensitivity analysis type	Sensitivity measure	Uncertainty analysis	Model type	Model outputs investigated	Model inputs perturbed	No of inputs	No of model runs
7	0	0	1	ADIFOR automatic differentiation for FORTRAN	Derivative	0	1D CTM	NO_2 photolysis rates, O_3 production	Aerosol mass, aerosol ext. coef., scattering albedo, RH, initial total ozone column, emissions of NOx and NMHCs	Not clear	Not clear
8	1	0	1	DDM	ppb	0	CIT, 3D photochemical model	O_3	VOC, NOx	Not clear	Not clear
9	1	0	1	Scenario	Comparison to BL values	0	MAQSIP, Eulerian grid model	O_3	HC emissions	6	9
10	1	0	1	Scenario	Comparison between results	0	Gaussian plume	Concentration of airborne pollutants	Algorithm	2	2
11	1	0	1	OAT, Scenario	Comparison between results	0	TCTM, 3D Eulerian	O_3	NOx, VOC	2	4
12	1	0	1	Scenario	Comparison to BL values	0	CMAQ	O_3	NOx, VOC, CO	3	12
13	1	0	1	DDM	ppm, concentration	0	CMAQ	O_3	NOx, VOC	2	Not clear
14	1	0	0	OAT	Change relative to BL	0	CMAQ	PM_{10}	PM_{10} emissions	7	14
15	1	0	1	Fractional factorial design	Comparison to BL values	0	MUSE	O_3	NOx, VOC	2	15

Index	Local SA	Global SA	Other type	Sensitivity analysis type	Sensitivity measure	Uncertainty analysis	Model type	Model outputs investigated	Model inputs perturbed	No of inputs	No of model runs
16	1	0	1	Scenario	Comparison to BL values	0	Global climate model	Aerosol concentration and properties	Emission inventories	3	3
17	1	0	0	OAT	Change relative to BL	0	TAPOM mesa scale model	Sulphate, nitrate, ammonium	Boundary conditions	1	1
18	1	0	0	OAT	Change relative to BL	0	CMAQ	PM	SO_2, NOx, NH_3, VOC, PC emissions, SO_2 sources differentiated	7	Not clear
19	0	1	0	Multiple linear regression with LHS	SRC uncertainty contribution	1	CIT, 3D photochemical model	$PM_{2.5}$, O_3	Concentrations, emission rates, reaction rates	17	50
20	1	0	0	OAT	Comparison between results	0	CMAQ	O_3, NO_2, $PM_{2.5}$	NOx, VOC emissions	2	2
21	1	0	1	DDM	ppb	0	CAMx	O_3	NOx, VOC emissions	Not clear	Not clear
22	1	0	1	HDDM	ppb	0	CMAQ	O_3	NOx, VOC emissions	Not clear	Not clear
23	0	0	1	Adjoint sensitivity analysis	Percentage response to fractional change	1	GEOS-CHEM	SO_2, NOx, NH_3, particles	Various emissions	Not clear	Not clear
24	1	0	1	OAT, DDM	ppb	0	CAMx	O_3	NOx, VOC emissions from various sources	Not clear	Not clear
25	1	0	0	OAT	Difference with BL normalised by emission reduction	0	CMAQ	$PM_{2.5}$, O_3	SO_2, NOX, PC, NH_3, VOC	5	100

Index	Local SA	Global SA	Other type	Sensitivity analysis type	Sensitivity measure	Uncertainty analysis	Model type	Model outputs investigated	Model inputs perturbed	No of inputs	No of model runs
26	1	0	0	OAT	Change relative to BL	0	PREVALP modelling system, multiple modules	O_3	VOC, temperature	3	3
27	1	0	1	HDDM	ppm	1	CAMx	O_3	Reaction rates, various emissions	Not clear	Not clear
28	1	0	1	OAT, Scenario	Change relative to BL	0	CMAQ	SO_2, NO_2, O_3, $PM_{2.5}$, sulphate, nitrate, sulphur and nitrogen deposition	Emission sectors, single pollutant emissions	12	12
29	0	1	0	Variance based, GP emulator	Main and total effects, variance contribution	1	GLOMAP	Cloud condensation nuclei	Parameters of aerosol microphysics module	8	104
30	1	0	1	OAT (screening) followed by differential SA	Change relative to BL	0	SIRANE, urban dispersion model	NOx	Various model parameters	12	24
31	1	0	1	Scenario	ppb	0	GEOS-CHEM	O_3	NOx from different sources, PAN	Not clear	Not clear
32	0	1	0	Variance based, RS-HDMR	First and second order sensitivity indices	1	RACM Photochemical box model	O_3	Model parameters	500	28500
33	1	0	1	Scenario	Comparison to BL values	0	RAMS-CMAQ	O_3	Various emission sources	1	2

Index	Local SA	Global SA	Other type	Sensitivity analysis type	Sensitivity measure	Uncertainty analysis	Model type	Model outputs investigated	Model inputs perturbed	No of inputs	No of model runs
34	0	1	0	Variance based, RS-HDMR	Sensitivity indices	1	RACM Photochemical box model	OH, HO_2	Model parameters	584	10000
35	1	0	1	Scenario	Comparison to BL values	0	CMAQ	NO_2, SO_2, CO, O_3, $PM_{2.5}$	Emissions inventory	1	4
36	1	0	0	OAT	Change relative to BL, comparison between results	0	Box model	HCHO	OH, HO_2, NO, background HCHO, dilution rate constant, V_d, boundary layer height	7	25
37	0	1	0	Variance based, GP emulator	Variance decomposition	1	GLOMAP	Cloud radiative forcing	Natural and anthropogenic aerosol emissions, aerosol precursor gas emissions, microphysical processes, structures of the aerosol model	28	168
38	1	0	0	OAT	Change relative to BL	0	Lagrangian photochemical box model	O_3	VOC, NOx emissions	2	13
39	1	0	1	Scenario	Comparison between results	0	CHIMERE Eulerian off-line CTM	NO_2, PM_{10}, O_3	Vertical mesh settings	1	3
40	1	0	0	OAT	Comparison to BL values	0	CALPUFF, puff dispersion model	CO, NO_2, $PM_{2.5}$	Various emissions, chemical transformations of NOX to nitrate aerosol	6	Not clear

Index	Local SA	Global SA	Other type	Sensitivity analysis type	Sensitivity measure	Uncertainty analysis	Model type	Model outputs investigated	Model inputs perturbed	No of inputs	No of model runs
41	1	0	1	OAT, Scenario	ppb	0	Multi-scale Sulfur Transport and Deposition Modeling system	O_3	Boundary conditions, species perturbed simultaneously (CO, NO, NO_2, NO_3, HNO_3, HNO_4, PAN, and N_2O_5), PAN	11	11
42	1	0	0	OAT	ppb	0	CMAQ	O_3	Emissions and source contributions	6	6
43	1	0	0	OAT	Change relative to BL	0	CMAQ	SO_2, NO_2, O_3	SO_2, NOx	2	2
44	1	0	0	OAT	Change relative to BL	0	CMAQ	$PM_{2.5}$	Various source regions	6	6
45	0	0	1	Adjoint sensitivity analysis	Normalised relative sensitivity	0	GEOS-Chem, STEM, AM3	O_3	NOX, VOC and CO emissions	Not clear	Not clear
46	1	0	1	OAT, ordinary differential equations	Change relative to BL	0	CMAQ	Nitrate	Various emissions, rh, T, deposition velocities, reaction probabilities	Not clear	Not clear
47	1	0	1	Scenario	Comparison between results	0	CMAQ	ratio of nitrate to non-sea salt sulfate	NOx, SO_2	2	2
48	0	0	1	Factor separation technique	Comparison between results	0	CAMx	O_3	Emission controls for different sectors: industry, power plant, transportation, residential, biogenic	31	32
49	1	0	1	OAT, HDDM	ppb	0	CMAQ	O_3	NOx, VOC, various source region	Not clear	Not clear

Index	Local SA	Global SA	Other type	Sensitivity analysis type	Sensitivity measure	Uncertainty analysis	Model type	Model outputs investigated	Model inputs perturbed	No of inputs	No of model runs
50	1	0	0	OAT	First order sensitivity coefficients	0	CMAQ	fine PM	$PM_{2.5}$, spatial and temporal allocation of fire emissions	Not clear	Not clear
51	1	0	1	HDDM	First and second order sensitivity coefficients	0	CMAQ	O_3 and $PM_{2.5}$ related deaths	NOx, VOCs, SO_2 regional anthropogenic emissions	Not clear	Not clear
52	1	0	1	OAT, HDDM	ppb	0	CAMx	O_3	NOx, VOC emissions, chemical reactions	Not clear	Not clear
53	1	0	1	OAT, Scenario	Change relative to BL	0	CMAQ	chemical composition of precipitation	Anthropogenic emissions for different years (2009, 2011)	1	2
54	1	0	1	OAT, Scenario	Comparison between results	0	GEOS-Chem	SO_2 loading	Meteorology and SO_2 emissions for 3 different years	2	6
55	1	0	1	OAT, Factorial design	Change relative to BL	0	CMAQ	O_3	NOX, VOC emissions by sector	Not clear	30
56	1	0	0	OAT	Comparison to BL values	0	CHIMERE	PM, CO	Diurnal variability, injection heights	2	4
57	1	0	1	Scenario	Change relative to BL	0	CHIMERE, MATCH	PM_{10}, $PM_{2.5}$, O_3	Climate settings, emissions	Not clear	Not clear
58	0	1	0	Variance based, GLM	Fraction of variance explained	0	WRF-Chem	SOA	Emissions, dry deposition, particle phase transformation	7	250
59	1	0	1	OAT, Scenario	Change relative to BL	0	WRF-Chem	$PM_{2.5}$	Residential and heating emissions	2	3

Index	Local SA	Global SA	Other type	Sensitivity analysis type	Sensitivity measure	Uncertainty analysis	Model type	Model outputs investigated	Model inputs perturbed	No of inputs	No of model runs
60	1	0	1	DDM	ppb	0	CMAQ	O_3	VOC, NOx emissions	2	Not clear
61	1	0	1	OAT, Scenario	Change relative to BL	0	CMAQ	O_3, $PM_{2.5}$	NOx, VOC emissions, split by source	Not clear	5
62	0	1	0	Variance based, FAST, GP emulator	Sensitivity coefficients, first-order, interactions, total effects	1	CMAQ	O_3	Emissions, boundary conditions, reaction rates	30	576
63	0	0	1	Adjoint sensitivity analysis	Proportion of contribution from a source	0	GEOS-Chem	$PM_{2.5}$	Emissions by sector and region	Not clear	Not clear

Appendix B

Supplementary figures for Chapters 3 and 4

Figure B.1 shows spatial distribution of the emissions of NO_x, SO_2, and NH_3 used as inputs in the FRAME model. The maps of NO_x and SO_2 emissions for the year 2012 were obtained from http://naei.beis.gov.uk/data/map-uk-das (last access: 9 March 2018). The NH_3 emission map was obtained from AQPI Summary Report – Emissions of Air Quality Pollutants – 1970-2011 (https://uk-air.defra.gov.uk/ assets/documents/ reports/cat07/1305031312_EoAQP1970-2011_pq.pdf, last access: 9 March 2018)

Figure B.2 shows annual average surface concentrations of particulate NH_4^+, NO_3^-, SO_4^{2-}, and annual wet and dry deposition of SO_y calculated by the FRAME model with baseline emissions for the year 2012.

Figures B.3 and B.4 show spatial distributions of regression coefficients for NH_3, NO_x, SO_2, HNO_3 and wet and dry deposition of NH_x and NO_y with respect to input emissions of the pollutant in brackets.

Figure B.5 shows spatial distributions of the relative uncertainties in surface concentrations of NH_3, NO_x, SO_2 and HNO_3 and dry and wet deposition of NOy and NHx for uncertainties of ± 4 %, ± 10 %, and ± 20 % in emissions of SO_2, NO_x and NH_3 respectively. The uncertainty values are represented as +/- range relative to the baseline value and with the full range represents the 95 % confidence interval.

Figures B.6 and B.7 show spatial distributions of the squared SRC values which represent the fractional contribution of the uncertainty in the input emissions given in brackets to the overall uncertainty in NH_3, NO_x, SO_2, HNO_3 and dry and wet deposition of NOy and NHx.

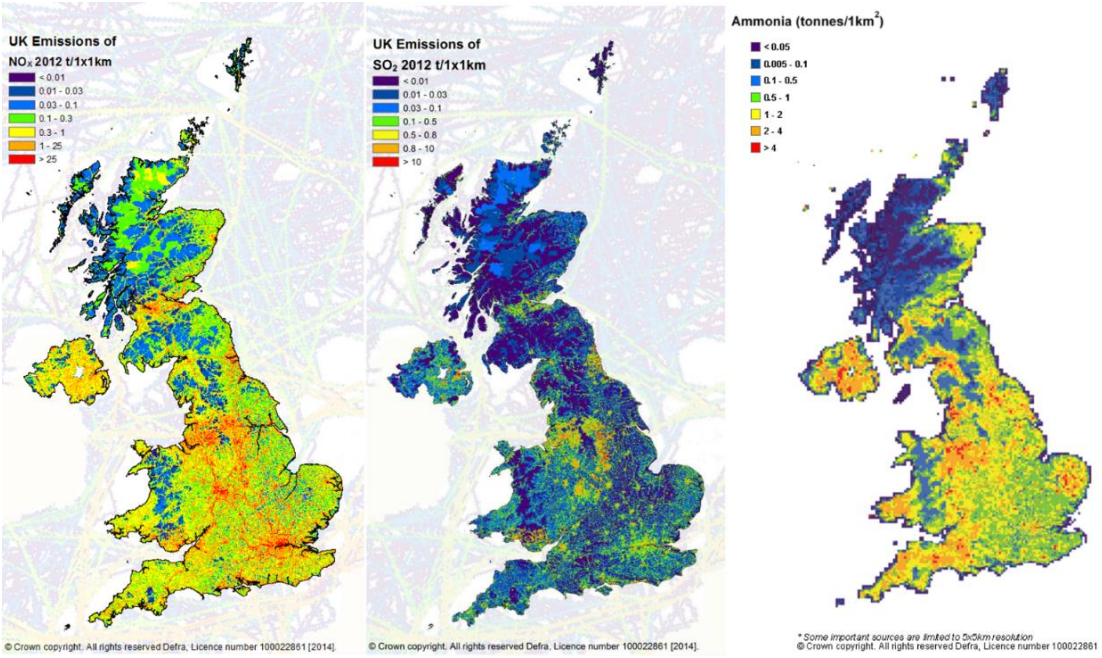

Figure 0.1 Spatial distribution of the UK NO_x, SO_2, and NH_3 emissions. The maps of NO_x and SO_2 emissions were obtained from http://naei.beis.gov.uk/data/map-uk-das, last access: 9 March 2018. The NH_3 emission map is obtained from AQPI Summary Report – Emissions of Air Quality Pollutants – 1970-2011 (https://uk-air.defra.gov.uk/assets/documents/reports/cat07/1305031312_EoAQP1970-2011_pq.pdf, last access: 9 March 2018).

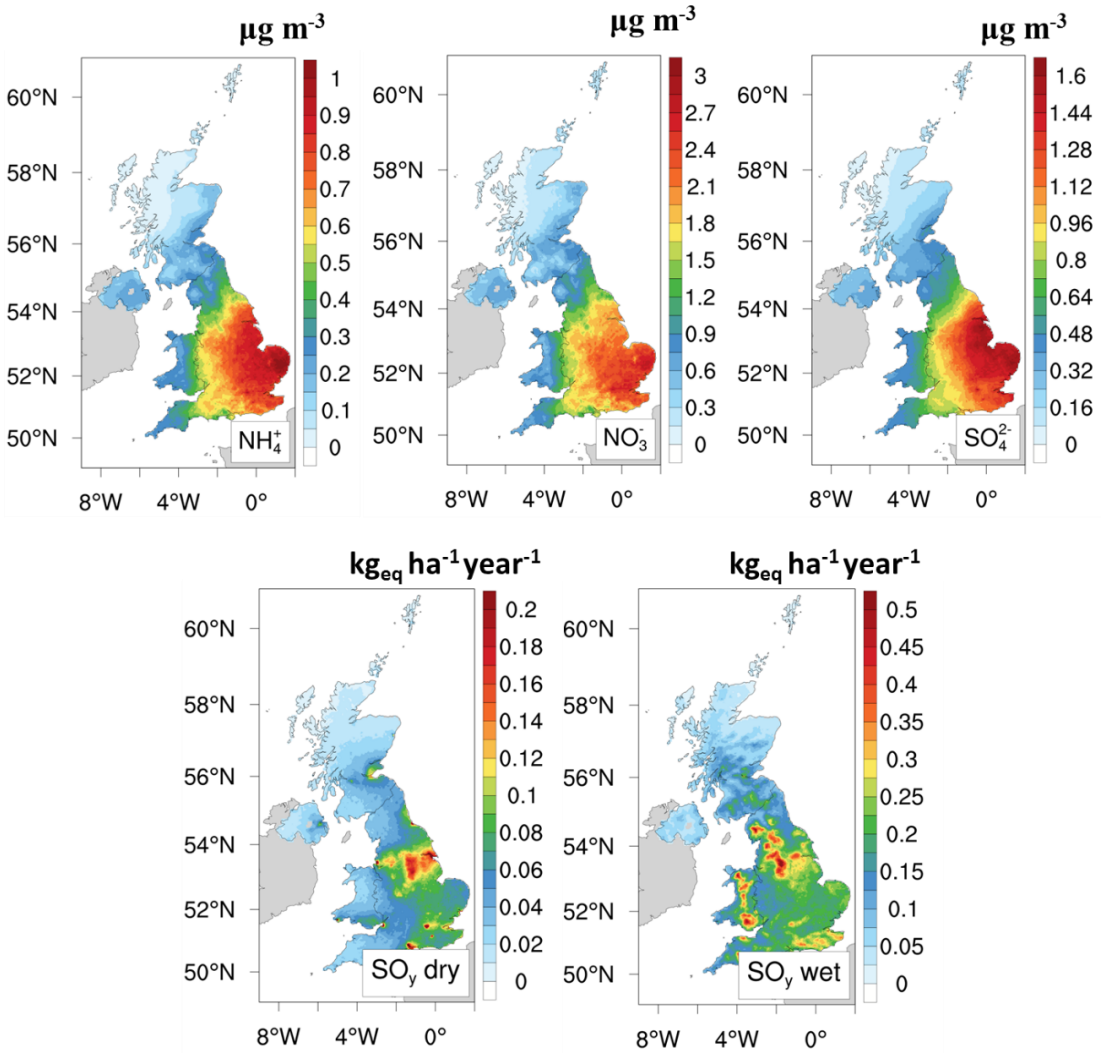

Figure 0.2 Annual average surface concentrations of particulate NH_4^+, NO_3^-, SO_4^{2-}, and annual wet and dry deposition of SOy calculated by the FRAME model for 2012.

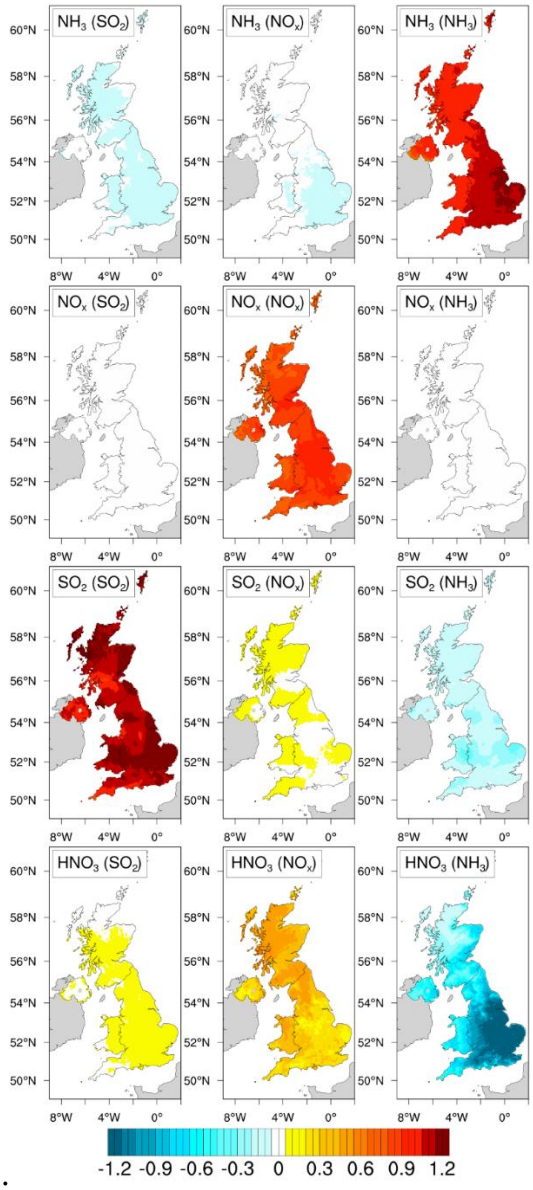

Figure 0.3 Spatial distributions (at the 5 km × 5 km model grid resolution) of RCs for NH_3, NO_x, SO_2, and HNO_3 as a function of variation in input emissions of SO_2, NO_x or NH_3. The model input emissions for which the RC quantifies the output variable sensitivity is given in the brackets in each panel.

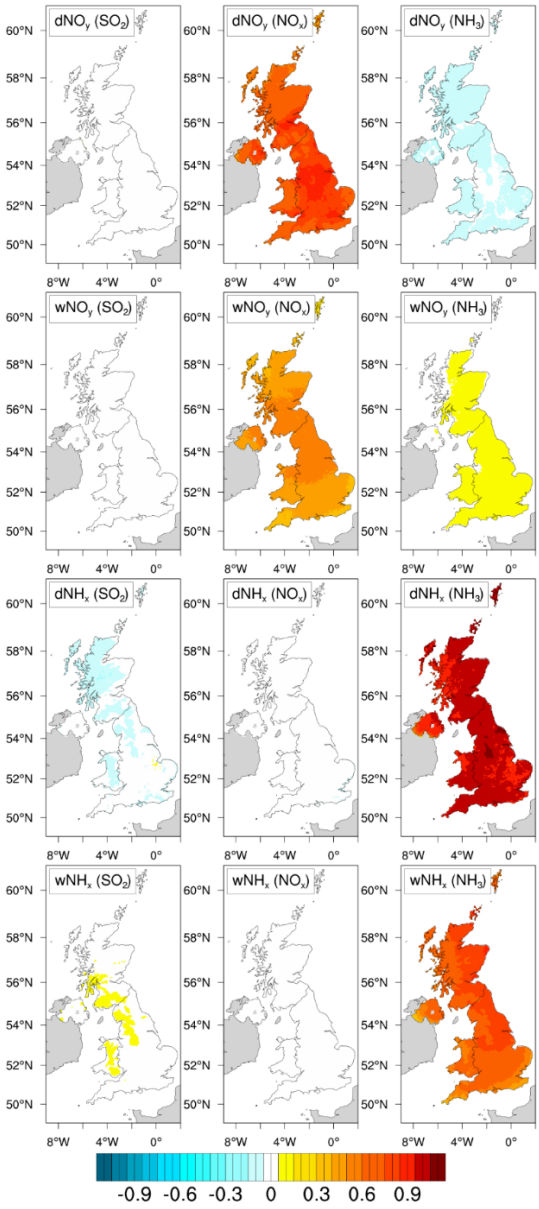

Figure B.4 Spatial distributions (at the 5 km × 5 km model grid resolution) of RCs for wet (w) and dry (d) deposition of NO_y and NH_x as a function of variation in input emissions of SO_2, NO_x and NH_3. The model input emissions for which the RC quantifies the output variable sensitivity is given in the brackets in each panel.

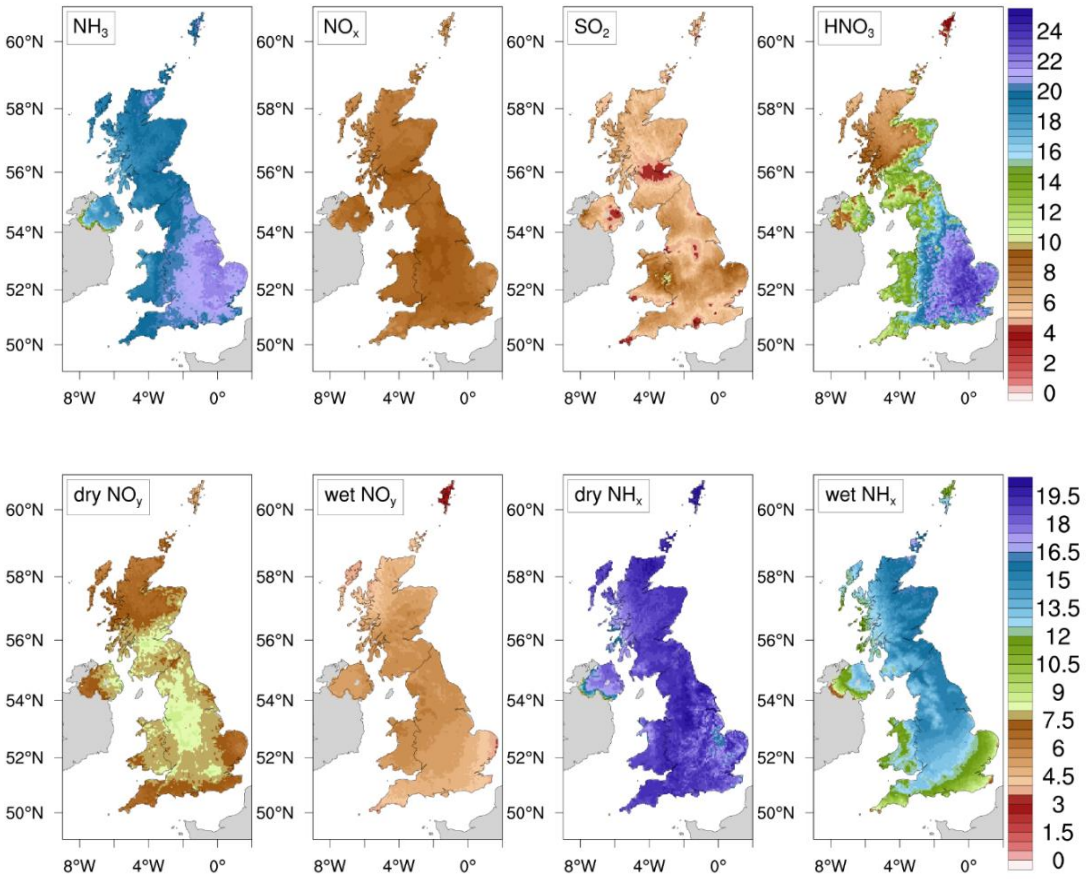

Figure B.5 Spatial distributions (at the 5 km × 5 km model grid resolution) of the relative uncertainties in surface concentrations of NH_3, NO_x, SO_2 and HNO_3 and dry and wet deposition of NO_y and NH_x for uncertainties of ± 4 %, ± 10 %, ± 20 % in emissions of SO_2, NO_x and NH_3 respectively. The uncertainty values are represented as a range of +/- the baseline value and represent the 95 % confidence interval.

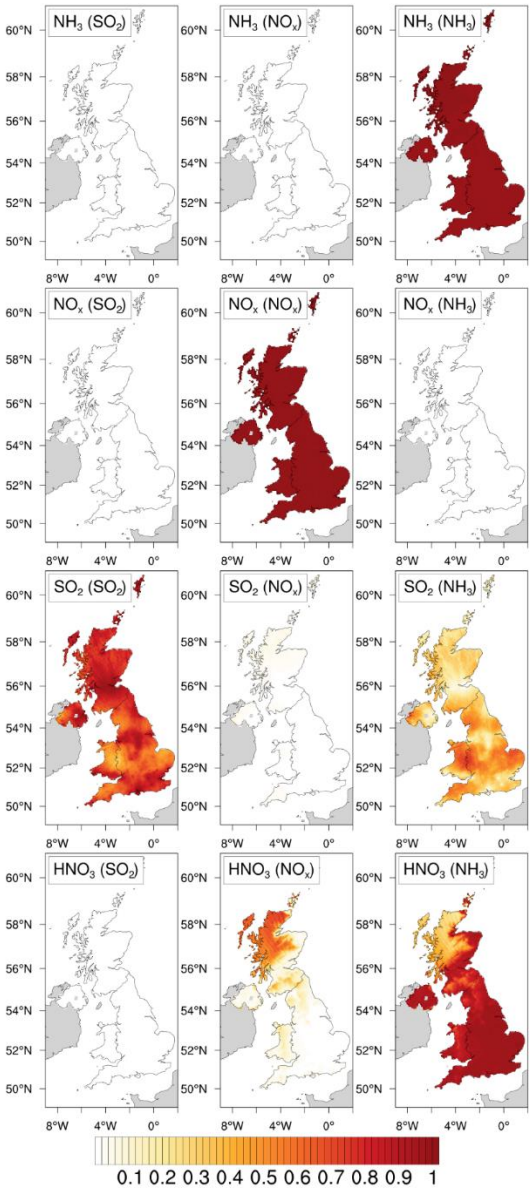

Figure B.6 Spatial distributions (at the 5 km × 5 km model grid resolution) of the squared SRC values which represent the fractional contribution of the uncertainty in the input emissions given in brackets to the overall uncertainty in NH_3, NO_x, SO_2 and HNO_3. The uncertainties in the input emissions are ± 4 %, ± 10 % and ± 20 % for SO_2, NO_x and NH_3 respectively.

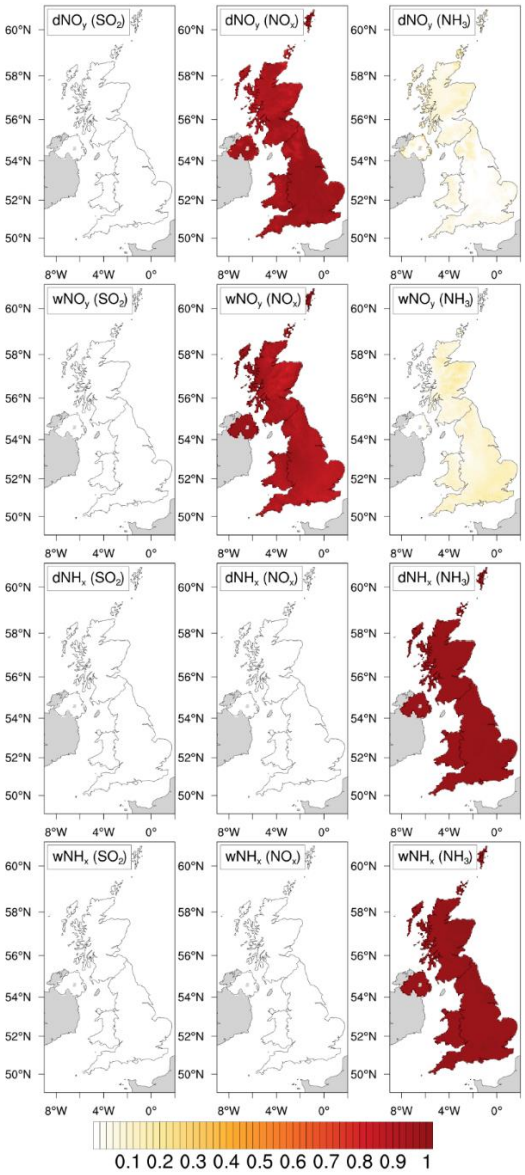

Figure B.7 Spatial distributions (at the 5 km × 5 km model grid resolution) of the squared SRC values which represent the fractional contribution of the uncertainty in the input emissions given in brackets to the overall uncertainty in the dry and wet deposition of NO_y and NH_x. The uncertainties in the input emissions are ± 4 %, ± 10 % and ± 20 % for SO_2, NO_x and NH_3 respectively

Appendix C

Supplementary figures for Chapter 5

Figure C.1 shows the spatial distribution of *k*-fold cross-validation errors for the Gaussian process emulators used to estimate the annual average surface concentrations of O_3, NO_2, and $PM_{2.5}$.

Figure C.2 shows the scatter plot of the first-order sensitivity indices against the total sensitivity indices. The grey lines indicate ± 3% fluctuation in the sensitivity index values, which were attributed to numerical errors in the calculation of sensitivity indices the analytical values of which are close to zero.

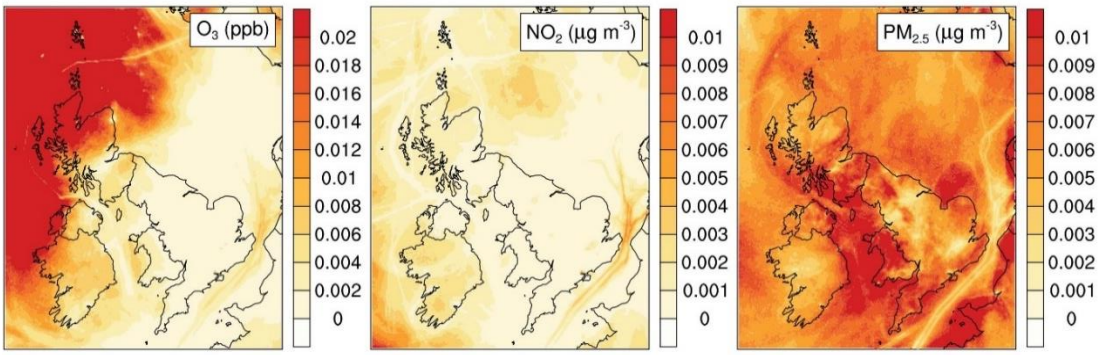

Figure C.1 Spatial distribution of k- fold cross validation error values for emulated annual average concentrations of O_3, NO_2, and $PM_{2.5}$.

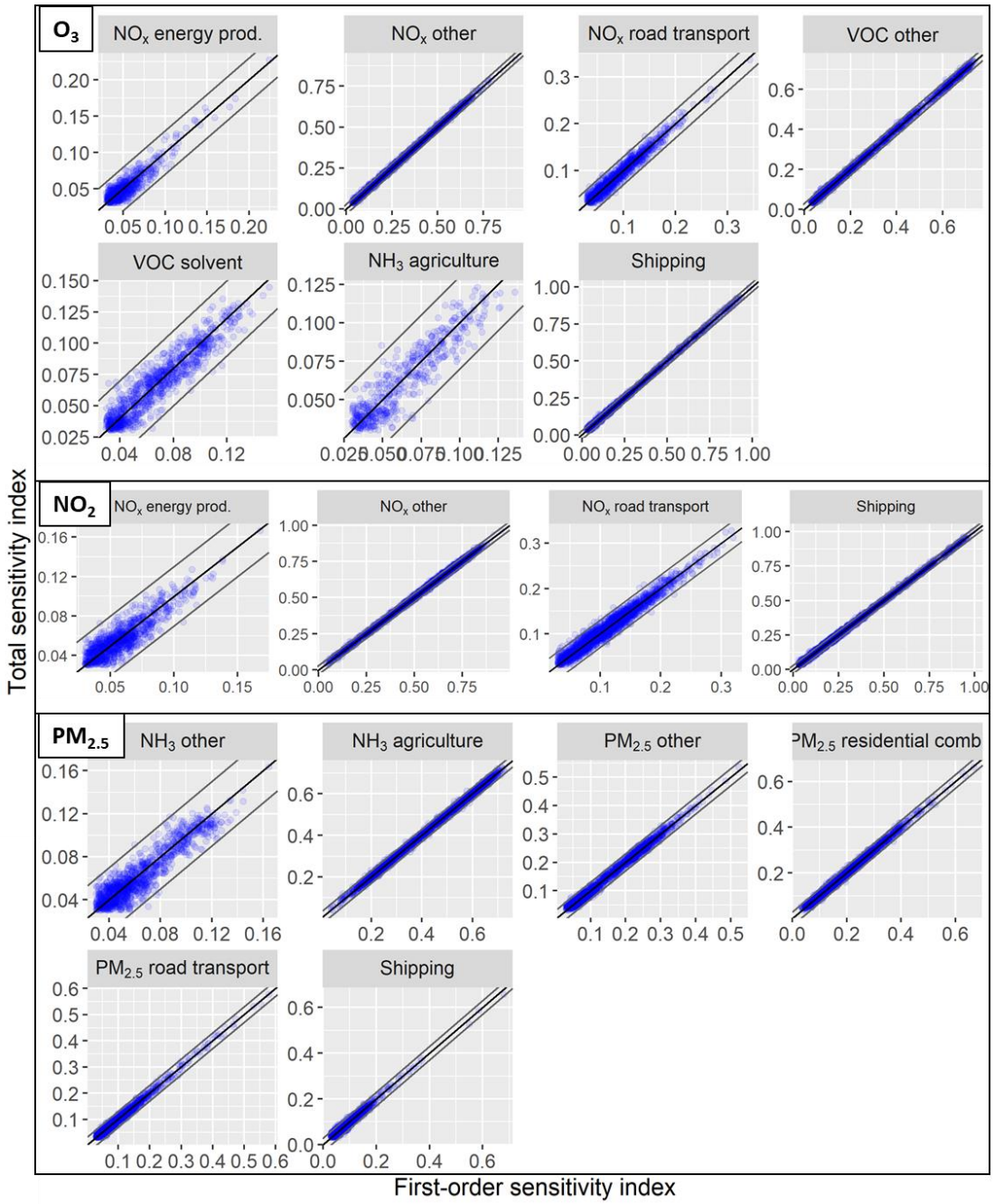

Figure C.2 Scaterplot of the first-order sensitivity indices against the total sensitivity indices for the inputs affecting the variation in modelled values of O_3, NO_2, and $PM_{2.5}$.